THESIS FOR THE DEGREE OF DOCTOR OF PHILOSOPHY
IN
THERMO AND FLUID DYNAMICS

Optimization of Chemical Kinetic Mechanisms and Numerical Simulations of Industrial Gas Turbine Burners

ABDALLAH ABOU-TAOUK

Division of Fluid Dynamics

Department of Applied Mechanics

CHALMERS UNIVERSITY OF TECHNOLOGY

Göteborg, Sweden, 2014

Optimization of Chemical Kinetic Mechanisms and Numerical Simulations of Industrial Gas Turbine Burners
ABDALLAH ABOU-TAOUK
ISBN 978-91-7597-029-5

Doktorsavhandling vid Chalmers tekniska högskola
Ny serie nr 3710
ISSN 0346-718X

Division of Fluid Dynamics
Department of Applied Mechanics
Chalmers University of Technology
SE-412 96 Göteborg, Sweden

Phone: +46-(0)31-7721000
Fax: +46-(0)31-7723872

Printed at Chalmers Reproservice
Göteborg, Sweden, 2014

Optimization of Chemical Kinetic Mechanisms and Numerical Simulations of Industrial Gas Turbine Burners

ABDALLAH ABOU-TAOUK

Division of Fluid Dynamics
Department of Applied Mechanics
Chalmers University of Technology

Abstract

Increasing demands on environmentally friendly energy conversion indicate that pollutants need to be reduced. Computational Fluid Dynamics is efficiently used today in turbulent reaction flow simulations to gain a deeper understanding of the combustion process and consequently be able to improve combustor design and reduce emissions. This thesis aims to investigate recent developments in turbulent reacting flow in the context of engineering type numerical analysis tools, applied to the main problem area of swirl-stabilized flexi-fuel flames. Combustion simulations involve a strong coupling between kinetics, transport and turbulence and their interactions. Fully detailed kinetic mechanisms are expensive in terms of computer time when coupled with Computational Fluid Dynamics, and the complexity of combustion chemistry must hence be downsized. Chemistry look-up tables and reduced reaction mechanisms are two well-known methods used today. Compared to chemical look-up tables, the use of a global mechanism involving a limited number of species is of obvious practical interest, specifically when dealing with complex burner geometries in the industrial applications featuring multiple inlets, dilution with burnt gases in recirculation zones and heat loss. The proposed optimization methodology for global schemes is based on the 1D balance equations for species mass fractions and temperature, and also laminar flame speed involved in the reduced mechanisms correctly reproducing the detailed chemistry solution. The optimizations are performed using a set-up of different tools, such as CANTERA®, CHEMKIN® and modeFRONTIER®. A new approach to sub-grid scale modeling is also suggested, which relies on the idea that effects and properties of the spatial filtering, inherent to Large Eddy Simulation solvers, could be directly accounted for when reducing chemistry and molecular transport properties. The optimized global schemes have been implemented in the CFD toolbox Ansys CFX® and used in numerical simulations (RANS, URANS/LES and LES turbulence models) of two different par-

tially premixed industrial gas turbine combustors and the test case of Sandia Flame D. The focus has been on grid generation and modeling of the CFD domain. Measured and predicted flow and flame dynamics, averaged temperature and species concentrations compare well for the different set-ups.

Keywords: Chemistry Reduction, Global Mechanism, Finite Rate Chemistry, Swirling Flow, Gas Turbine Combustion, Partially Premixed Flames, RANS, SAS-SST, LES,

List of Publications

This thesis is based on the work contained in the following papers:

I A. Abou-Taouk and L. E. Eriksson , 2011, Optimized Global Mechanisms For CFD Analysis of Swirl-Stabilized Syngas Burner for Gas Turbines, *ASME Turbo Expo 2011*, June 6-11, Vancouver, Canada

II A. Abou-Taouk, R. Whiddon, I. R. Sigfrid and L. E. Eriksson , 2011, CFD Investigation of Swirl-Stabilized Flexi-Fuel Burner Using Methane-Air Mixture for Gas Turbines, *The 20th ISABE Conference*, ISABE 2011-1122, September 12-16, Göteborg, Sweden

III A. Abou-Taouk and L. E. Eriksson, Evaluation of Optimized 3-step Global Reaction Mechanism for CFD Simulations on Sandia Flame D , 2011, *The 6th Symposium on Numerical Analysis of Fluid Flow and Heat Transfer*, ICNAAM 2011-0604, September 18-25, Halkidiki, Greece

IV A. Abou-Taouk, R. Whiddon, I. R. Sigfrid and L. E. Eriksson, A Four-Step Global Reaction Mechanism for CFD Simulations of Flexi-Fuel Burner for Gas Turbines, 2012, *7th International Symposium on Turbulence, Heat and Mass Transfer*, Palermo, Italy

V I .R. Sigrid, R. Whiddon, A. Abou-Taouk, R. Collin, and J. Klingmann, Experimental Investigations of an Industrial Lean Premixed Gas Turbine Combustor With High Swirling Flow, 2012, *ASME Gas Turbine India Conference*, GTIndia 2012-9681, Mumbai, India

VI A. Abou-Taouk, S. Sadasivuni, D. Lörstad and L. E. Eriksson, Evaluation of Global Mechanisms for LES Analysis of SGT-100 DLE Combustion System, 2013, *ASME Turbo Expo 2013, GT2013-95454*, San Antonio, Texas, USA

VII B. Farcy, A. Abou-Taouk, L. Vervisch, P. Domingo and N. Perret, Two approaches of chemistry downsizing for simulating selective non catalytic reduction DeNOx Process, *Fuel*, 118 (2014) 291-299

VIII A. Abou-Taouk, B. Farcy, P. Domingo, L. Vervisch, S. Sadasivuni and L. -E. Eriksson, 2014, A new approach for Large Eddy Simulation of gas turbine partially premixed combustion: Implicit modeling using optimized chemistry, *To be submitted to Combustion Theory and Modeling*

Other relevant publications

IX B. Farcy, A. Abou-Taouk, L. Vervisch, P. Domingo, N. Perret, Numerical Modeling of Selective Non Catalytic Reduction DeNOx Process, 2013, *7th European Combustion Meeting*, 25-28 June, Lund, Sweden

Acknowledgments

This work would not have been possible without the support of a number of organizations and individuals. It was carried out at the Department of Applied Mechanics, Division of Fluid Dynamics, at Chalmers University of Technology. The CFD computations in the thesis were made at Chalmers Center for Computational Science and Engineering (C3SE). The financial support of the Swedish Energy Agency, Siemens Industrial Turbomachinery AB, Finspång, Sweden, GKN Aerospace Engine Systems Sweden and the Royal Institute of Technology through the Swedish TURBO POWER research program is greatly acknowledged.

First and foremost, I would like to express my great appreciation to my supervisor, Professor Lars-Erik Eriksson, for his wonderful supervision, guidance and support, and for sharing his knowledge and ideas with me. I am grateful to all of my colleagues and friends at the Division of Fluid Dynamics, and particularly PhD student Lars Ellbrant and Dr. Mohamad El-Alti for all their invaluable help and pleasant discussions with me during the work. The administrative support of Ulla Lindberg-Thieme and Monica Vargman is gratefully acknowledged.

I will not forget the industry and here, especially, and many thanks go to Dr. Jenny Larfeldt, Dr. Darioush Gohari Barhaghi and Dr. Daniel Lörstad at Siemens Industrial Turbomachinery AB in Finspång, Sweden. I appreciate the helpful discussions we had and sharing knowledge and burner geometries with me. I would also like to acknowledge Siemens Industrial Turbomachinery Ltd, Lincoln, UK, and especially Dr. Ghena Bulat and Dr. Suresh Sadasivuni for helpful discussions and permission to use the Turchemi test case.

In this PhD work, I also made a three-month visit to CORIA - INSA, Rouen, France. Here, I would like to thank Professor Luc Vervisch, Professor Pascale Domingo and PhD student Benjamin Farcy for the inspiring and encouraging time, for sharing knowledge and for the joint collaboration in publishing a number of articles.

Collaboration with Lund University is also acknowledged. Special thanks here go to Dr. Ivan Sigfrid and Dr. Ronald Whiddon for providing the validation data used in the CFD work concerning the down-

scaled SGT-750 test burner.

My warmest gratitude and deepest feelings go to my mother, my father, my four sisters, my wife Douaa and my wonderful two daughters Sabah and Laila. The work could never have been done without your support and encouragement.

Finally, I would like to thank God, Allah, the almighty, for giving me the good health and power to carry out five years of PhD work.

Nomenclature

Upper-case Roman

A_i	pre-exponential factor
$\mathcal{A}_i$	ensemble of species involved in reaction i
B_k	backward reaction rate
C_μ	constant in k-ε turbulence model
D_{th}	thermal diffusivity
E_{a_i}	activation energy
F_k	forward reaction rate
$[I]$	molar concentration
K_c	equilibrium constant
$L_{\nu k}$	von karman length scale
P_{in}	inlet reactor pressure
P_k	turbulent production term
RR_i	reaction rate
R	gas constant
S_{ij}	strain rate tensor
S_L	laminar flame speed
S_T	turbulent flame speed
S_{SAS}	source term in SAS model
S	swirl number
T	temperature
T_{adi}	adiabatic flame temperature
T_{in}	inlet reactor temperature
T_{out}	outlet reactor temperature
V	reactor volume
W_j	molecular weight of species j
Y	mass fraction
$Y^{(k)}$	species mass fraction

Lower-case Roman

$f_i(\phi)$	correction function

h_0	total enthalpy
k	turbulent kinetic energy
$\dot{m}$	mass flow rate
$n_{j,i}$	reaction orders of species j in reaction i
p	pressure
u_i	cartesian components of velocity vector
u	axial velocity component
v	radial velocity component
w	tangential velocity component
$\widetilde{T}$	spatially filtered temperature

Greek Symbols

ϕ	equivalence ratio
β	temperature exponent
$\beta^\star$	constant in k-ω turbulence model
δ_{ij}	kronecker delta
δ_L	flame thickness
ε	dissipation of turbulent kinetic energy
μ	laminar dynamic viscosity
μ_t	turbulent eddy viscosity
ν	kinematic viscosity ($\nu = \mu/\rho$)
ρ	density
ρ_u	unburned gas mixture density
τ_{ij}	viscous stress tensor
τ_{res}	residence time
τ_c	chemical time scale
τ_m	turbulence mixing time
u'	turbulent intensity
Δ	filter size
Ξ	SGS flame wrinkling factor

Abbreviations

CFD	Computational Fluid Dynamics
CFL	Courant-Friedrichs-Lewy
CSP	Computational Singular Perturbation
DES	Detached Eddy Simulation
DLE	Dry Low Emission
DNS	Direct Numerical Simulation
EDC	Eddy Dissipation Concept
EDM	Eddy Dissipation Model
FRC	Finite Rate Chemistry

IEA	International Energy Agency
LCV	Low Caloric Value
LDV	Laser Doppler Velocimetry
LES	Large Eddy Simulation
LTH	Lund University
MFL	Mass Flow Controllers
M3	Meredith 3-step reaction mechanism
PIV	Particle Image Velocimetry
PLIF	Planar Laser-Induced Fluorescence Imaging
PaSR	Partially Stirred Reactor
PSR	Perfectly Stirred Reactor
RANS	Reynolds Averaged Navier-Stokes
RPL	Rich Pilot Lean
RNG	Re-Normalisation Group
SAS	Scale Adaptive Simulation
SGS	Sub Grid Scale
SCADA	Supervisory Control Data Acquisition
SNCR	Selective Non Catalytic Reduction
SIT	Siemens Industrial Turbomachinery
UHC	Unburned HydroCarbons
URANS	Unsteady Reynolds Averaged Navier-Stokes
WALE	Wall Adaptive Local Eddy Viscosity
WD2	Westbrook Dryer 2-step reaction mechanism

Chemical Compounds

CH_4	methane
CO_2	carbon dioxide
CO	carbon monoxide
H_2	hydrogen
H_2O	water
NO_x	nitrogen oxides
O_2	oxygen

Contents

Chapter 1

Introduction

1.1 Motivation

COMBUSTION processes play a central role in today's energy intensive society for household and industrial heating, power generation, propulsion (transport and communication), waste management and process industry. In the future, regulations on emissions, new technology improvements, increased use of nuclear power, biomass energy and other renewable energy still seem not to be sufficient to decrease the strong dependency on fossil fuels, Figure 1.1. Thus, combustion and its control are essential to our existence. It is anticipated that combustion will remain the dominant source of power for at least the next three to four decades (Grundy (2008); IEA (2013)). Nuclear energy has seen significant growth between 1971 and 2011, Figure 1.2. However, after the most recent accident in Japan in 2011, great pressure has been put on governments such as in Germany and Japan to decrease use of this energy source and stop production of new nuclear power plants. Figure 1.2 shows statistics of the world energy supply from 1971 to 2011 published by the International Energy Agency (IEA). As we know today, combustion of fossil fuels (liquids, solids and gases) still accounts for more than 80% of the total energy consumption in the world. Renewable sources of energy such as solar, wind, heat and geothermal are growing slowly but are far from being able to meet today's energy demands. In the future, fossil fuels will still dominate as the primary source of energy, and this source includes combustion. There is currently almost full agreement that human use of fossil fuels affects the Earth's climate. However, scientists have not yet come to full agreement on how great this impact is and how serious the effects can be, although it seems clear that emissions of greenhouse gases must be reduced if warming of the planet is to be reduced. Reducing

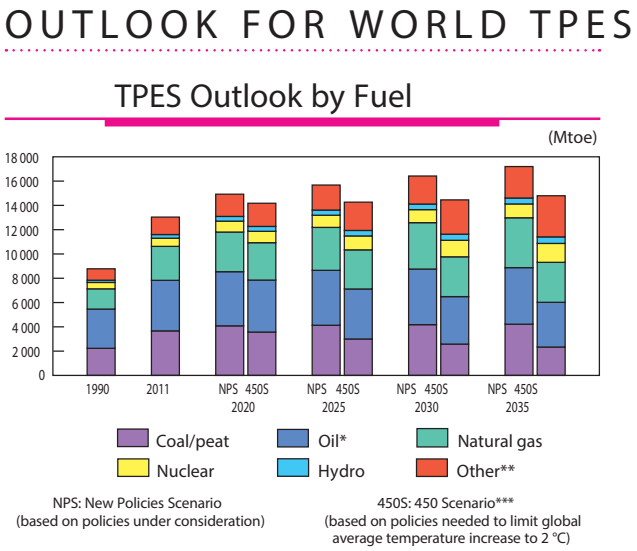

Figure 1.1: International Energy Agency energy consumption scenario for the next 20 years based on different policies

negative environmental impacts and developing a sustainable energy system require improved combustion technology in terms of emissions and efficiency. For ideal stoichiometric combustion of hydrocarbon fuels, the reactants are fuel and oxidizer and the products are carbon dioxide (CO_2) and water (H_2O). In an incomplete combustion process, however, emissions such as soot, carbon monoxide (CO), nitrogen oxides (NO_x) and Unburned Hydro Carbon (UHC) are produced. The release of greenhouse gases, such as CO_2, is considered the main source of global warming. Regulatory requirements to limit the emissions of pollutants and global warming imply an increasing need of optimization of energy conversion processes. To accomplish this, numerical simulation tools become more and more important for investigating turbulent combustion because of the high cost of experimental testing and prototyping. Detailed simulations increase our understanding of turbulent flame structures and dynamics and are used to test and improve existing turbulent combustion models for industrial Computational Fluid Dynamics (CFD) tools, which are then validated against experimental data.

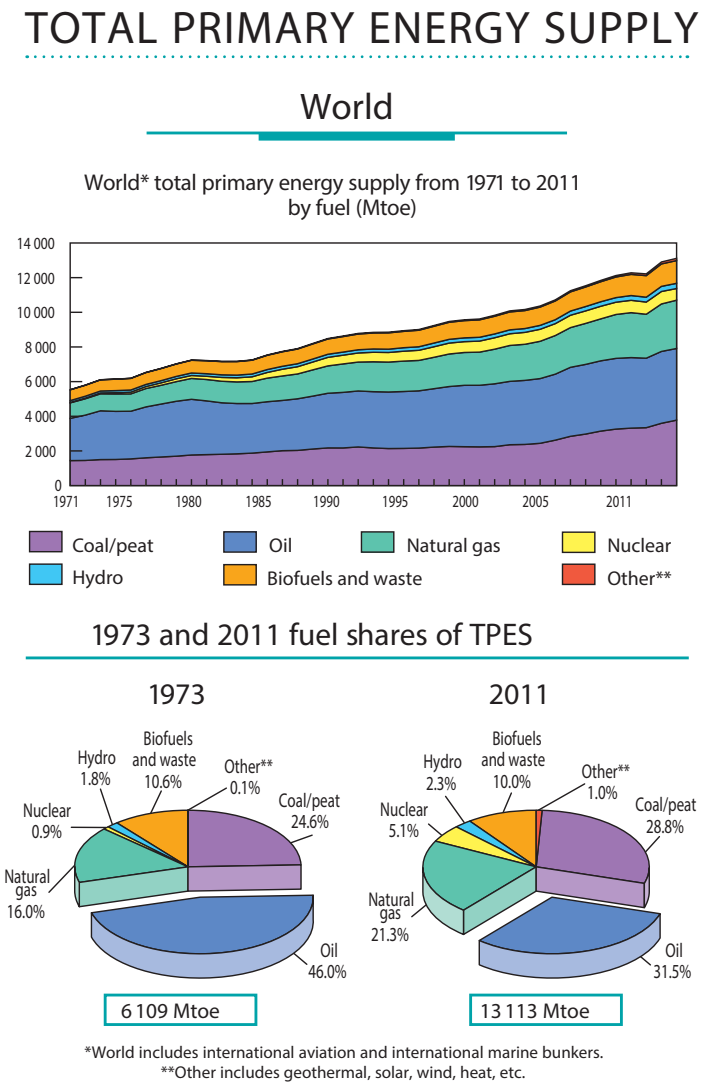

Figure 1.2: Total world energy supply

In the past few years, the development of combustor technology in the gas turbine community has followed a general trend towards fuel flexibility and increased use of bio fuels, Genrup & Thern (2013). Fuel flexibility is a term often used to describe the growing trend for gas turbines to be operated on a variable set of fuels. These fuels are typically of the Low Caloric Value (LCV) type. The opportunity to operate on flexi-fuel is important since fossil fuels are a limited energy source. The use of syngas fuel (a mixture of methane (CH_4), CO and hydrogen (H_2)) in combustors is becoming more attractive since this is a common denominator for many gasification processes based on either bio fuels or fossil fuels. One difficulty with these types of gases is that

they have a lower energy content per unit volume. This implies that the time needed for complete combustion increases. Further, the high content of hydrogen increases the risk of obtaining flashbacks or extinguishing the flame. These phenomena can cause serious damage to different components in the gas turbine. Siemens Industrial Turbomachinery AB, Finspång, Sweden has developed a new premixed Dry Low Emission (DLE) burner (4^{th} generation) that is used in the SGT-750 industrial gas turbine. This burner can be operated by both liquid and gaseous fuels. A scaled down version of this test burner was experimentally investigated at Lund University, Sweden (Sigfrid *et al.* (2011*a*,*b*, 2012, 2013*a*,*b*, 2014); Sigfrid (2013); Whiddon (2014)), and used in this work for validation of the turbulent reactive flow simulations using different turbulent combustion models. The SGT-100 industrial gas turbine studied experimentally by the DLR Institute of Combustion Technology, Stuttgart, Germany (Stopper *et al.* (2010, 2013)), was simulated with a 3D-LES flow solver using a new sub-grid scale model approach developed in the present work.

1.2 Background

The integration of detailed kinetics into turbulent flame simulations is one of the most difficult challenges in the combustion community today. The complexity of combustion chemistry must be downsized to reduce both the number of degrees of freedom and the stiffness of the partial differential equations solved simultaneously with the flow. Chemistry downsizing has been addressed previously, providing reduced chemical schemes (Jones & Lindstedt (1988); Franzelli *et al.* (2010)) or using chemical look-up tables obtained either from low-dimensional manifold projection (Bykov & Maas (2007)) or from one- or multi-dimensional canonical combustion problems, such as flamelets (Peters (1986); Oijen *et al.* (2001); Nguyen *et al.* (2010)). Both of these techniques have recently benefited from automated optimization tools. In the case of reduced chemistry, the rates of global schemes were found from an optimization procedure (Meredith & Black (2006); Franzelli *et al.* (2010); Abou-Taouk & Eriksson (2011); Abou-Taouk *et al.* (2012, 2013, 2014); Farcy *et al.* (2014)). In the context of the table look-up construction, it was proposed to determine the progress variable from all species of a detailed chemical scheme with optimization, Niu *et al.* (2013).

When it comes to industrial applications, e.g. a gas turbine where the burner is often fed by several streams for fuel, cold and heated air, recirculated burnt gases are used, and higher pressures and regions of premixed and partially premixed mixtures are obtained in the combus-

tor. In these complex flow situations, the full tabulation of chemistry may become cumbersome because of too large a number of control parameters (fuel, oxidizer, dilution, heat loss etc.) that are necessary to parameterize for the look-up table.

One method for solving this is to use a reduced global scheme solving for respective species in the CFD simulations, instead of the tabulated chemistry of a complex scheme. Using global mechanisms in CFD simulations is advantageous because only a few species are of interest in many industrial applications. In general, to be able to use CFD as a design tool in gas turbine combustors, it is necessary to correctly predict the fuel reaction rates, the combustor exit temperature and the CO and NO_x composition. The reduced mechanism also offers solutions that are significantly cheaper in both CPU time and memory than tabulation methods. Several different reduced reaction mechanisms for hydrocarbon mixtures are described in the literature (Meredith & Black (2006); Westbrook & Dryer (1984); Jones & Lindstedt (1988); Slavinskaya & Unkhoff (2008); Marzouk & Huckaby (2010); Novosselov & Malte (2008); Abou-Taouk *et al.* (2013, 2012); Fedina & Fureby (2011)). A number of published global reaction mechanisms have shown that these schemes have the capacity to mimic several aspects of the flames despite the simplified chemistry. The drawback of most of the published global schemes is that they are not flexible enough to cope with a wide range of operation conditions (e.g. equivalence ratio and pressure variations) as are present in most industrial gas turbines.

The complexity of turbulent combustion has to do with the unresolved problem in how the exact manner in which combustion and turbulence affect each other. Turbulent flows are characterized by a large range of length and time scales, Figure 1.3. The turbulent spectrum is divided into three different regions. The first region, I, corresponds to the generation of large energy containing scales. The intermediate region stands for the inertial subrange, where the energy is transferred from large to small scales. In the third region, III, the small scales are dissipated. Depending on which turbulence model is used, different amounts of the turbulent spectrum are resolved and modeled. More information about the turbulence cascade process is available in different turbulence books.

The book by Wilcox (2004) summarizes very well the properties of turbulence and different types of turbulence models available today. Reynolds Averaged Navier-Stokes (RANS) models are very important turbulence models for engineers in everyday work. The models are robust, and the turnaround time for the simulations is short. However, the RANS models give only the mean solution of a problem since the

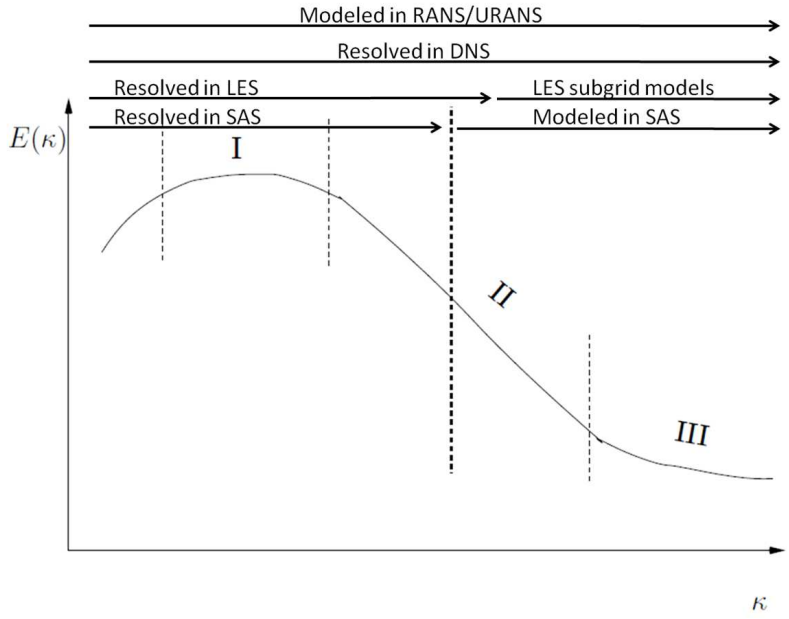

Figure 1.3: The turbulent spectrum, Wilcox (2004)

effects of the fluctuations are modeled, which is not always very useful in the design of practical systems. Further, RANS simulations cannot address the unsteadiness and instabilities obtained for a reacting flow where the flow-flame interacts at different scales. The other extreme is to use Direct Numerical Simulation (DNS), where all the scales are resolved and the flow equations are solved without any modeling assumptions. However, DNS is extremely expensive in terms of the number of grid cells that must be resolved for all the scales of the flow and will not be possible to use in the industry in the near future for the kind of applications considered here. Large Eddy Simulation (LES) resolves large-scale turbulent mixing and models small scales of the flow. The LES simulation can give a good prediction of the flame front dynamics, which is of great help for NO_x predictions. The grid resolution in LES simulations specifies the range of scales that are resolved; large numbers of grid cells are thus still needed for LES simulations compared to RANS models. Between the RANS models and the LES model, we have the hybrid RANS/LES models. These models switch to LES mode in unsteady flow if the resolution of the grid is satisfied and to an unsteady RANS mode close to the walls. Examples of the hybrid RANS-LES models are the Scale Adaptive Simulation (SAS) and the Detached Eddy Simulation (DES) models. The SAS approach represents a new class of URANS models. Different from the RANS formulations, the SAS model adjusts the turbulence length scale to the local flow. As a

measure of the local flow length scale, a boundary layer length scale introduced by von Karman is generalized for arbitrary 3D flows.

The most common way to study turbulent reacting flows is to use turbulence-combustion interaction models together with well-known turbulence models. This has been done for RANS turbulence models before, and many combustion models have been proposed. A fast chemistry assumption is often made for turbulent reacting flow. This means that turbulent motions control the reaction rate and hence simplify the description of the reacting flow to that of a mixing problem. The eddy-breakup model (Spalding (1971, 1976)) and the Eddy Dissipation Model (EDM), based on the work by Magnussen & Hjertager (1976), are examples of such models. The EDM is well known and often used in industry. In the EDM model, the chemical reaction rate is governed by the turbulence mixing rate, ϵ/k.

More elaborate models also take into account finite rate chemistry, for example the Eddy Dissipation Concept (EDC) by Gran & Magnussen (1996), PDF methods (Pope (1985)), flamelet models (Peters (1986)) and the Partially Stirred Reactor (Golovitchev *et al.* (2000)). The EDC model is an extension of the EDM model that includes detailed chemical mechanisms in turbulent reacting flows. It assumes that the reaction occurs in small turbulent structures, called the fine scales. These small scale structures can be captured as a part of the cell, where Kolmogorov-sized eddies containing combustion species are situated so close together that mixing on the molecular level takes place. The EDC model evaluates the volume of each cell, where mixing on a molecular scale occurs, and treats this part of the cell as a Perfectly Stirred Reactor (PSR).

The increase in computer power in recent years has made the reacting flow simulations feasible using LES, which resolves some of the unsteady structures and flow-flame interactions, and the uncertainty of the combustion modelling is then narrowed to the smallest scales of the flow. However, some procedure must be proposed to formally account for the unresolved fluctuations of species concentrations and temperature, to account for the LES spatial averaging (filtering) procedure. The thickness of the flame front is less than the typical LES grid resolution, which indicates that the whole reaction zone is filtered out and cannot be resolved. The modelling challenge raised by Large Eddy Simulation (LES) of turbulent flames has been the subject of numerous studies (Boudier *et al.* (2008); Pitsch (2006); Fiorina *et al.* (2010); Subramanian *et al.* (2010); Janicka & Sadiki (2005); Cavallo-Marincola *et al.* (2013); Duwig *et al.* (2011); Bulat *et al.* (2013); Abou-Taouk *et al.* (2014); Fureby (2008, 2010); Selle *et al.* (2004); Kuenne *et al.* (2011)).

1.3 The SGT-100 and the SGT-750 Industrial Gas Turbines

Prototypes of the burners used in the SGT-100 (Figure 1.4) and SGT-750 (Figure 1.5) industrial gas turbines were used in the present work as test cases for the turbulent combustion simulations. Both burners are premixed/partially premixed DLE burners and were supplied by Siemens Industrial Turbomachinery in Sweden and the UK. A testing and measurement campaign for the SGT-100 burner was previously carried out at the DLR Institute of Combustion Technology, Stuttgart, Germany, for various operating pressure conditions (Stopper *et al.* (2010, 2013)). A downscaled SGT-750 test burner was studied at Lund University, Sweden, by Sigfrid *et al.* (2011*a*,*b*, 2012, 2013*a*,*b*, 2014); Whiddon (2014) for various operating conditions and atmospheric pressures.

The SGT-100 engine has a power output ranging from 4.35 to 5.7 MW and the burner consists of a main burner, pilot burner, radial swirler and double skinned can combustor. Fuel (gas) is injected from two different locations. There are 12 main injection holes at the entrance of the swirler slot and two gas injection holes on the side wall of each swirler vane. Pilot (gas) is injected into the groove between the pilot face and main burner. The SGT-750 engine has a power output

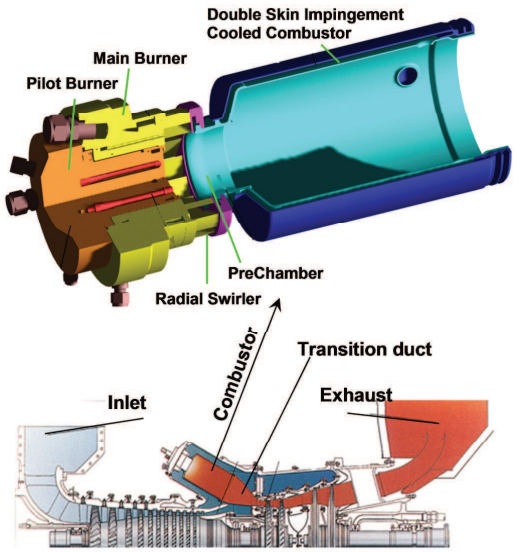

Figure 1.4: SGT-100 industrial gas turbine combustor (top) with a cross-sectional view of the gas turbine showing the location of the combustor, Abou-Taouk *et al.* (2013)

of 36 MW, and the burner consists of a complex arrangement of fuel and air premix ducts and swirler vanes, involving a main premixed flame (MAIN), a partially premixed pilot flame (PILOT) and a confined rich premixed lean flame (RPL), shown in Figure 1.4. The air and fuel are premixed before the combustion process takes place. The RPL flame burns at rich conditions in a pre-combustion chamber, creating hot gases with high amounts of radicals. This hot gas is then mixed downstream of the RPL with premixed fuel/air from the MAIN and PILOT systems, which augments the overall flame in the tube.

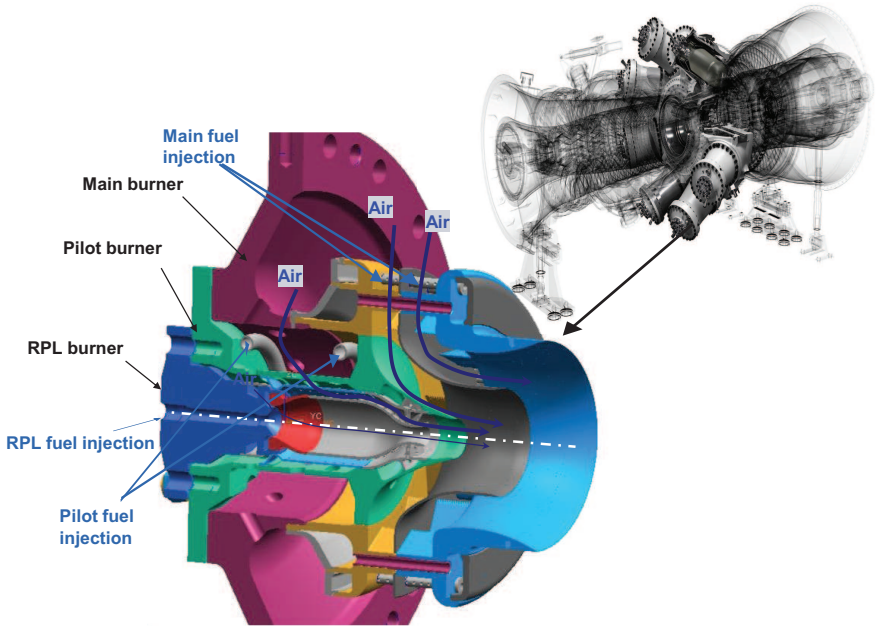

Figure 1.5: SGT-750 industrial gas turbine combustor (left) with a view of the gas turbine (right) showing the location of the combustor; pictures taken from Persson (2012) and SIT (2014)

1.4 Objectives of the Thesis and Achievements

The main objective of the thesis was to develop a methodology for optimizing global schemes in order to apply it for turbulent combustion studies. The secondary objective was to validate the optimized global schemes in premixed and partially premixed combustion by simulating prototypes of the SGT-100 and SGT-750 industrial test burners studied experimentally at the DLR Institute of Combustion Technology, Stuttgart, Germany (SGT-100), and the Departments of Energy Sciences and Combustion Physics in Lund University (SGT-750), Sweden. The third objective was to investigate the CFD modeling in the context of geometry set-up, boundary conditions, mesh type and size, and turbulence modeling with respect to industry applications. The main achievements of this thesis are listed below:

Development of a methodology for optimizing global schemes in order to apply it for numerical studies. Different tools have been investigated, e.g. CANTERA, CHEMKIN®, and an in-house code in the context of PSRs was developed. An optimization strategy was developed using modeFRONTIER® as the optimization software coupled to the CHEMKIN® software. Different models have been investigated and used in the work, such as PSRs, 1D propagating flames and homogenous reactors.

Optimization of several global schemes for methane-air and syngas mixtures using the PSR model and the 1D propagating flame model. The global schemes reproduce the emissions and temperatures well compared to the detailed reaction mechanisms.

Validation and evaluation of optimized global schemes in turbulent reaction flow simulation using a prototype of the SGT-100 burner and the downscaled SGT-750 test burner, and the test case of Sandia Flame D. Both RANS and hybrid URANS/LES models were investigated using different operation conditions.

Optimization of a two-step global scheme for simulating the selective non-catalytic reduction $DeNO_x$ process using the homogenous reactor in the CHEMKIN® software. The global scheme is obtained from an automated optimization of the chemical rate parameters and reproduces most of the expected NO_x conversion trends.

CFD modeling strategy in the context of different geometry features, mesh type and size, and investigation of different flow and combustion models. The prototype of the SGT-100 and the downscaled SGT-750 test burners are modelled with upstream cavities, swirling vanes and cooling slots. The mesh consists completely of hexahedral cells, and the mesh size is dependent on the turbulence model used.

LES modeling strategy, which implies a new approach based on optimized chemistry for LES of gas turbine partially premixed combustion. The method accounts for the effects of LES filtering (for a given filter size) on chemistry by simultaneously optimizing, from reference detailed chemistry, the Arrhenius coefficients and the mass/thermal diffusion coefficients of a limited number of species. The new sub-grid scale modeling approach is applied with LES for the SGT-100 industrial gas turbine burner.

Chapter 2

Gas Turbine

GAS turbines are generally divided into two groups, industrial gas turbines and aircraft propulsion gas turbines. The design of a gas turbine for propulsion needs to take into account effects of forward speed and altitude, take-off, climb, cruise and landing, power/weight ratio and different weather conditions, Saravanamuttoo *et al.* (2001). The most important requirements for an industrial gas turbine are long life, where there are usually 100000 hours between major overhaul, being able to operate over a wide load and speed range, being robust in installation, burning different fuels and, finally, simplicity in maintenance. The size and weight for an industrial gas turbine are not as critical as for aircraft gas turbines. A modern industrial gas turbine can reach an electrical efficiency in the order of 40% and NO_X emissions below 15 ppmV (corrected to 15 $\%$ O_2 dry), Siemens (2014).

Gas turbines basically involve three main sections, see Saravanamuttoo *et al.* (2001); Japikse & Baines (1997):

- **The compressor**, which draws air into the engine, adds energy to the air and pressurizes it.
- **The combustion system**, in which fuel is injected into the combustion chambers, where it mixes with the air. The combustion produces a high temperature mixture due to the release of chemical energy in the fuel, and a high pressure gas stream that enters and expands through the turbine section.
- **The turbine**, in which hot combustion gas expands through the turbine and spins the rotating blades. Depending on the purpose of the gas turbine, the shaft can be connected to different arrangements, e.g. to spin a generator to produce electricity, or to drive propellers on ships or propellers on aircraft (turboprop). For turbojet engines, the turbine only drives the compressor and the re-

maining pressure and energy of the gas stream are used to create a high speed jet.

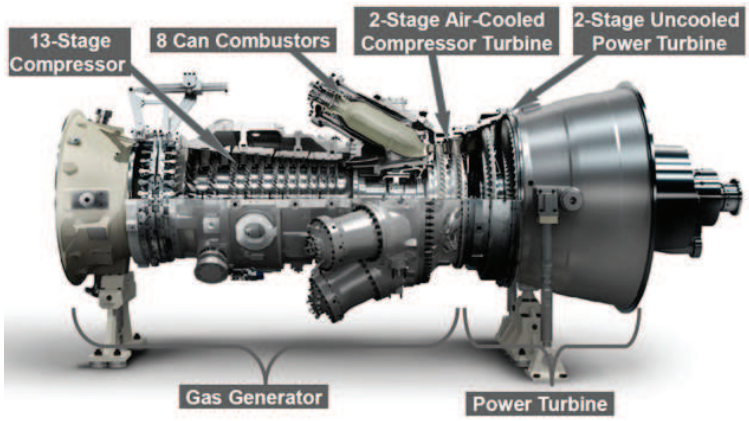

Figure 2.1: SGT-750 industrial gas turbine

Gas turbines can also have a single shaft, a twin shaft or even a triple shaft arrangement (Saravanamuttoo *et al.* (2001), Japikse & Baines (1997), Moustapha & Zelesky (2003), Walsh & Fletcher (2004)). The industrial gas turbines are of two types: (1) heavy frame engines and (2) aero-derivative engines. Heavy frame engines are characterized by lower pressure ratios (typically below 20) and tend to be physically large. Aero-derivative engines are derived from aircraft gas turbines and operate at very high compression ratios (typically in excess of 30). Aero-derivative engines tend to be very compact and are useful where smaller power outputs are needed.

2.1 General Combustion Systems

The design of a gas turbine combustor system is a complex process since it involves turbulent flow, complicated chemistry and/or two-phase flows. Also, depending on the flame arrangement, the flame can reach a maximum temperature of 2200 K - 2400 K, hence requiring a working cooling arrangement. The high temperature can also imply large damage risk for upstream components since the flame for certain conditions can propagate in the upstream direction. One key to a gas turbine's fuel-to-power efficiency is the temperature at which it operates or, more specifically, the turbine inlet temperature. Higher temperatures generally mean higher efficiencies, which in turn can lead to more economical operation. For the combustor, this implies the need for high

combustion efficiency ($> 99\%$) and low pressure loss ($1\% - 5\%$), Saravanamuttoo *et al.* (2001). The most common fuels for gas turbines are natural gas and liquid petroleum. Stationary industrial gas turbines normally operate using natural gas. However, the development of combustor technology is currently following the general trend towards fuel flexibility and increased use of bio fuels. Today's requirement and demand for low emissions imply that the development for low-emission combustion systems is going towards the direction of lean mixtures, e.g. a mixture with an excess of air compared to the amount of available fuel.

The purpose of the combustor is to burn the air supplied from the compressor with the fuel mixture in a continuous process and hence increase the mixture temperature before it expands in the turbine. After ignition of the mixture, the flame must be self-sustaining. Depending on the necessary residence time, weight and volume, the combustor arrangements can be widely different. The combustor can be of the type can (tubular), tubo-annular (cannular) or annular arrangement, Saravanamuttoo *et al.* (2001).

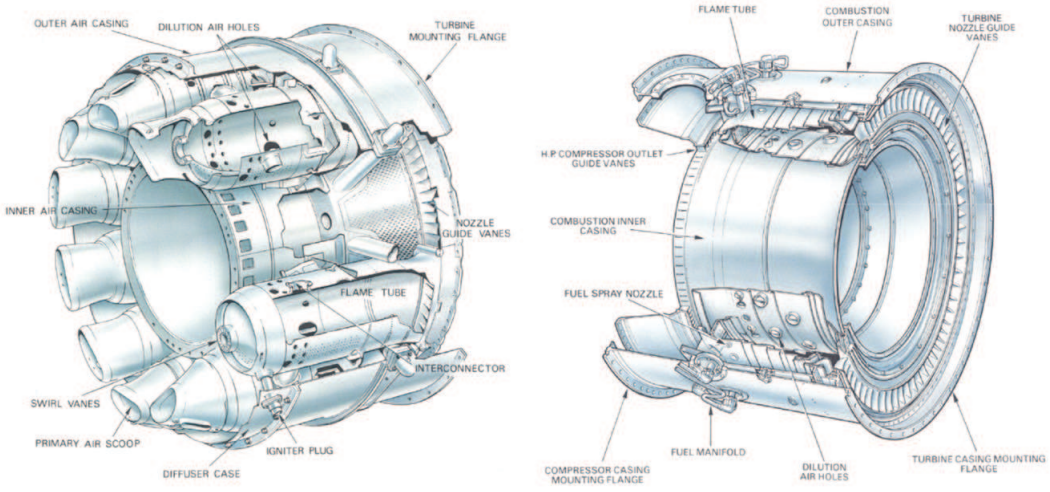

Figure 2.2: Left: tubo-annular (cannular) combustor system, right: annular combustor system, Saravanamuttoo *et al.* (2001)

The most common arrangement for industrial gas turbines is a cannular system; see Figure 2.2, where a number of flame tubes are fitted inside a common casing. This arrangement is easy to test experimentally. The most important factors that the combustor must fulfill are to deliver an even temperature distribution in front of the turbine blades, to minimize pollutions such as NO_X, CO and UHC, and to provide a stable flame arrangement in a stream of air moving at high velocity (up to 40 m/s - 70 m/s).

2.2 Combustor Zones

The burners operate in different modes depending on the required power output. The combustion chamber is often divided into different zones, Figure 2.3. First, there is a primary zone where combustion starts and the equivalence ratio is rather high. Very often the flame is stabilized here by bluff body stabilization or by a swirling flow arrangement. In the second zone, the local equivalence ratio is decreased through an increase in supplied air. The third and last combustion zone is introduced downstream in the burner before the exit. The aim of this zone is to obtain the target air temperature at exit by a dilution of excess air.

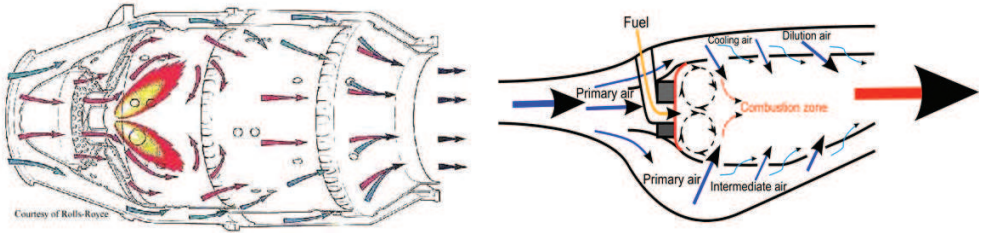

Figure 2.3: Different combustion zones in a combustor

2.3 Environmental Combustion Considerations

Regulatory requirements for limiting the emissions of pollutants and global warming imply an increasing need for optimizing energy conversion processes. The ozone balance in the atmosphere can certainly be changed by an increased amount of oxides of nitrogen. Both nitric oxide (NO) and nitrogen dioxide (NO_2), where they together are referred as NO_x, are present in the atmosphere. NO_x also reacts to form smog and acid rain. Many researchers and agencies have reported a steady increase of NO_x and N_2O since the middle of the nineteenth century. One of the reasons behind this increase is the steady increase of combustion of hydrocarbon fuels. The major products from combustion are CO_2 and H_2O. Today CO_2 is a substantial source in the atmosphere balance, and concerns for a global warming effect are also being raised.

NO_x production is divided into four formation routes according to Warnatz *et al.* (2006): the thermal route (Zeldovich NO), the prompt route, the N_2O route and the fuel-bound route. Thermal NO_x, which is the primary cause of the NO_x production in a gas turbine, has obtained

the name thermal due to the high activation energy in the reaction of the N_2 -oxidation (due to the triple bond in the N_2 molecule). Consequently, the N_2 molecule is sufficiently fast only at high temperatures (Warnatz *et al.* (2006)). From a combustion perspective, the highest flame temperature is obtained slightly to the fuel rich side. The flame temperature is indeed the most important factor that affects NO_x production. The obvious way to lower the flame temperature and consequently the NO_x production is to operate well away from the stoichiometric condition. Therefore, the combustion mixtures should be fuel lean or fuel rich, although this results in increasing production of CO emissions, see Figure 2.4.

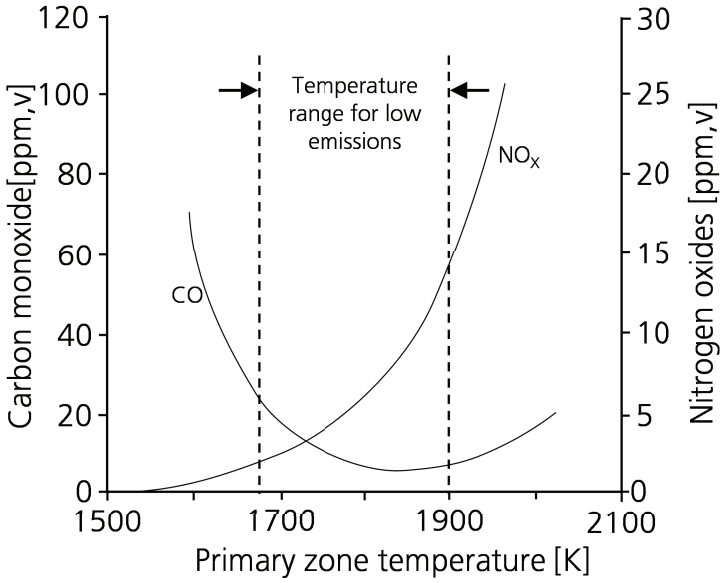

Figure 2.4: Primary zone temperature influence on emissions for typical gas turbine combustion, Lefebvre (1999)

There exist different methods to decrease NO_x production. Staged combustion is a method that operates at both fuel lean and fuel rich conditions. The idea is to run fuel rich at the first stage to minimize the amount of NO_x, HCN and NH_3. In the second stage, the products are rapidly mixed with air to obtain a fuel lean condition. The benefit of this method is that the N_2 produced in the first stage is not converted to thermal NO_x, due to the steadily decreased combustion temperature, Warnatz *et al.* (2006). Even a third stage can be used to introduce an additional amount of fuel to decrease NO concentrations, Warnatz *et al.* (2006). A different method is to introduce water injection or dilute the gas with nitrogen, whose additional heat capacity de-

creases the flame temperature and consequently reduces NO_x concentrations (Figure 2.4). Further improvements of NO_x emissions have been made using lean premixed combustion, numerically and experimentally studied by several researchers, such as Irannezhad (2012); Cheng *et al.* (2009); Johnson *et al.* (2005); Abou-Taouk *et al.* (2013). The lean premixed combustion lowers the flame temperature, and NO_x emissions therefore decrease. Important issues to consider regarding lean premixed combustion are to have the mixture well mixed, to be aware of the technical challenges caused by the lean blow off limit and flame pressure oscillations. Moving towards leaner equivalence ratios implies lower flame speed and consequently lower reaction rates. This means that the flame sensitivity to changes in temperature and concentrations increases, such as occurs when there exist pressure oscillations. All the methods mentioned above are regarded as primary measures. However, these modifications are often not sufficient, so post-combustion processes are necessary. Well-known methods are to use a catalytic converter for vehicles. For stationary industrial gas turbines, a catalyst is often used to convert NO with the addition of ammonia to N_2 and H_2O. This method is called selective catalytic reduction. However, it is also possible to use selective non-catalytic reduction methods, as are used in the present work and described by Farcy *et al.* (2014).

Chapter 3

Combustion

THE combustion process requires some understanding of fundamental concepts and definitions, which shall be described in this section. Turns (1996) defines a combustion process as "Combustion transforms energy stored in chemical bonds to heat that can be utilized in a variety of ways." The combustion process mainly consists of exothermic reactions, oxidation processes, high temperatures and radiation. Combustion in a gaseous medium is classified depending on how fuel and oxidizer are mixed and burned. Typically, the combustion modes are classed as non-premixed, partially premixed and premixed combustion. If the fuel and oxidizer are mixed prior to the combustion, the type is called premixed, while if the mixing occurs simultaneously it is called non-premixed. Each of these types is further divided based on whether the flow is laminar or turbulent. The initiation of the burning process is called ignition. Once the mixture is ignited, the burning process continues, provided that the mixture is within the so-called flammability limits.

3.1 Chemical Fundamentals

Combustion involves release of energy from chemical reactions. A chemical reaction is the exchange and/or rearrangement of atoms between colliding molecules. The atoms are conserved, while the molecules are not conserved. Theoretically, it is possible to generally describe a hydrocarbon fuel by a complete reaction formulated by:

$$\mathrm{C_mH_n} + (\mathrm{m} + \mathrm{n}/4)\mathrm{O_2} = \mathrm{mCO_2} + (\mathrm{n}/2)\mathrm{H_2O} \tag{3.1}$$

This reaction can be used to calculate how much energy is released when the fuel and oxygen react into CO_2 and H_2O. If the reaction is complete, e.g. all the fuel and oxidizer consume each other completely,

forming only CO_2 and H_2O, then this condition is called a reaction with a stoichiometric condition. If there exists an excess of fuel over the oxygen, the mixture is called fuel rich, and if there is an excess of oxygen, it is called fuel lean. The equivalence ratio (ϕ) of a mixture is defined as:

$$\phi = \frac{\mathrm{Y_{fuel}/Y_{oxidizer}}}{(\mathrm{Y_{fuel}/Y_{oxidizer}})_{\mathrm{stoichiometric}}} \tag{3.2}$$

where Y_i is the mass fraction of the fuel and oxidizer.

The mass fraction, Y_i, is the ratio of the mass m_i of the species i and the total mass $m = \sum(m_i)$ of the mixture ($Y_i = m_i/m$). The mole fraction X_i of species i denotes the ratio of the mole number, n_i of species i to the total mole number, $n = \sum(n_i)$, of the mixture ($X_i = n_i/n$). The molar weight, M_i, of species i is the mass of 1 mole of this species. The following relation holds:

$$\mathrm{Y_i = X_i M_i / \sum_{j=1,S} (M_j X_j)} \tag{3.3}$$

$$\mathrm{X_i = (Y_i/M_i) / \sum_{j=1,S} (Y_j/M_j)} \tag{3.4}$$

Practically, the complete reaction is almost never obtained and the final composition includes species that are not defined from the stoichiometric reaction. Therefore, chemical equilibrium considerations are useful where the temperature is rather constant and most radical reactions are completed (downstream of the flame). In the reaction zone, where high temperature gradients and a large number of radicals (highly reactive species) are located, the chemical equilibrium approach is often not applicable. The second law of thermodynamics provides criteria for the position of equilibrium and, in the case of a system at constant temperature and pressure, this may be represented by a minimum in the free enthalpy (Gibbs free energy), G=H-TS.

3.2 Premixed Flame Characteristics

The structure of a typical premixed flame usually consists of three separate zones, a preheat zone, a reaction zone (inner layer) and a post-flame zone (product zone), shown in Figure 3.1. In the preheat zone, only a small amount of heat is produced by chemical reactions; instead, the gas mixture is heated by diffusion from the reaction zone. The reaction zone (or often called the flame front) normally starts at the inflexion point in the temperature profile. In the reaction zone, a high temperature increase occurs due to a fast release of energy in a narrow

region. Due to the high temperature, the concentration of radicals is large and the hydrocarbon fuel degrades to short fuel fragments. This layer is also responsible for keeping the reactions ongoing. The last layer, namely the postflame zone, is responsible for the recombination reactions. The equilibrium concentrations will be reached in this zone. The concentrations of recombining radicals are low, and therefore the temperature will not change significantly. Mainly H_2O and CO_2 are formed for a stoichiometric mixture, while O_2 will be found for a lean mixture. For a fuel rich mixture, CO and H_2 will be found since the hydrocarbon fuel will degrade due to the high reaction zone temperature.

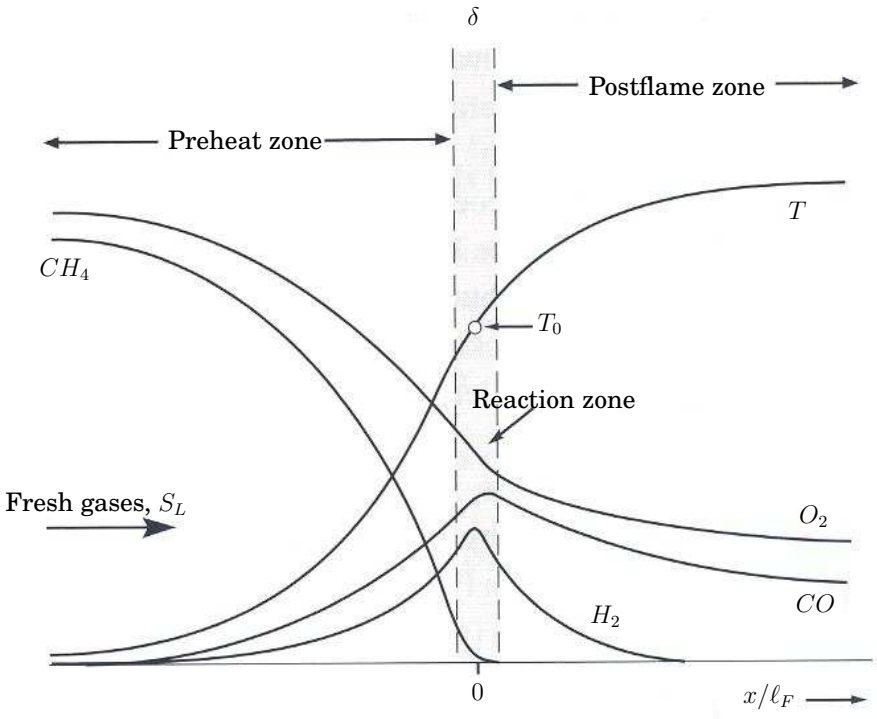

Figure 3.1: Structure of a premixed methane flame, taken from the thesis of Irannezhad (2012)

3.3 Perfectly Stirred Reactor Model

The PSR is an ideal constant pressure reactor in which perfect mixing is assumed inside the control volume, due to high diffusion rates or forced turbulent mixing. This means that the rate of conversion of reactants to products is controlled by chemical reaction rates and not

by mixing processes. In addition to the fast mixing, the modeling of PSR requires that the flow through the reactor must be characterized by a residence time, τ_{res}, which is defined according to: $\tau_{res} = V\rho/\dot{m}$, where V is the reactor volume, ρ is the density inside the reactor and $\dot{m}$ is the mass flow through the reactor. The PSR reactor is assumed to operate at steady state, so no time dependence is included in the equations. Figure 3.2 illustrates the conceptual representation of a PSR reactor.

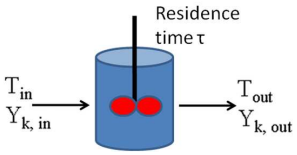

Figure 3.2: Schematic picture showing the PSR model

Reactants are introduced through the inlet with a given species composition and temperature. The reactor pressure is specified, so that the conservation equations determine the volume outflow. All properties are uniform inside the reactor (mass fractions, temperature and pressure). The gas leaving the reactor has the composition and temperature of the reactor, $T_{out} = T$ and $Y_{i,out} = Y_i$. There is no heat loss, which means that the reactor is adiabatic. Figure 3.3 shows an example of temperature prediction using different reaction mechanisms in a PSR reactor.

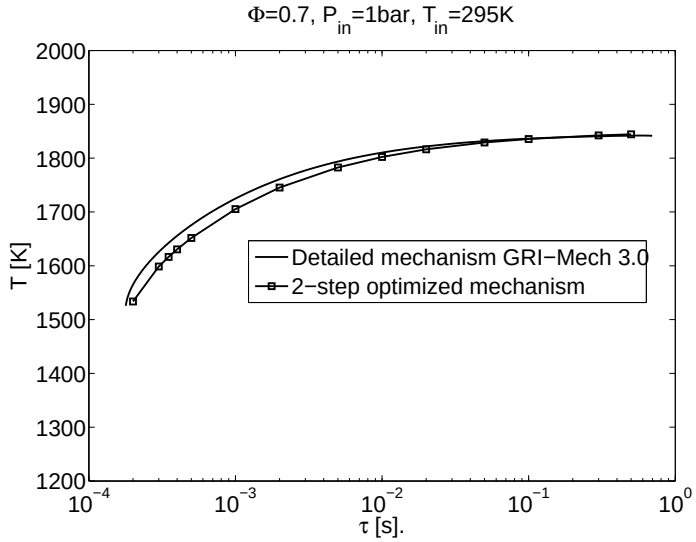

Figure 3.3: Comparison of temperature versus residence time in a PSR reactor using two different schemes, Abou-Taouk & Eriksson (2011)

3.4 1D Premixed Flames

One-dimensional (1D) propagating laminar flame into a premixed gas is a basic problem in combustion, both for theory and for numerical methods. The interest in numerically solving this problem comes mainly from the detailed comparison that can be made between experiments, theory and computations. The 1D laminar propagating flame can also be used to validate chemical models, which was done in the present work. Finally, laminar flames are often used as the elementary building blocks of turbulent flames in many flamelet theories, Peters (1986); Oijen *et al.* (2001); Nguyen *et al.* (2010). Considering a tube with fresh gases to the left and burned gases to the right (1-D), a propagating laminar premixed flame would be somewhere in between, moving with a constant speed. If the frame of reference is moving with the propagating flame, the solution to the problem becomes time independent. Figure 3.4 shows results in the form of species profiles using the 1D premixed flame model. In general, the predictions made by the optimized global mechanism are good when compared to the detailed scheme. More information on the results and how the optimization is performed can be found in Abou-Taouk *et al.* (2013).

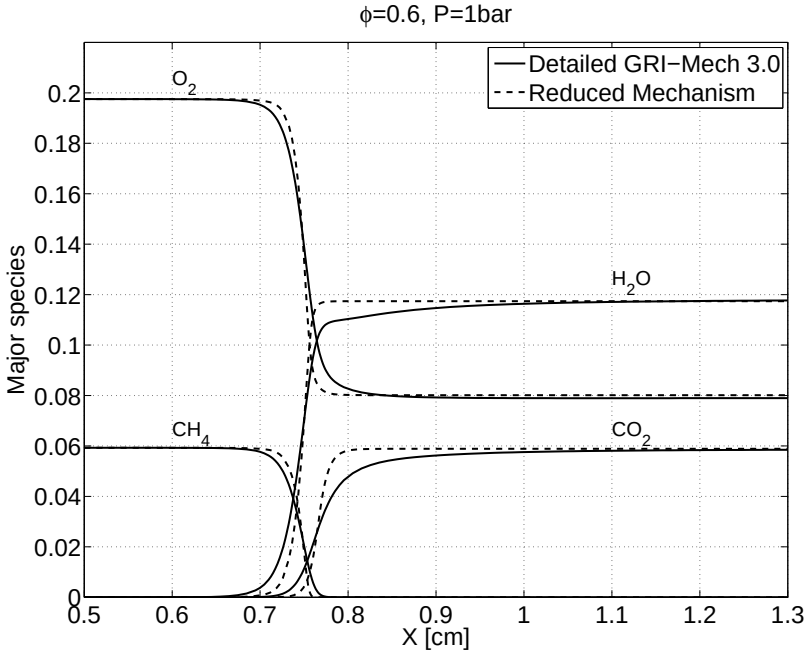

Figure 3.4: Species profiles *vs* position for $\phi = 0.6$. Line: reference flame (GRI-Mech 3.0). Dashed line: optimized global scheme, Abou-Taouk *et al.* (2013)

3.4.1 Conservation Equations, Laminar Flame Speed, S_L, and Adiabatic Flame Temperature, T_{adi}

The conservation equations for the laminar 1D premixed flames can been found in many books on turbulent combustion, e.g. Poinsot & Veynante (2001). The conservation of mass and species and the energy equations describe a wave propagating from the burnt to the fresh gas at a speed that reaches a constant value of the laminar flame speed, S_L, when transients are ignored. This velocity has a certain value for a given fuel/oxidant mixture at a specific temperature, pressure and equivalence ratio.

In a 1D propagating laminar flame, a combustion wave will propagate either as a deflagration or a detonation wave. In a deflagration wave, the propagation is at subsonic speed (laminar flame speed in the order of 0.5 m/s - 1 m/s for most hydrocarbon fuels), see Figure 3.5, and the pressure is almost constant over the reaction zone. A detonation wave propagates at supersonic speed (laminar flame speed in the order of 1000 m/s for most hydrocarbon fuels) and a large pressure difference is obtained. Only deflagration is considered here, and the velocity of the deflagration is called laminar flame speed, S_L (also called burning velocity or normal combustion velocity). For a steady-state 1D laminar flame calculation, where the flame remains in a fixed position, the inlet velocity needs to match the laminar flame speed. In CHEMKIN®, the flame is usually fixed at the x-position equal to the mid point of the domain. The problem to solve is an eigenvalue problem: the unknowns are the profiles of temperature, species and velocity, as well as the S_L, which is the eigenvalue of the problem, Karman & Penner (1954).

Several laminar flame theories have been proposed in the past, the objective of each being the determination of fundamental flame attributes. Classification of these theories has been carefully described by Kuo (2005); Glassman (1996); Warnatz *et al.* (2006). Determination of the laminar flame speed from theoretical analyses falls into three theories: the thermal theories, the diffusion theories and the comprehensive theories. In the theory of Mallard & Chatelier (1883) (which is a thermal theory) one can observe that the laminar flame speed has a strong dependence on the temperature and therefore also a strong dependence on the equivalence ratio. Mallard & Chatelier (1883) proposed that the flame propagation is due to the propagation of heat back through layers of gas. Improvements were made to the thermal theories by Zeldovich *et al.* (1985) and Semenov (1942), which also included the diffusion of molecules (not radicals or atoms) as well as heat. Their conclusions were that the controlling mechanism for the reaction zone

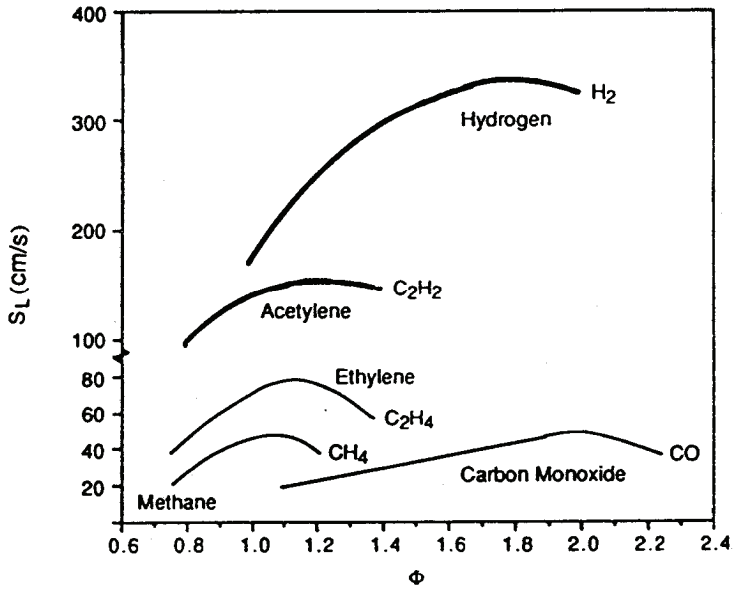

Figure 3.5: Laminar flame speed vs. the equivalence ratio of some species, $T = 295K$**,** $P = 1atm$

was due to the heat and diffusion of molecules. Tanford & Pease (1947) proposed a diffusion theory based on the idea that it is the diffusion of radicals that is the most important controlling mechanism in the reaction zone, not the temperature gradient, as required by the thermal theories.

The theory of Mallard & Chatelier (1883) gives the laminar flame speed and the reaction zone thickness according to equations 3.5, in which S_L, δ_L, D and $\bar{W}$ are the laminar flame speed, flame thickness, heat diffusivity and average reaction rate, respectively.

$$s_L \propto \sqrt{D\overline{W}} \qquad \delta_L \propto \frac{D}{s_L} \tag{3.5}$$

The adiabatic flame temperature, T_{adi}, is the theoretical flame temperature obtained for a given fuel/oxidant mixture at a specific pressure without any heat loss. Due to energy losses in a burner, such as radiation, cooling and partially premixed systems, the adiabatic flame temperature is often not attained. Assuming a stoichiometric mixture, a preliminary hand calculation can be made by assuming a single step reaction in the combustion process, according to reaction 3.1. However, additional reactions, especially dissociation of products such as CO_2 and H_2O, take place at high temperatures. These reactions are endothermic and decrease temperature levels. Consequently, the hand calculation can be far from reality since no dissociation is considered.

3.4.2 Convergence of the 1D Flame Code

Even though the 1D propagating laminar flame is a basic problem, the process of obtaining a converged solution is always a challenge due to the non-linear problem. If initial solutions for T and for all species Y_i are too far from the solution, it is difficult to obtain convergence. Furthermore, when new reduced chemical schemes with new constants are introduced, convergence problems for the 1D flame code may be encountered due to an improper modeling of the chemistry. Consequently, it is important to carefully choose the maximum and minimum bounds for the Arrhenius parameters during the optimization process. Unfortunately, this is an iterative process and depends largely on the experience of the user. Finally, since the computation is pushed outside the flammability limits (especially in the chosen optimization process), it is important to have continuation techniques in the iterative solution process.

The chosen commercial software, CHEMKIN®, uses the continuation technique, which is included for the 1D propagating laminar flame. The software also uses an adaptive grid, and the largest grid size was set to 0.1 mm while the smallest one depends on the chemical scheme and the transport properties. A coarser mesh is used in the diffusion/convection zones, while more refined grids are used in the reaction/diffusion zones. The number of adaptive grid points, the maximum number of grid points allowed, and starting and ending position of the domain must also be set in the 1D flame code. Finally, it is important to optimize parameters such as settings of the absolute and the relative tolerances, the maximum gradient and curvature allowed between grid points and use of a specified temperature profile in the code in order to decrease the simulation time and obtain convergence. From a numerical point of view, decreasing the reaction exponents for the global mechanisms (which are used in the present work) causes increased stiffness, Poinsot & Veynante (2001).

3.4.3 Transport Properties

The mass diffusion coefficients and the heat diffusion coefficients have important roles when computing flames. Assuming equal diffusivities for all species has a significant effect on flame speed, especially towards richer equivalence ratio conditions. Very often, the Lewis numbers ($Le_k = D_{th}/D_k$) are set to unity. This assumption is used in many theoretical approaches and is true for most species except for very light molecules, such as H_2, visible in Figure 3.6, which have Lewis numbers of the order of 0.3, Poinsot & Veynante (2001); Pitsch (2012). Very often,

the commercial softwares have different options for how the transport properties should be calculated. In CHEMKIN®, one can use mixture-average properties or fully multi component transport properties. The software also provides the option to use one's own user routines for calculating the transport properties for the mixture. The diffusion coefficients calculated by common packages may exhibit larger error margins than are generally expected, Warnatz *et al.* (2006).

CH_4	O_2	H_2O	CO_2	H	O	OH	HO_2
0.97	1.11	0.83	1.39	0.18	0.70	0.73	1.10

H_2	CO	H_2O_2	HCO	CH_2O	CH_3	CH_3O
0.3	1.10	1.12	1.27	1.28	1.00	1.30

Figure 3.6: Lewis numbers of some reacting species occurring in methane-air flames, Pitsch (2012)

Chapter 4

Turbulent Combustion Modeling

NUMERICAL techniques for combustion are important tools for both engineers and research specialists designing new combustor devices. However, combustion is a multi-disciplinary research topic and involves consideration to several different areas, see Figure 4.1. Combustion also involves a large range of chemical time and length scales. An example of this is that, in most practical combustion applications, fuel oxidation times are small, while the times required for CO oxidation to CO_2 are longer. Combustion usually involves a broad range of scales in space and time that need to be accurately resolved. The dynamic range of scales between chemical/molecular processes compared to the scales of a real combustor can reach several orders of magnitude.

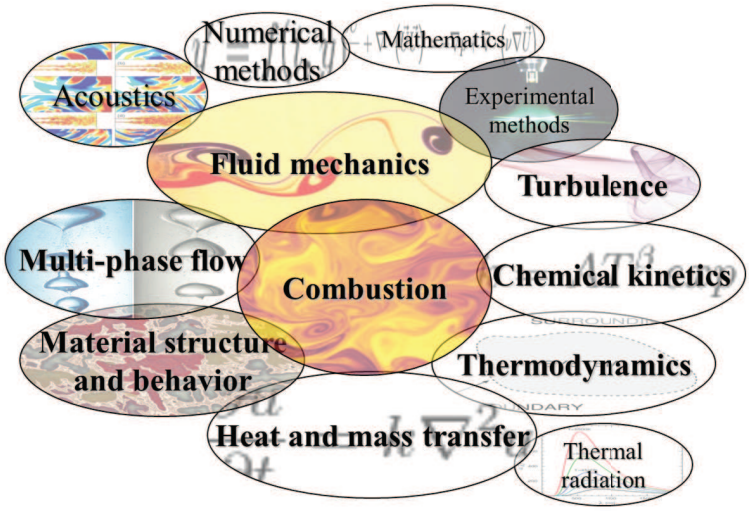

Figure 4.1: Combustion is a multi-disciplinary topic, picture taken from Gustafsson (2010)

4.1 Introduction

Solving a non-reacting compressible flow (aerodynamics) requires five equations: the continuity equation (solving for the density), the momentum equations (solving for the three velocities) and the energy equation (solving for pressure or enthalpy or temperature or energy). The unknown variables that are not solved for in the energy equation can be obtained from the equation of state. This implies that, for a non-reacting compressible flow, the number of degrees of freedom and the number of equations are five. For the reacting flow case (combustion), all these equations are still needed. In addition, the composition of the mixture (distribution of the mass fractions, Y_i) need to be solved for. The number of species is N and one additional transport equation is therefore required for each species. However, the conservation of the total mass must also be fulfilled and, consequently, the reacting flow case contains $5 + (N - 1)$ equations. The number of species is, indeed, one of the main contributions to the cost of the chemistry integration in a reactive flow simulation.

In turbulent combustion modeling, the interaction between chemistry and turbulence also needs to be modeled. Turbulence can enhance the chemical reaction or, in extreme cases, quench the flame because of the strong flow accelerations through the flame front induced by heat release and because of the large changes in viscosity related to temperature changes, Poinsot & Veynante (2005); Peters (2000). In the past, the industrial standard for turbulent reacting flow analysis consisted of RANS calculations that use two-equation models for turbulence and very simplified chemistry for heat release. Hence, the unsteady motions that govern mixing were difficult to capture by this approach. The turbulence-combustion interaction was often modeled by Eddy Break Up models (EBU) or Eddy Dissipation Models (EDM) (Spalding (1971)). Today, the state of the art in numerical combustion modeling is to use LES methods to numerically resolve the large scale turbulence and to model the subgrid turbulence and chemistry. This allows a more accurate representation of turbulence, kinetics and the turbulence-combustion interaction that is not attainable with RANS calculations.

Growing computer resources have allowed for more elaborate detailed chemistry models to be included in the form of tabulation methods and different optimization approaches, such as the Eddy Dissipation Concept (EDC) by Gran & Magnussen (1996), PDF methods (Pope (1985)), flamelet models (Peters (1986)) and the Partially Stirred Reactor model by Golovitchev *et al.* (2000). The state of the art models also imply that calculation of minor species needed for accurate prediction

of NO_x and CO, lean blowout, and flashbacks can be performed.

There are mainly three different parts to be considered when simulating a reacting flow; these are:

1. Describing the chemistry (kinetic modeling)
2. Closure of filtered terms (combustion modeling)
3. Turbulence modeling

These topics will be briefly reviewed and discussed in the following sections.

4.2 Modeling of Chemistry

The integration of detailed kinetics into turbulent flame simulations is today one of the most difficult challenges in the combustion community. Detailed reaction mechanisms for conventional and bio fuels are huge and contain hundreds of species and thousands of reactions. Chemistry reduction aims to lower the order of the system of differential conservation equations to be integrated by reducing the effective number of chemical species to be considered in the simulation. There are a number of strategies for chemistry reduction, such as automatically identifying the fast and slow time scales of the chemical system in order to decouple them, manifold generation and tabulated chemistry (consists of storing the chemical source terms in tables to avoid repeated calculations), automatically optimizing global and skeletal mechanisms using sensitivity analysis, reaction flow analysis or different reactor models.

4.2.1 Manifold Generation and Tabulated Chemistry Approaches

There are numerous variants of manifold generation and tabulated chemistry approaches; some require computations prior to the simulation for the conditions expected to be encountered, while others evaluate chemical terms during the simulation. Common to all tabulated chemistry techniques is the need for a well optimized algorithm for storing and searching data in the table in order to be efficient.

The manifold generation method attempts to project the complete reaction system onto a lower dimensional system by using different assumptions. According to this approach, Peters (1985) proposed identifying the fast time scales of the chemical system and making the assumption that the species are both at a quasi steady state (Warnatz

et al. (2006)) and equilibrium. Consequently, the system reduces to solving only for the slow evolving species. The Computational Singular Perturbation (CSP) method is a similar approach but is extended for the reactions with the assumption that partial equilibrium is valid for the reactions, Lam & Goussis (1994). What can be seen is that the partial equilibrium assumption provides satisfactory results only at high combustion temperatures. At lower temperatures, the reaction times are slower than the characteristic time of combustion, and the partial equilibrium condition is not consequently established (Warnatz *et al.* (2006)). A more mathematical approach to identifying low dimensional manifolds based on eigenvalue analysis of the species evolution was proposed by Maas & Pope (1992*b*). The fast and slow evolving species are also identified in this approach. As for the CSP methods, problems are encountered at low temperatures. Improvements for the low temperature region were proposed by Ren & Pope (2006).

The flamelet models for turbulent premixed flames are also different approaches. They are based on being able to describe the turbulent premixed flame as laminar premixed flamelets, PSRs, steady non-premixed flamelets, unsteady non-premixed flamelets or even partially premixed 2D flamelets. These approaches are generally applicable in the zone of large Damköhler numbers with turbulent scales larger than the flame thickness (Glassman (1996)). Examples of models belonging to this category are flamelet modeling based on a reaction progress variable or using level-set methods, and flamelet generated manifolds. See de Goey *et al.* (2003); Oijen & Goey (2000); Bray & Libby (1976); Bray & Moss (1977); Williams (1985) for more information about these models.

4.2.2 Skeletal Reaction Scheme

Several different reduced reaction mechanisms of hydrocarbon mixtures are described in the literature. The skeletal mechanisms usually contain hundreds of reactions and a few dozen species. The skeletal mechanisms are commonly developed by employing strategies such as sensitivity analysis of the reaction rate constants (identifies the rate-limiting steps), species bounding (Tianfeng & Chung (2007)), reaction flow analysis (determines the characteristic reaction paths) and/or computational singular perturbation techniques (Tianfeng & Chung (2008)). The focus in the present work has not been on the skeletal mechanisms; nevertheless, the benefits of the skeletal mechanisms are that they well capture the ignition sequences, the ignition delay time and NO_x compared to global schemes. However, due to the large num-

ber of species and reactions, the computation cost is typically high.

4.2.3 Global Reaction Scheme

Reviewing the literature in the context of optimization of global mechanisms, it seems that there are mainly three common strategies that are used: 0D reactor calculations (such as perfectly stirred reactors, homogenous reactors or plug flow reactors), 1D calculations simulating a freely propagating flame (such as 1D laminar premixed flames) and determining the limiting steps of the chemistry using quasi-steady state and/or partial equilibrium approximations. A focus on developing reliable global reaction mechanisms for combustion of hydrocarbons emerged during the 1980s, Jones & Lindstedt (1988); Westbrook & Dryer (1984).

Zero Dimensional Calculations: Meredith & Black (2006) reported an automated and efficient generation of global mechanisms that are valid over a broad range of operating conditions. In brief, they applied robust optimization techniques (sequential quadratic programming algorithm), along with a robust PSR model, to obtain several global schemes that provide the best possible match with detailed chemistry. The mathematical functionality of the various Arrhenius parameters is quite different, and what Meredith & Black (2006) found was that simultaneous optimization of these parameters proved to be extremely difficult due to their hugely different behavior. Nevertheless, they report very good results with three-/five -step global mechanisms for methane and JP8 combustion cases. Meredith & Black (2006) excluded combustion parameters such as laminar flame speed and flame species profiles in the optimization. Elliott *et al.* (2003) and his co-workers used a multi-objective genetic algorithm approach to develop global schemes for the combustion of hydrogen/ air mixtures. The multi-objective structure of the genetic algorithm employed allowed the incorporation of both PSR and laminar premixed flame data in the inversion process. Elliott *et al.* (2003) reported very good results for the species fully burned conditions in PSR calculations, and laminar flame speeds and species profiles in PREMIX simulations, over a wide range of operating conditions.

Freely Propagating Flame Calculations: Franzelli *et al.* (2010) derived a two-step global mechanism for kerosene combustion based on the freely propagating flame approach. They reported accurate predictions of laminar flame speed, adiabatic flame temperature, CO levels at equilibrium and autoignition delays for a wide range of equivalence ratios. The approach was based on the introduction of correction func-

tions, dependent on the local equivalence ratio, for the fuel oxidation (reaction 1) and the CO oxidation (reaction 2), to compensate and predict better results at rich combustion. The solution proposed is a tabulation of the reaction constants as proposed by other authors before, see Fernandez-Tarrazo *et al.* (2006); Boudier *et al.* (2008).

Determining the Limiting Reaction Steps: The results of the work of Westbrook & Dryer (1984) and Jones & Lindstedt (1988) allowed new one-step and two-step global mechanisms for hydrocarbons fuels to be derived, and these are still used today in the industry. In the single-step mechanism, the fuel and oxidizer react to CO_2 and H_2O. The weakness of the single step is that, by assuming that the reaction products are only CO_2 and H_2O, the total heat of the reaction is over-predicted. To account for this, a two-step model for hydrocarbons was suggested by Westbrook and Dryer. A four-step global reaction mechanism was also derived by Jones & Lindstedt (1988), which is also well known. This mechanism includes the H_2 species, and the benefits of this species are mainly obtained at the rich side, see also Abou-Taouk *et al.* (2014). Peters (1985) proposed a four-step global mechanism consisting of seven species for methane-air mixtures (starting from a detailed mechanism by Smooke (1991)). The four reaction rates are determined from limiting steps of the chemistry, using quasi steady state and partial equilibrium approximations.

Andersen *et al.* (2009) modified the two-step mechanism of Westbrook & Dryer (1984) and the four-step mechanism of Jones & Lindstedt (1988) in order to account for oxy-fuel conditions. The approach used was based on the backward rates being calculated by evaluating the forward rates divided by the equilibrium constant at a series of temperatures, and then fitting an Arrhenius expression to the results, to obtain an individual expression for the reverse reaction. The tests of the refined schemes were done using a plug flow reactor. The major species concentrations predicted by the modified mechanisms confirm that the modified schemes constitute an improvement for oxy-fuel conditions. Compared to the original schemes, the prediction of the CO fully burned conditions concentration has been improved, Andersen *et al.* (2009).

4.3 Modeling of Combustion

RANS and LES modeling of turbulent combustion differ in their modeling strategy. Development of RANS combustion models started around 40 years ago with the work of Spalding (1971). On the other hand, LES combustion modeling has only been performed for around 15 years.

Consequently, the combustion models differ between these strategies, and many of the RANS turbulent combustion models have been extended for the LES applications.

4.3.1 RANS Modeling

Several combustion models exist for RANS modeling: e.g. models based on turbulent flame speed correlations, the G-equation model, the Bray Moss Libby model, flame surface density models, PDF models, modeling of turbulent scalar transport terms, the EBU model, finite rate chemistry models based on global mechanism chemistry and the Arrhenius approach, and the EDM model. Only the latter two have been used in the present work. For more detail about the models, see books by Poinsot & Veynante (2001, 2005); Veynante & Vervisch (2002); Glassman (1996); Warnatz *et al.* (2006); Pitsch (2012); Peters & Kanury (2001).

4.3.2 LES Modeling

LES in reacting flow simulations resolves the larger scales and flow-flame interactions of the flow, and models the sub-grid scales, where the uncertainty of the combustion modelling is narrowed to the smallest scales of the flow. The thickness of the flame front is generally much smaller than a typical LES filter size, which indicates that the whole reaction zone is filtered out and cannot be resolved. Therefore combustion principally exists as a sub-grid phenomenon in LES and requires being modeled.

There are mainly two strategies in using LES in turbulent premixed combustion; either the approach is based on resolving the flame, such as thickened flame models (Colin *et al.* (2000)) and linear eddy models (Chakravarthy & Menon (2000)), or capturing the flame dynamics without resolving it (level set G-equation model (Peters & Kanury (2001)) and flame surface density approaches (Hawkes & Cant (2001)). The present combustion modeling used in the LES simulation is close to the thickened flame approach and consequently will be described in this section. The thickened flame approach is an attractive solution method to propagate a premixed flame on a given coarse LES mesh by artificially thickening the flame. The idea was proposed by Butler & O'Rourke (1977); O'Rourke & Bracco (1979) and follows theories of laminar premixed flames (Williams (1985)). Basically, the flame speed,

S_L, and the flame thickness, δ_L, may be expressed as:

$$s_L \propto \sqrt{D_{th} A} \qquad \delta_L \propto \frac{D_{th}}{s_L} \tag{4.1}$$

where D_{th} is the thermal diffusivity and A the pre-exponential factor. If the thermal diffusivity is increased by a factor F while the pre-exponential factor is decreased by F, the correct laminar flame speed is preserved. However, the mixing in the non-reacting zones will also be affected. Légier *et al.* (2000) proposed a dynamic thickened flame approach where the thickening factor, F, is active only in the flame. In addition, artificially thickening the flame implies that the interaction of the turbulence and flame (wrinkling) is modified (Colin *et al.* (2000); Angelberger *et al.* (1998)). Colin *et al.* (2000) proposed an efficiency factor to account for the sub-grid wrinkling.

4.4 Turbulent Flame Speed

Turbulence is an important factor to account for in designing a combustor burner. The mass consumption rate per unit area in a premixed laminar flame is simply $\rho_u S_L$, where ρ_u is the unburned gas mixture density. The main effect of turbulence on combustion is to increase the combustion rate and therefore also the increase in the chemical energy release rate and, hence, the power output for a given size of a combustor. At turbulent conditions, a similar consumption rate can be specified: $\rho_u S_T$, where S_T is the turbulent flame speed. Velocity, temperature, pressure, density and species concentrations will fluctuate in a turbulent flow. The characteristic time scales for these parameters will decide to what degree the mentioned parameters will affect the heat release, the chemical reactions and the flame dynamics. In low intensity large scale turbulence dominated flow, the premixed laminar flame will appear as a wrinkled laminar flame with an increased effective area compared to a simple planar laminar flame. Higher turbulence intensity creates laminar flamelets within turbulent eddies. At very high turbulence intensities, the laminar flame structures dissolve into a distributed reaction zone. Generally, the chemistry is unaffected by the flow field if the characteristic time (τ_c) of the reaction is much smaller than the characteristic time (τ_t) associated with flow fluctuations. The chemistry (energy release, flame structure and reaction rates) could be affected if the contrary condition ($\tau_c > \tau_t$) is fulfilled. On the basis of calculating the increase in flame surface area in a large scale low intensity turbulent flow field, Damköhler suggested $S_T = S_L + u'$ for the turbulent flame speed, in which u' is the turbulent

intensity ahead of the flame front (e.g. wrinkling as the main mechanism controlling the turbulent flame).

The turbulent flame speed can be calculated using different approaches and correlations (Zimont & Lipatnikov (1995); Gülder (1990); Peters (1999) or see Kuo (2005) for a simple review). In LES the turbulent flame speed calculation is narrowed to the increase of the flame surface due to subgrid corrugation of the flame. From experimental data (Abdel-Gayed *et al.* (1984); Abdel-Gayed & Bradley (1989)) or theoretical analysis (Yakhot *et al.* (1992)), the following expression has been proposed for the turbulent flame speed:

$$\frac{S_T}{S_L} = 1 + \alpha(\frac{u'}{S_L})^n \tag{4.2}$$

where α and n are constants of the order of unity, and u' is the subgrid scale turbulence level. This expression thus gives the enhancement of the resolved flame speed due to subgrid wrinkling.

4.5 Scales and Regimes for Turbulent Combustion

Turbulent combustion involves various lengths, velocity and time scales describing the turbulent flow field and the chemical reactions. Diagrams defining combustion regimes in terms of dimensionless numbers as functions of these scales have been proposed by many researchers, such as Williams (1985); Abdel-Gayed & Bradley (1989); Peters (1999); Borghi (1988). These diagrams indicate whether the flow contains flamelets (thin reaction zones), pockets or distributed reaction zones, Figure 4.2, and can be a support to select and develop the relevant combustion model for a given problem. The turbulent Reynolds number reads:

$$Re = \frac{u'\ell_t}{\nu} \tag{4.3}$$

which compares the turbulent transport to viscous forces, and where ℓ_t is the turbulent integral scale and ν the kinematic viscosity of the flow. The Damköhler number compares the turbulent time scale, τ_t, and the chemical time scale, τ_c, and can be expressed as:

$$Da = \frac{\tau_t}{\tau_c} \tag{4.4}$$

τ_c may be estimated as the ratio of the thickness, δ_L, and the propagation speed, S_L, of the laminar premixed flame. τ_t can be estimated

from the turbulent integral scale ℓ_t and the u', as $\tau_t = \ell_t/u'$. Based on these scales, the Damköhler number becomes:

$$Da = \frac{\tau_t}{\tau_c} = \frac{\ell_t}{\delta_L}\frac{S_L}{u'} \tag{4.5}$$

where a length scale ratio (ℓ_t/δ_L) and a velocity ratio (S_L/u') are visible. What can be observed is that, for $Da >> 1$, the chemical time is short compared to the turbulent one and consequently corresponds to a thin reaction zone. In this regime, turbulence cannot interfere with the flame and it may then be described as a laminar flame. This regime is called the flamelet regime or thin wrinkled flame regime. On the other hand, $Da << 1$ implies a slow chemical reaction. Reactants and products will be mixed by turbulent mixing before the reaction. The transition between the chemical time scale and the smallest turbulence time scale (the Kolmogorov scale) is described in terms of the Karlovitz number, Ka:

$$Ka = \frac{\tau_c}{\tau_k} = \frac{\delta_L}{\ell_k}\frac{u_k}{S_L} \tag{4.6}$$

The Kolmogorov structures in terms of the size (ℓ_k) and the velocity (u_k) are given by Tennekes & Lumley (1972) and are defined in equation 4.7.

$$\ell_k = (\frac{\nu^3}{\varepsilon})^{1/4}, u_k = (\nu\varepsilon)^{1/4} \tag{4.7}$$

where ε is the dissipation of the turbulent kinetic energy, k. The turbulent integral scale, ℓ_t, may be written as:

$$\ell_t = (\frac{u'^3}{\varepsilon}) \tag{4.8}$$

Reynolds, Re, Damköhler, Da, and Karlovitz, Ka, numbers are related to each other as:

$$Re = Da^2 Ka^2 \tag{4.9}$$

Figure 4.2 illustrates the classification of premixed flame regimes. Laminar flames occur at Re numbers less than unity. All the other regimes are within the turbulent premixed category. The following turbulent premixed flame regimes are proposed by Peters (2000):

1. $Ka < 1$: **Flamelet regime or thin wrinkled flamelets regime**. Two subdivisions may be made here based on the velocity ratio v'/S_L. If $v'/S_L < 1$, the turbulent intensity is smaller than the flame speed and laminar flame propagation dominates the flame front corrugation. Large scales of turbulence are larger than the flame thickness and can not interact with the internal structure of

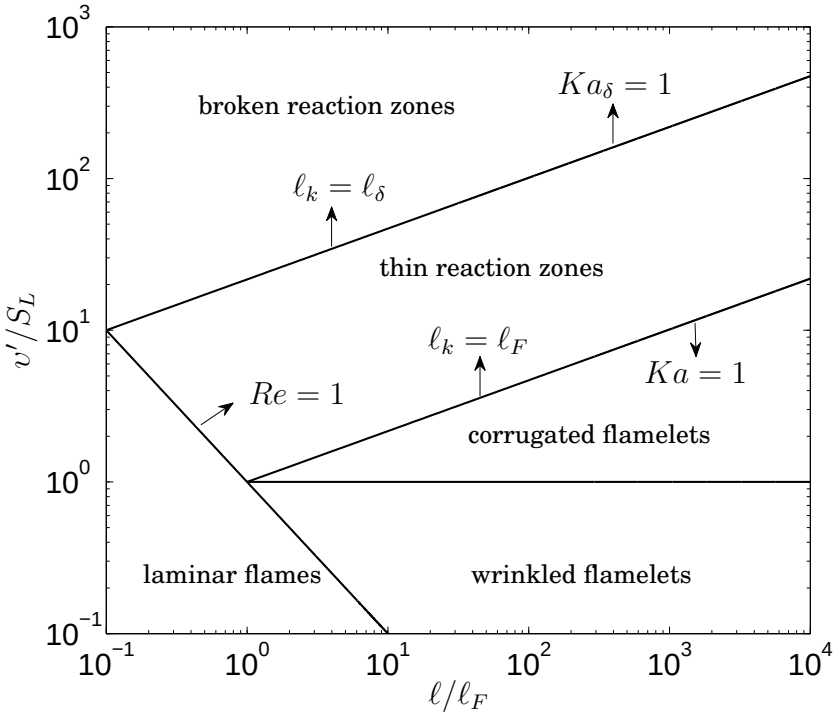

Figure 4.2: Turbulent premixed combustion regimes diagram, Peters (2000)

the flame. The corrugated flamelets regime is obtained for $v'/S_L > 1$, where larger structures become able to interact with the flame front, leading to pockets.

2. $Ka > 1$: **Thin reaction zones regime**. This zone can also be termed the thickened wrinkled flame regime. Turbulent motions are able to penetrate into the preheat zone and both affect and thicken it. However, the reaction zone is unaffected and remains thin and close to a laminar reaction zone.

3. $Ka > 100$ $(Ka_\delta > 1)$ **Broken reaction zones regime**. This zone can also be called the thickened flame regime or even well-stirred reactor. The small scales of turbulence can enter both the preheat and the reaction zones, and the flame is strongly affected by turbulent motions, possibly leading to local quenching of the flame. No laminar flame structure can be seen.

Most practical turbulent flames are either in corrugated flamelets or thin reaction zones regimes.

Chapter 5

Methodology

In this section, the balance equations for conservation of mass, momentum and energy are first formulated. Second, the LES turbulent reacting flow equations are described. Third, the multiobjective optimization strategy of the reaction rate coefficients is described. Finally, the source of errors and the CFD modeling strategy are discussed.

5.1 Balance Equations for Reacting Flows

The balance equations for conservation of mass, momentum and energy are formulated in this section. These equations are well established and can be found in most textbooks on fluid mechanics and turbulent reaction flow, e.g. Wilcox (2004); Kuo (2005); Glassman (1996); Lefebvre (1999); Turns (1996); Warnatz *et al.* (2006); Peters (2000); Poinsot & Veynante (2005); Veynante & Vervisch (2002).

5.1.1 Conservation of Mass

The total mass conservation (continuity equation) reads:

$$\frac{\partial \rho}{\partial t} + \frac{\partial (\rho u_i)}{\partial x_i} = 0 \tag{5.1}$$

where ρ is the fluid density and u_i is the velocity component in the x_i direction.

The mass conservation equation for a species (N species with $k = 1, ..., N$) can be written as (Poinsot & Veynante (2005)):

$$\frac{\partial \rho Y_k}{\partial t} + \frac{\partial}{\partial x_i} \left(\rho (u_i + V_{k,i}) Y_k \right) = \dot{\omega}_k \tag{5.2}$$

where $\dot{\omega}_k$ is the reaction rate of species k and Y_k is the mass fraction for species k. $V_{k,i}$ is the diffusion velocity of species k in the x_i direction and is obtained by solving the system:

$$\nabla X_p = \sum_{k=1}^{N} \frac{X_p X_k}{D_{pk}}(V_k - V_p) + (Y_p - X_p)\frac{\nabla P}{P} + \frac{\rho}{P}\sum_{k=1}^{N} Y_p Y_k (f_p - f_k) \quad (5.3)$$

for $p = 1, ..., N$, where P is the pressure, and f_p and f_k are the external forces. $D_{pk} = D_{kp}$ is here the binary mass diffusion coefficient of species p into species k, see Williams (1985). The diffusion of mass based on the temperature gradients (Soret effects) is neglected. Considering a mixture of two species (volume forces and pressure gradients are neglected) and using the conservation of mass species, equation 5.3 becomes

$$V_1 Y_1 = -D_{12}\nabla Y_1 \quad (5.4)$$

which is the Fick's law, see Glassman (1996); Kuo (2005). Using the Hirschfelder and Curtiss approximation, Curtiss & Hirschfelder (1949), the diffusion velocity can be written as

$$V_k = -D_k \nabla X_k / X_k \quad (5.5)$$

where D_i is the diffusion coefficient written as

$$D_k = -\frac{1 - Y_k}{\sum_{j \neq k} X_p X_k / D_{jk}} \quad (5.6)$$

Coefficient D_k is the diffusion coefficient of species k into the rest of the mixture. The Lewis number, defined as $Le_k = D_{th}/D_k$, links the heat diffusivity, D_{th}, to the diffusion coefficient, D_k. The heat diffusivity is defined by the following expression: $D_{th} = \lambda/\rho C_p$, where λ is the heat conductivity. The Lewis number usually varies by small amounts in the flame fronts (Poinsot & Veynante (2005)). It should also be mentioned that only $N - 1$ species transport equations are needed since the sum of mass fractions must be unity: $\sum_{k=1}^{N} Y_k = 1$. The total mass conservation equation should be recovered if all species equations are added, and the terms $\sum_{k=1}^{N} Y_k V_{k,i} = 0$ and $\sum_{k=1}^{N} \dot{\omega}_k = 0$ are used. However, using the Hirschfelder and Curtiss approximation implies that the global mass is not conserved. Two methods exist to fulfill the global mass conservation. The first method is often used in the existing CFD codes, where only N-1 species equations are solved. The last species mass fraction, N, is obtained by solving $Y_N = 1 - \sum_{k=1}^{N-1} Y_k$. This simplification should be used only in strongly diluted mixtures (for example in air). In the second method, the global mass conservation is obtained by

a correction velocity, V_a, which is added to the convection velocity, u_i, in equation 5.2.

5.1.2 Conservation of Momentum

The conservation of momentum can be written as

$$\frac{\partial(\rho u_j)}{\partial t} + \frac{\partial(\rho u_i u_j)}{\partial x_i} = -\frac{\partial p}{\partial x_j} + \frac{\partial \tau_{ij}}{\partial x_i} + \rho \sum_{k=1}^{N} Y_k f_{k,j} \tag{5.7}$$

where $f_{k,j}$ is the body force acting on species k in direction j. This equation is closed by assuming a Newtonian fluid, i.e. the viscous stress tensor (τ_{ij}) is given by the Newton law and can be written as

$$\tau_{ij} = \mu(2S_{ij} - \frac{2}{3}S_{mm}\delta_{ij}) \tag{5.8}$$

$$S_{ij} = \frac{1}{2}(\frac{\partial u_i}{\partial x_j} + \frac{\partial u_j}{\partial x_i}) \tag{5.9}$$

where S_{ij} is known as the strain-rate tensor. Both equations 5.1 and 5.7 are the same for reacting and non-reacting flow.

5.1.3 Conservation of Energy

The range of velocities in a combustor is very often low, e.g. $M \ll 0.3$. Assuming also constant pressure, the energy equation can be written as (Poinsot & Veynante (2005); Veynante & Vervisch (2011))

$$\frac{\partial(\rho h_t)}{\partial t} + \frac{\partial(\rho u_i h_t)}{\partial x_i} = \frac{\partial p}{\partial t} + \frac{\partial(J_i^h + u_j \tau_{ij})}{\partial x_i} + u_i f_{k,i} \tag{5.10}$$

where J_i^h is the enthalpy diffusion and $h_t = h + u_j u_j/2$ is the total enthalpy. The enthalpy, h, includes both the sensible energy ($\int_{T_0}^{T} C_p dT$) and the chemical energy ($\sum_{k=1}^{N} Y_k \Delta h_k(T)$). The enthalpy diffusion is described by the Fourier law (Veynante & Vervisch (2011))

$$J_i^h = -\frac{\mu}{Pr}\left[\frac{\partial h}{\partial x_i} + \sum_{k=1}^{N}(\frac{Pr}{Sc} - 1)h_k \frac{\partial Y_k}{\partial x_i}\right] \tag{5.11}$$

where Sc is the Schmidt number defined according to

$$Sc = \frac{\mu}{\rho D_k} \tag{5.12}$$

D_k is here the molecular diffusivity of species k relative to the major species. Pr in equation 5.11 is the Prandtl number written as

$$Pr = \frac{\mu C_p}{\lambda} \tag{5.13}$$

where C_p is the calorific capacity at constant pressure and λ is the thermal conductivity. The assumption of a unity Lewis number ($Le = Sc/Pr = 1$) is very often made to be able to simplify the enthalpy diffusion equation 5.11.

5.2 LES Modeling Strategy

In a typical LES simulation, the flame thickness is generally much smaller than the LES filter size. Consequently, the modeling challenge raised by LES of turbulent flames is that some procedure is needed to account for the unresolved fluctuations of species concentrations and temperature, formally to account for the LES spatial averaging (filtering) procedure.

A new approach to sub-grid scale modeling is proposed in this work, Abou-Taouk *et al.* (2014), which relies on the idea that effects and properties of the spatial filtering inherent to LES solvers can be directly accounted for when reducing the chemistry and molecular transport properties. Using these chemical schemes and transport properties in LES modeling would then provide a good estimation of the behavior of the largest scales of turbulent flames.

Introducing a mass weighted Gaussian filtering operation of characteristic filter size Δ

$$\overline{\rho}\widetilde{Y}_i(\underline{x},t) = \int_{-\infty}^{+\infty} \rho(\underline{x}',t) Y_i(\underline{x}',t) G_\Delta(\underline{x}-\underline{x}') d\underline{x}' \,, \tag{5.14}$$

and applying it to $\rho(\underline{x},t)$, $Y_i(\underline{x},t)$ and $T(\underline{x},t)$ provides $\overline{\rho}(\underline{x},t)$, $\widetilde{Y}_i(\underline{x},t)$ and $\widetilde{T}(\underline{x},t)$. For a number of $M < N$ species reacting according to a reduced global scheme, it is proposed that the filtered quantities be obtained by the following modeled equations:

$$\frac{\partial \overline{\rho}\widetilde{Y}_i}{\partial t} + \nabla \cdot \left(\overline{\rho}(\widetilde{\mathbf{u}} + F(\phi)[\mathbf{V}_i(\widetilde{Y}) + \mathbf{V}_a(\widetilde{Y})])\widetilde{Y}_i \right) = \Xi \dot{\omega}_i(\widetilde{Y},\widetilde{T}) \,, \tag{5.15}$$

$$\begin{aligned}\frac{\partial\overline{\rho}\widetilde{T}}{\partial t} &+ \nabla\cdot\left(\overline{\rho}\widetilde{\mathbf{u}}\widetilde{T}\right) = \frac{1}{C_p}\nabla\cdot\left(F(\phi)\lambda\nabla\widetilde{T}\right)\\ &- \frac{1}{C_p}\sum_{i=1}^{N}\rho C_{p_i}Y_iF(\phi)(\mathbf{V}_i(\widetilde{Y})+\mathbf{V}_a(\widetilde{Y}))\cdot\nabla\widetilde{T} \qquad (5.16)\\ &- \frac{1}{C_p}\Xi\sum_{i=1}^{N}h_i\dot{\omega}_i(\widetilde{Y},\widetilde{T})\,.\end{aligned}$$

Here, $V_i(\widetilde{Y})$ indicates that the $\widetilde{Y}_i$ are directly used in the definition of V_i (idem for V_a and $\dot{\omega}_i$). Parameters $F(\phi)$ (correction factor to the transport properties) and $\dot{\omega}_i(\widetilde{Y},\widetilde{T})$, the chemical rates of the reduced scheme, are determined from an automated optimization procedure discussed in the next section. Ξ is an SGS flame wrinkling factor, see Veynante & Vervisch (2002).

5.3 Optimization Approach

Multiobjective optimization of the reaction rate coefficients for different fuels has previously been performed using different kinds of algorithms and reactor models, see Meredith & Black (2006); Franzelli *et al.* (2010); Elliott *et al.* (2003). In the present work, mainly three different models have been used for the optimization, namely the 0D models of the PSR (Abou-Taouk & Eriksson (2011); Abou-Taouk *et al.* (2012)), the isothermal homogenous reactor (Farcy *et al.* (2014)) and the propagating 1D laminar flamespeed model (Abou-Taouk *et al.* (2013, 2014)). All the optimization has been based on the Genetic Algorithm (GA). What was found in the present work is mainly that optimization based on the PSR model yields multiple reaction rate coefficient solutions that give accurate predictions of the species concentrations. However, further investigations of these global schemes have shown that almost all these solutions fail to predict the species concentration profiles and the laminar flame speed in a 1D propagating flame. In contrast to this, optimization based on 1D laminar flame models provide consistently good reduced mechanisms that predict both laminar flame speed and species concentration profiles.

5.3.1 Reaction Rate Calculations

In a combustion process, the net chemical production or destruction rate of each species results from a competition between all of the chemical reactions involving that species. The reaction rates based on the

Arrhenius expression are written as

$$\dot{\omega}_i = A_i f(\phi) \prod_{j \in \mathcal{A}_i} \left(\frac{\rho Y_j}{W_j} \right)^{n_{j,i}} T^{\beta_i} \exp\left(-E_{a_i}/(RT)\right) \ , \tag{5.17}$$

where $\mathcal{A}_i$ is the ensemble of species involved in reaction i, ρ denotes the density and W_j is the molecular weight of species j. Multi-objective optimization may be used to determine the main parameters, namely the pre-exponential factor, $A_i f(\phi)$, including a correction $f(\phi)$ that depends on the equivalence ratio, the temperature exponent, β_i, the activation energy, E_{a_i}, and $n_{j,i}$, the reaction orders of species j in reaction i. The method consists of coupling the solution of given laminar premixed flames with an optimization procedure that dynamically adjusts A_i, E_{a_i}, β_i, $n_{j,i}$, $f(\phi)$ and $F(\phi)$ to match a set of reference laminar flames computed with fully detailed kinetics, for example GRI-Mech 3.0 (Smith *et al.* (1999)) for methane-air flames. $F(\phi)$ is a correction factor introduced to the mixture-averaged molecular diffusion coefficients (the mass and thermal diffusion), which is similar to the one introduced in the thickened flame model, see Colin *et al.* (2000); Boileau *et al.* (2008). In the present work, however, it is determined simultaneously with the chemical parameters in order for the filtered flame to be resolved by the LES mesh, reproducing the species profiles observed in a Gaussian filtered reference detailed chemistry flame, see Figure 5.1 and Figure 5.2, which show temperature and species profiles predicted by an optimized global mechanism with higher mass and thermal diffusion, Abou-Taouk *et al.* (2014).

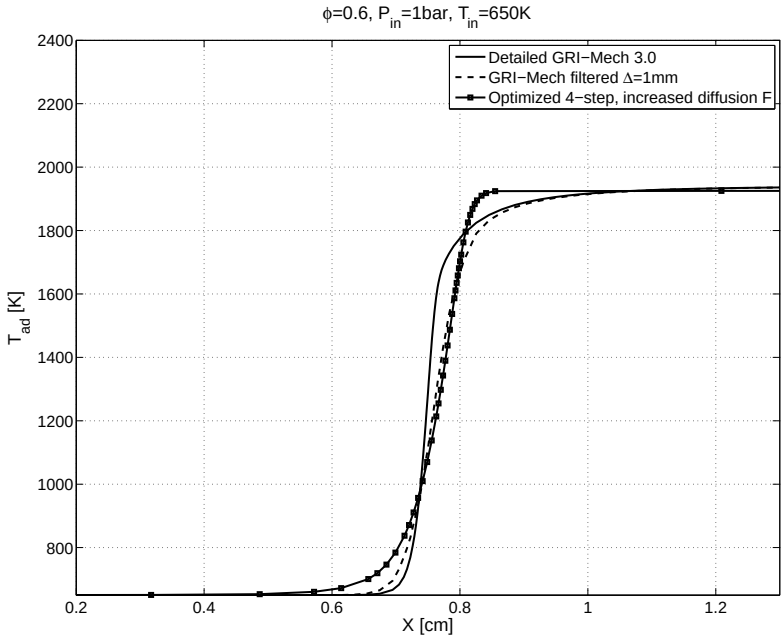

Figure 5.1: Temperature profiles vs position for reference density weighted filtered ($\Delta = 1mm$) reference flame (Gri-Mech 3.0) and the optimized mechanism with higher diffusion by Abou-Taouk *et al.* (2014)

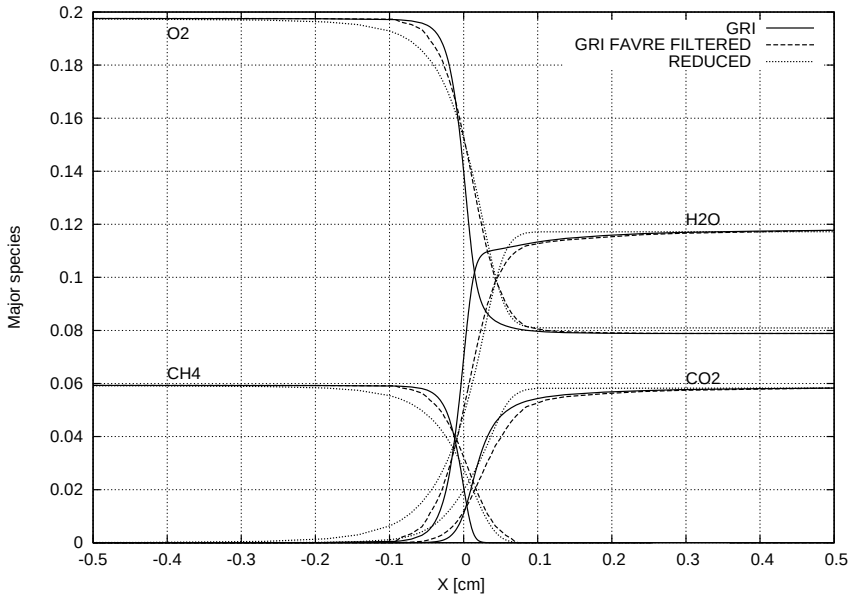

Figure 5.2: Species profiles *vs* position for $\phi = 0.6$. Line: reference flame (GRI-Mech 3.0). Dashed line: Reference density weighted filtered reference flame ($\Delta = 1mm$). Dotted: Optimized mechanism with higher diffusion by Abou-Taouk *et al.* (2014)

5.3.2 Optimization Set-up

In this process, the software CHEMKIN® for chemistry is coupled with the optimization toolbox ModeFRONTIER®, visible in Figure 5.3. In practice, starting from a given set of parameters, $(A_i, \beta_i, E_{ai}, n_{j,i})$, the following procedure is followed:

- Chemical trajectories are computed using the detailed chemistry GRI-Mech 3.0, Smith *et al.* (1999); results are stored.
- Three different scenarios are then obtained depending on the chosen reactor model:
  - 0D reactor: The target data are defined in order to match $T^{\text{ref}}, Y_k^{\text{ref}}$ at selected residence time, τ_{res}, for different sets of (P, T_{in}, ϕ) conditions.
  - 1D laminar flame speed model: The target data are defined in terms of laminar flame speed, $S_L(\ell)^{\text{ref}}$, species profiles $Y_j^{\text{ref}}(x, \ell)$ and temperature $T^{\text{ref}}(x, \ell)$ for the selected points, where ℓ denotes a given (P, T_{in},ϕ) condition.
  - 1D laminar flame speed model with filtering: The chemical trajectories are Gaussian filtered at a chosen filter size Δ and the solutions are stored as a reference, in terms of flame speed $S_L(\ell)^{\text{ref}}$, filtered species profiles $\widetilde{Y}_j^{\text{ref}}(x, \ell)$ and filtered temperature profile $\widetilde{T}^{\text{ref}}(x, \ell)$.
- The selected points that were simulated with the detailed mechanism are also simulated with the global scheme; the difference from the detailed chemistry solution is measured over target optimization points $N_s =$ distributed among the selected points, with an objective function, $\mathcal{F}_Y$:
  - In a 0D reactor:

$$\mathcal{F}_Y\left((A_i, \beta_i, E_{a_i}, n_{j,i})_{i=1,..,N}\right) = \sum_{\ell=1}^{N_{\text{fl}}}\sum_{k=1}^{N_s}\frac{|Y_{\text{j}}(t^k,\ell) - Y_{\text{j}}^{\text{ref}}(t^k,\ell)|}{Y_j^{\text{ref}}(t^k,\ell)} + \sum_{\ell=1}^{N_{\text{fl}}}\sum_{k=1}^{N_s}\frac{|T_{\text{j}}(t^k,\ell) - T_{\text{j}}^{\text{ref}}(t^k,\ell)|}{T_j^{\text{ref}}(t^k,\ell)}$$

  - In a 1D flame speed model:

$$\mathcal{F}_Y\left((A_i, \beta_i, E_{a_i}, n_{j,i}))_{i=1,..,N}\right) = \sum_{\ell=1}^{N_{\text{fl}}}\sum_{k=1}^{N_s}\frac{|Y_{\text{j}}(t^k,\ell) - Y_{\text{j}}^{\text{ref}}(t^k,\ell)|}{Y_j^{\text{ref}}(t^k,\ell)}$$

– In a 1D flame speed model with filtering:

$$\mathcal{F}_Y\left((A_i, f, \beta_i, E_{a_i}, n_{j,i}, F)_{i=1,..,N}\right) = \sum_{\ell=1}^{N_{\text{fl}}} \sum_{k=1}^{N_s} \frac{|\widetilde{Y}_{\text{j}}(t^k,\ell) - \widetilde{Y}_{\text{j}}^{\text{ref}}(t^k,\ell)|}{\widetilde{Y}_j^{\text{ref}}(t^k,\ell)}$$

Here T is the adiabatic flame temperature and t_k is the selected points. $\mathcal{E}_{\mathcal{S}_\mathcal{L}}$ is the error in flame speed and $\mathcal{E}_\mathcal{T}$ is the error in adiabatic flame temperature. The correction function for the transport properties, F, is used only in the approach where the 1-D laminar flame speed solution is filtered. Error functions in laminar flame speed, $\mathcal{E}_{\mathcal{S}_\mathcal{L}}$, and adiabatic flame temperature, $\mathcal{E}_\mathcal{T}$, were introduced in the methods above that are based on the laminar flame speed model. These functions are defined by the following expressions:

$$\mathcal{E}_{S_L} = \frac{|S_L^{\text{ref}}(\ell) - S_L(\ell)|}{S_L^{\text{ref}}(\ell)}, \mathcal{E}_T = \frac{|T_b^{\text{ref}}(\ell) - T_b(\ell)|}{T_b^{\text{ref}}(\ell)} \tag{5.18}$$

- A new set of parameters, $(A_i, \beta_i, E_{a_i}, n_{j,i})$, is determined so as to minimize function $\mathcal{F}_Y$ defined above and to ensure that the errors on the flame speed and adiabatic temperature (equation 5.18) are within 5% and 1%, respectively.

- The process is repeated, *i.e.* the specified flames in a 1-D flame speed model or the selected points in a reactor model are then recomputed with new parameter sets (designs) with the global scheme. The number of designs can be between 5000 and 20000 global schemes depending on the chosen model.

- The best set of parameters $(A_i, \beta_i, E_{a_i}, n_{j,i}, F(\phi))$ fulfilling the requirements are chosen and frozen. A new optimization starts for the 0-D reactors and the laminar flame speed approach (without any filtering) that aims to optimize the correction factor $f(\phi)$ in front of the pre-exponential factor for rich conditions.

- The final results in terms of $(A_i, \beta_i, E_{ai}, n_{j,i})$, the molecular diffusion factor $F(\phi)$ and the correction factor $f(\phi)$ are tabulated to be introduced in the CFD simulation.

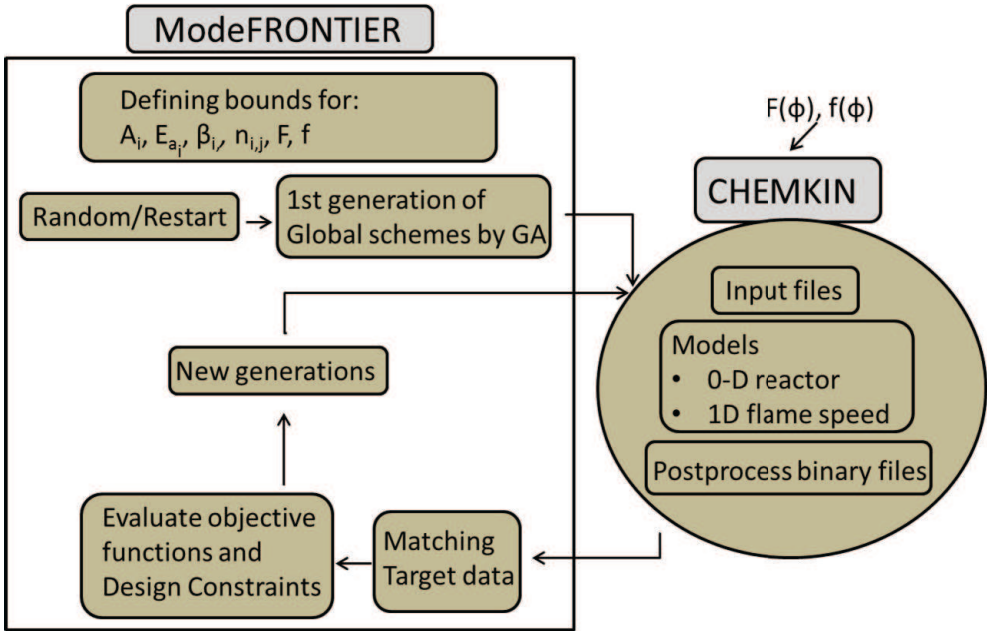

Figure 5.3: Schematic layout of the optimization process

5.4 Numerical Method

5.4.1 Ansys CFX Settings

ANSYS CFX® uses a finite volume method to solve the compressible Navier-Stokes equations. The originally generated grid is converted into finite volumes by the solver, which is used to conserve relevant quantities such as mass, momentum and energy. The software uses a coupled solver, which solves the equations for u, v, w, p as a single system. This solution approach uses a fully implicit discretization of the equations at any given time step. The high resolution scheme (which is a bounded second-order upwind biased discretization) was applied for discretization in space and time for all simulations.

5.4.2 Source of Errors

There are various sources of errors in performing a turbulent reactive flow simulation, where Figure 5.4 displays an illustration of overall disciplines involved in a simulation. Reducing the sources of error is critical if accurate and reliable prediction of combustion systems of practical and technical importance is desired. The overall difficulty in these types of simulations in general is that all of the phenomena in the combustor process are strongly coupled.

Effective strategies to decrease simulation errors are to increase the order accuracy of discrete approximations and/or to use a refined mesh in regions of large gradients. Contributions to the sources of error due to the discretization of diffusion and source terms decreases with increased grid quality. The inflow conditions and the grid resolution are found to be crucial in determining the flow characteristics. The present work has used only hexahedral meshes since they yield high orthogonality, low expansion factors and low numerical errors. Generally, the inflow conditions applied often introduce flow instabilities at different conditions. This problem can usually be solved by shifting the inflow plane upstream, see Irannezhad (2012); Janicka & Sadiki (2005). Consequently, critical upstream geometrical features were included in this work to decrease the dependency on the boundary conditions and create a correct representation of the turbulent flow field entering the combustor.

In LES, the combination of accurate discretization and integration schemes with large numerical efficiency plays a central role, in particular for complex flows in geometrically complicated flow domains, Veynante & Vervisch (2002). The need for reliable and accurate predictions in a reasonable time requires a compromise on numerical accuracy, the range of scales resolved and testing for numerical accuracy, since computer power is limited (Ren & Pope (2006); Veynante & Vervisch (2002)). While this task is relatively easy in RANS simulations, it is more difficult in the LES context. The most commonly used LES procedure is to couple the filter length scale, Δ_f, and the grid spacing, Δ_g. The solution should converge to a DNS as the grid is refined (Gullbrand (2003)), and not towards the solution of the filtered equations. However, if Δ_f is fixed, then LES will not approach a DNS solution as the grid is refined. A refined grid implies that more turbulence length scales are resolved and the influence from the SGS models is reduced. A grid-independent solution is therefore difficult to determine, Kempf *et al.* (2002). In the present work, the mesh convergence for LES was done by checking that the statistics remain the same when a larger period of time was included. A more rigorous check is to compare statistics for two different meshes (mean flow and turbulence statistics).

Accurate predictions also require high quality experimental data in the context of measured boundary conditions in order to be able to match the chosen statistics. Finally, the chosen turbulence and combustion model will introduce different types of errors with respect to their prediction capabilities.

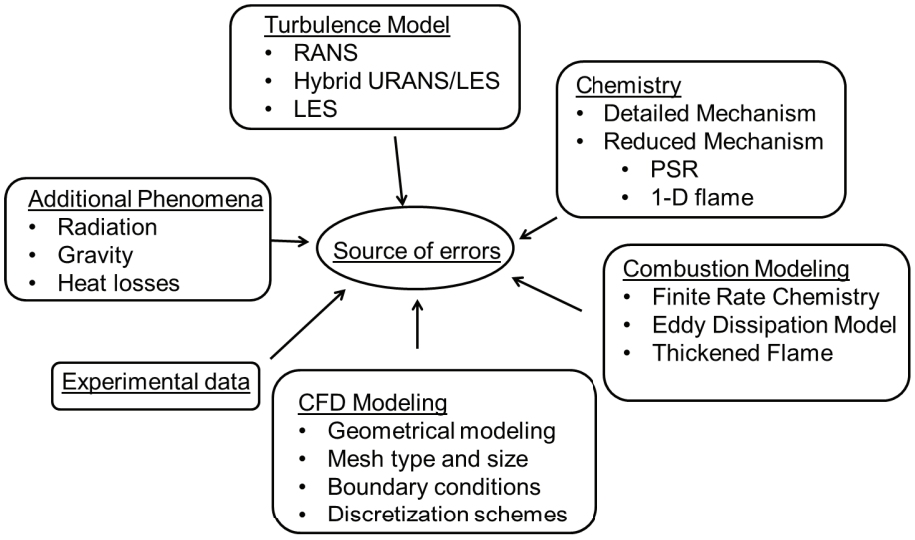

Figure 5.4: Source of errors in performing a reactive CFD simulation

5.5 CFD Modeling

5.5.1 Grid Generation and CFD-Domain

This work has used only structured hexahedral (hex) cell meshes for all CFD simulations (both the SGT-100 and the downscaled SGT-750 test burners and the Sandia Flame D burner). The reason for using this mesh type rather than the tetrahedral mesh type is that hex cells give a lower numerical dissipation (the mesh cells are aligned with the direction of the general flow) and lower cell count (a factor of 5-8 lower). It is extremely important to keep the cell count down since it is directly proportional to the simulation time needed for a converged solution.

Downscaled SGT-750 test burner

The downscaled SGT-750 test burner is investigated experimentally and numerically only in the primary zone, and no cooling air or dilution air is supplied to the combustion. In the experiments and the simulations, both natural gas (methane-air) and syngas mixtures were used. The burner consists of a main premixed flame, a partially premixed pilot flame and a confined rich premixed lean flame, which produces radicals that support both the pilot and the main flame. The combustor has two different combustion zones and consists of three concentric sections visible in Figure 5.5. The first section is the RPL section, where the first combustion zone is located. The RPL can be operated

from lean to rich conditions to satisfy combustion stability issues, see Sigfrid *et al.* (2011*a*); Whiddon (2014), and to obtain low NO_X concentrations (Sigfrid *et al.* (2011*b*)). To the primary zone, both the second section (the PILOT system) and the third section (the Main system) provide fuel and air. After the burner configuration, there is a throat followed by the Quarl, which decreases the velocity due to the expansion and increases the recirculated mass flow compared to burners with a straight nozzle (sudden expansion) for the same swirl number, Syred & Beér (1974).

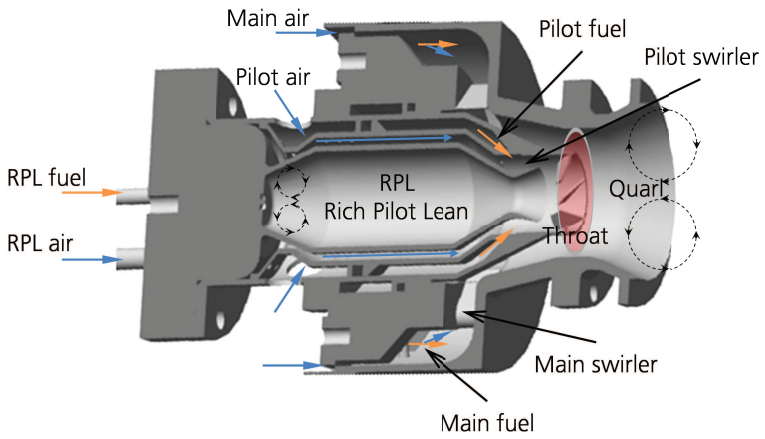

Figure 5.5: Schematic cross section of the downscaled SGT-750 test burner with recirculation zones, taken from Sigfrid (2013)

The atmospheric set-up and the experimental testing were performed by Dr. I. Sigfrid and Dr. R. Whiddon (Whiddon (2014); Sigfrid (2013)) at Lund University. The experimental testing included measurements of the lean stability limit and flame diagnostic through OH-PLIF PIV. Tests were conducted at both atmospheric conditions with preheated air (650 K) and at elevated pressure up to 9 bar. Figure 5.6 shows a photo taken when the burner was running at full operating conditions.

The CFD geometry and the separate inlets for the three different systems are shown in Figure 5.7. All the massflow rates and the preheat temperatures were provided by LTH for the CFD simulations.

At the beginning of the project, Dr. D. G. Barhaghi at Siemens Industrial Turbomachinery AB, Sweden, provided us with the geometry and a tetra mesh for the downscaled SGT-750 test burner. Very early in the project, we decided to create a structured hex cell mesh where all the upstream cavities, the fuel injectors, the cooling ribs and the holes, and the swirler vanes for the main and RPL systems would be included in the CFD domain. Consequently, the grid generation of the

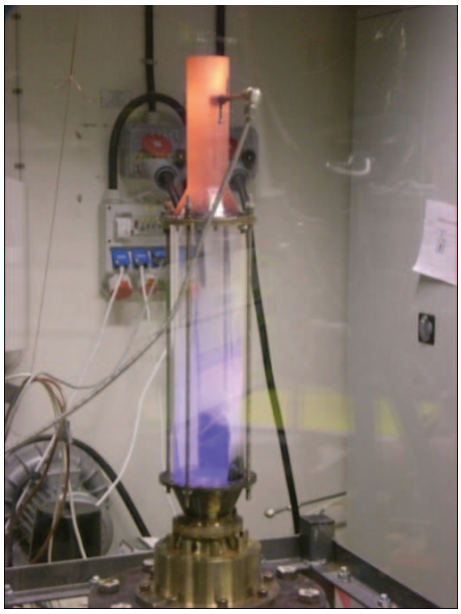

Figure 5.6: The liner after the burner glowed orange due to the hot combustion gases

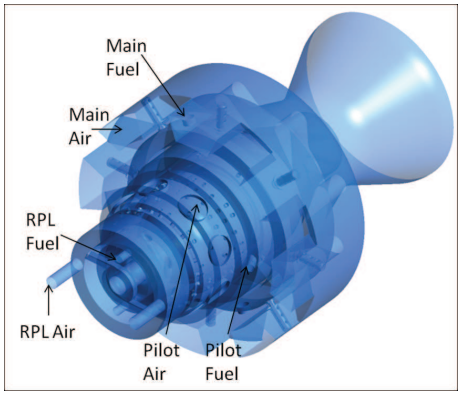

Figure 5.7: Configuration of the burner where the CFD domain inlets are visible

scaled 4^{th} generation DLE flexi-fuel burner required a large amount of time, approximately five months work using the commercial software ICEMCFD®. A grid independence study was done both for the steady-state and transient simulations. To decide whether the grid is mesh independent, transient averaged data such as temperatures and major species (CH_4, CO_2 and CO) were compared for different hexahedral grids at different planes downstream in the burner. The number of cells finally used was between 9 and 17 million cells for the RANS and hybrid URANS/LES models. Figure 5.8 - Figure 5.13 show some pic-

tures of the hex mesh for the downscaled SGT-750 test burner used.

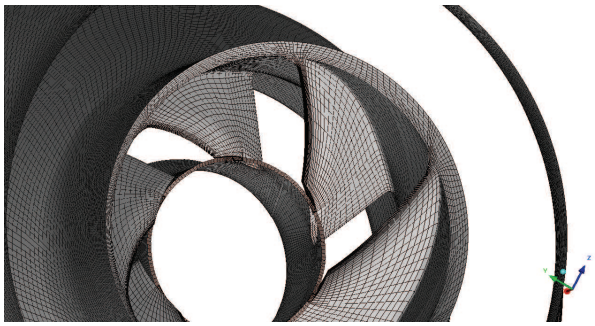

Figure 5.8: Swirler vanes for the RPL and PILOT systems

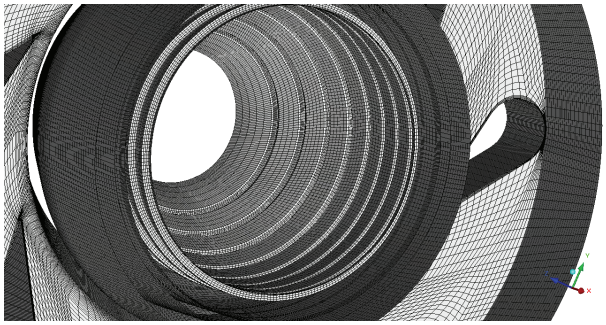

Figure 5.9: Swirler vanes for the MAIN system and ribs

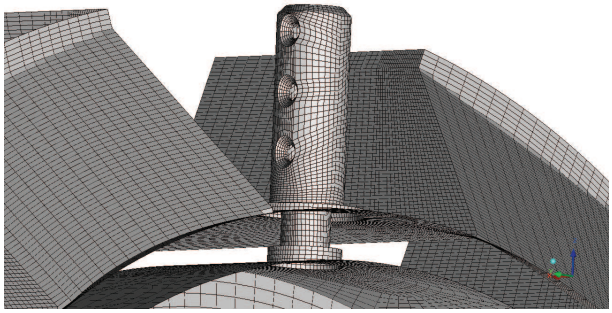

Figure 5.10: Fuel injectors for the MAIN system - Rods

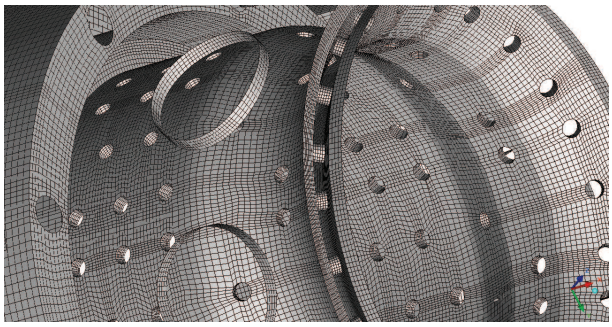

Figure 5.11: Cooling holes and cavities

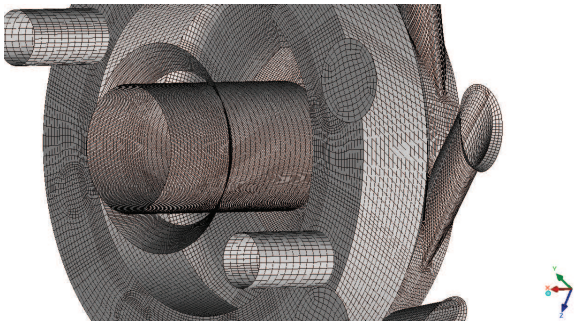

Figure 5.12: Inlets and cavities upstream in the burner

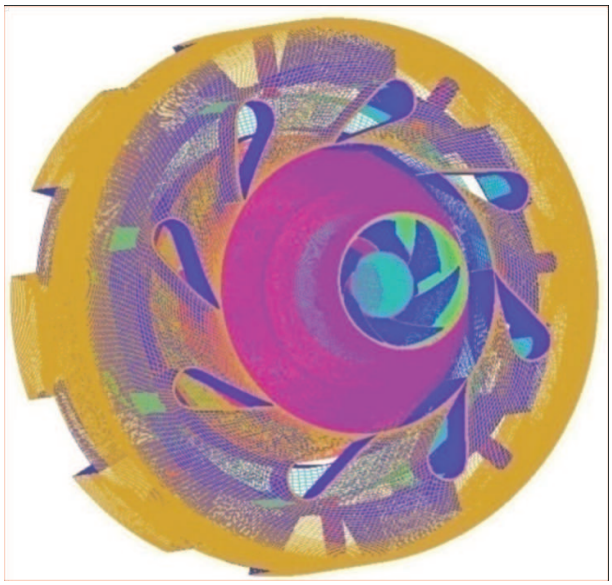

Figure 5.13: Front view showing the different parts in the burner

SGT-100 Burner

The SGT-100 DLE burner consists of a main burner, pilot burner, radial swirler and double skinned can combustor. Fuel (natural gas) is injected at two different locations. There are 12 main injection holes at the entrance of the swirler slot and two gas injection holes on the side wall of each swirler vane. Pilot (gas) is injected into the groove between the pilot face and main burner. The flow passes the swirler vanes and turns into the prechamber, followed by a sudden expansion into the combustion chamber. The geometric swirl number, S_g, in the burner is 1.3, based on the following expression:

$$S_g = \frac{2}{3}\frac{[1-(D_{si}-D_{so})^3]}{[1-(D_{si}-D_{so})^2]}tan\gamma \tag{5.19}$$

where D_{si} and D_{so} are the inner and the outer diameter of the swirler, and γ is the swirler vane angle. The burner has a partially premixed combustion system with both premixed and non-premixed combustion regimes. Tests were previously carried out at the DLR Institute of Combustion Technology, Germany, for various operating pressure conditions, 1 to 6 bar. A comprehensive set of measurements was made for this configuration in order to describe the flame and its dynamics. More specifically, PLIF and chemiluminescence imaging were applied to determine the flame structures and the stabilization region. PIV was used to measure the flow velocities, while (1D) laser Raman scattering was used to quantitatively measure the major species concentrations (CH_4, O_2, H_2O, CO_2, CO, H_2 and N_2) and the temperature, see Stopper *et al.* (2010, 2013).

The mesh provided by Dr. G. Bulat at Siemens Industrial Turbomachinery Ltd, UK, was modified to include a structured mesh around the 36 fuel inlets and the inlets of the cooling air. The mesh size was 8.5 million cells for all CFD simulations (based on RANS and hybrid RANS/LES models) and 24.5 million cells for the LES simulations. Figure 5.14 - Figure 5.16 show some pictures of the CFD domain and the hex mesh for the SGT-100 DLE burner used.

The SGT-100 DLE burner has previously been numerically investigated by Bulat *et al.* (2013) using LES with a sub-grid pdf model. The chemistry was modeled by a 15-step reaction mechanism using 19 species. The conclusions of that work were basically that the flow field, and both the temperature and species in the inner shear layer, were accurately predicted. The burner was also found to have regions of diffusion combustion regimes, and the local extinction of the flame was shown to be due to local chemistry/turbulence effects rather than large scale mixing.

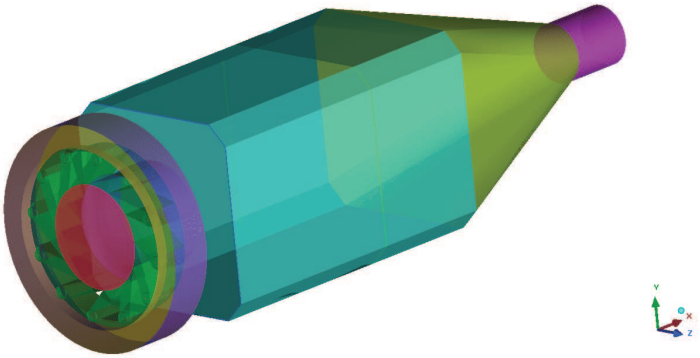

Figure 5.14: CFD domain for the SGT-100 DLE burner

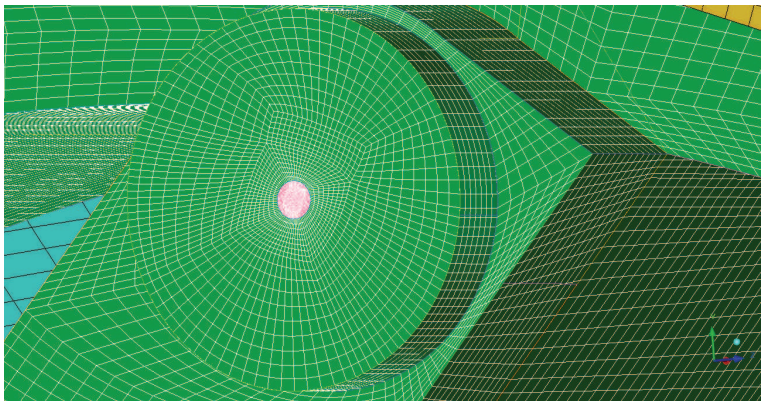

Figure 5.15: Front view from the upstream cavities showing the fuel inlet directed towards the axial direction

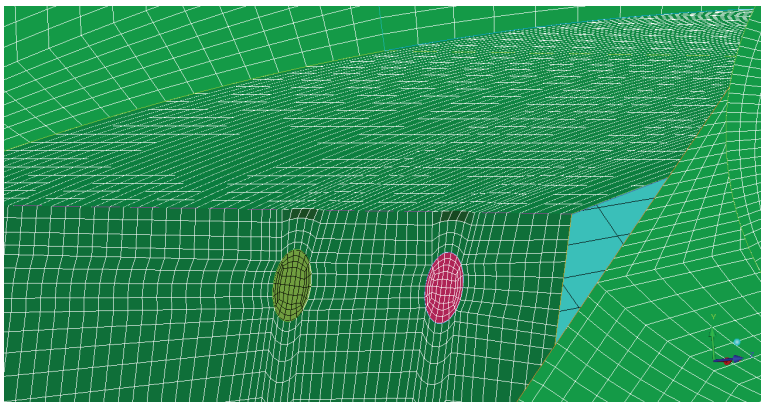

Figure 5.16: Side view showing the fuel inlets located in between the vanes and directed towards the tangential direction

Chapter 6

Summary of Papers

THIS chapter gives a short summary of the work done and the results reported in the eight papers on which this thesis is based.

6.1 Paper I

A. Abou-Taouk and L.-E. Eriksson, 2011, Optimized Global Mechanisms For CFD Analysis Of Swirl-Stabilized Syngas Burner For Gas Turbines, *ASME Turbo Expo 2011*, June 6-11, Vancouver, Canada

6.1.1 Division of the Work

My contribution, in addition to being the lead author, was to perform the optimization of the kinetics, validate it and set up and perform the CFD simulations. The geometry was supplied by Siemens Industrial Turbomachinery AB, Sweden, and the experiment was carried out at Lund University. L. E. Eriksson was involved in the work leading to the optimization methodology chosen and supervised the writing.

6.1.2 Results and Discussion

This paper presents the derivation and evaluation of kinetic optimization (a two-step global mechanism for methane-air mixture) using PSR calculations. The global mechanism consists of the fuel oxidation into CO and H_2O, and the $CO-CO_2$ equilibrium reaction. The swirl burner investigated operates at both lean and rich conditions. To ensure good agreement at rich conditions, correction functions dependent on the local equivalence ratio are optimized and tabulated for CFD. The range of validity of the global mechanism is $\phi = 0.5 - 1.6$, atmospheric pressure and inlet temperatures corresponding to $295K - 650K$. Comparing the

optimized global mechanism with the reference detailed mechanism, GRI Mech 3.0, the results show that the fully burned conditions of the gas temperature and emissions are reasonably well predicted. However, since the laminar flame speed parameter was not included in the optimization, it is overpredicted for higher ϕ.

A downscaled SGT-750 test burner was numerically investigated. The burner consists of a main premixed flame, a partially premixed pilot flame and a confined rich premixed lean flame which produces radicals that support both the pilot and the main flame. The CFD results are compared with experimental results obtained in an atmospheric version of the burner test rig at Lund University, see Whiddon (2014); Sigfrid *et al.* (2010, 2011*a*,*b*, 2012, 2013*a*,*b*, 2014). Both RANS and hybrid URANS/LES results were computed using the combined FRC-EDM turbulence-chemistry interaction model. The CFD results show reasonably good agreement with flame visualization and gas composition. The results of the two-step global mechanism show good agreement with experimental data for the CO value, while the global schemes by Westbrook & Dryer (1984) failed in their predictions of the CO emissions downstream in the burner.

6.2 Paper II

A. Abou-Taouk, R. Whiddon, I. Sigfrid and L. -E. Eriksson , 2011, CFD Investigation Of Swirl-Stabilized Flexi-Fuel Burner Using Methane-Air Mixture For Gas Turbines, *The 20th ISABE Conference*, ISABE 2011-1122, September 12-16, Göteborg, Sweden

6.2.1 Division of the Work

My contribution, besides being the lead author, was to perform the CFD simulations and validation thereof. I. Sigfrid's contribution was to choose the test settings, set up the emission sampling system and perform the PIV measurement. R. Whiddon performed the OH-LIF measurements. L. E. Eriksson supervised the writing.

6.2.2 Results and Discussion

The second paper presents more numerical results for the downscaled SGT-750 test burner. The CFD simulations were performed using three different configurations of the liner, a cylindrical liner, a quartz liner with a square cross-section and an unconfined flame (without liner). Both RANS and hybrid URANS/LES results were computed using the

two-step optimized global scheme by Abou-Taouk & Eriksson (2011) and the combined FRC-EDM turbulence-chemistry interaction model. The results are compared with high quality experimental data in the form of emission data, PIV data and OH-PLIF from an atmospheric burner test rig at Lund University, Sigfrid *et al.* (2010, 2011*a*,*b*, 2012, 2013*a*,*b*, 2014).

The results for the cylindrical liner show that the emission data (CO and O_2) are well predicted with the CFD simulations. The results from the second case with the square cross-section liner show that the velocity field and the flame position are well predicted with the SAS-SST model, while the steady-state RANS fails in some regions. The velocity field in the open liner (unconfined flame) is not well captured by the CFD simulations. The poor prediction may be due to the co-flow introduced around the burner in the CFD simulation to model the experiment set-up without a liner. This co-flow may influence the flame downstream in the burner. Also, in the experimental set-up, a fan is located above the burner to extract the exhaust gases. This fan is not included in the CFD and may thus also contribute to the differences between the measured and predicted velocity fields.

6.3 Paper III

A. Abou-Taouk and L.-E. Eriksson, Evaluation of Optimized 3-step Global Reaction Mechanism for CFD Simulations on Sandia Flame D , 2011, *The 6th Symposium on Numerical Analysis of Fluid Flow and Heat Transfer*, ICNAAM 2011-0604, September 18-25, Halkidiki, Greece

6.3.1 Division of the Work

My contribution, in addition to being the lead author, was to set up and perform the CFD simulations. L. E. Eriksson supervised the writing.

6.3.2 Results and Discussion

The aim in this article was to use a well-known test case, Sandia Flame D, to be able to validate the optimized two-reaction mechanism in the previous work. The Sandia Flame D consists of a main jet with a mixture of 25% methane and 75% air by volume. This jet is located in a co-flowing gas stream of air, and the flame is stabilized by a pilot. Experimental data from the Sandia National Laboratories (Sandia (2014)) were used. The RNG k-epsilon turbulence model was used

for the RANS simulations. The reason for this choice was the existing validation report by Gobby (2009), where the WD2 global mechanism (Westbrook & Dryer (1984)) is used together with the RNG k-epsilon model on the Sandia Flame D. Two different global mechanisms were used: the optimized two-step global reaction mechanism by Abou-Taouk & Eriksson (2011) and the global mechanism by Westbrook & Dryer (1984). The combined turbulence-chemistry interaction model, FRC-EDM, in Ansys CFX, was chosen for all CFD analyses. The CFD results with the two-step global mechanism showed good agreement with the experimental data based on emission, velocity and temperature profiles, while the WD2 global mechanism showed poor agreement with the emission profiles.

6.4 Paper IV

A. Abou-Taouk, R. Whiddon, I. R. Sigfrid and L. E. Eriksson, A Four-Step Global Reaction Mechanism for CFD Simulations of Flexi-Fuel Burner for Gas Turbines, 2012, *7th International Symposium on Turbulence, Heat and Mass Transfer*, Palermo, Italy

6.4.1 Division of the Work

My contribution, besides being the lead author, was to optimize the kinetics for the syngas mixture and validate the mechanism, and to perform the CFD simulations and the validation thereof. I. Sigfrid chose the test settings, set up and performed PIV measurements, derived and calculated turbulence length and time scales (for PIV and CFD), and performed the POD analysis (for PIV and CFD). R. Whiddon was in charge of the OH-LIF measurements. L. E. Eriksson supervised the writing.

6.4.2 Results and Discussion

In this paper, a four-step global mechanism was optimized for syngas combustion using both PSR and propagating flame simulations. Comparisons of the four-step mechanism with the reference detailed reaction mechanism show that the adiabatic flame temperature, the laminar flame speed and the emissions at fully burned conditions are well predicted. The range of validity of the global mechanism is equivalence ratios $0.4 - 1.8$, atmospheric pressure and inlet temperatures corresponding to $295K - 650K$.

The mechanism was used in CFD modelling of the downscaled SGT-750 test burner. The CFD results were compared with PIV images, OH-pLIF and POD analysis. CFD results show that the velocity field, the temperature and the flame dynamics are well predicted compared to PIV and OH-pLIF data.

6.5 Paper V

I .R. Sigrid, R. Whiddon, A. Abou-Taouk, R. Collin, and J. Klingmann, Experimental Investigations of an Industrial Lean Premixed Gas Turbine Combustor With High Swirling Flow, 2012, *ASME Gas Turbine India Conference*, GTIndia 2012-9681, Mumbai, India

6.5.1 Division of the Work

My contribution was to perform the CFD simulations and supply the CFD results. I. Sigfrid was the lead author and chose the test settings, set up and performed PIV measurements, derived and calculated turbulence length and time scales, and evaluated the results. R. Whiddon performed the OH-pLIF measurements and the post-processing thereof. R. Collin and J. Klingmann supervised the writing.

6.5.2 Results and Discussion

In this paper, PIV and OH-pLIF measurements were conducted in an atmospheric set-up with a downscaled SGT-750 test burner. The results are used to discuss the effect of varying the fuel gas composition on combustion and fluid mechanical properties, e.g. recirculation zone and velocity fluctuations. Relevant time and length scales are also derived. The PIV measurements and OH-pLIF measurements are compared to CFD simulations.

6.6 Paper VI

A. Abou-Taouk, S. Sadasivuni, D. Lörstad and L. -E. Eriksson, Evaluation of Global Mechanisms for LES Analysis of SGT-100 DLE Combustion System, 2013, *ASME Turbo Expo 2011, GT2013-95454*, San Antonio, Texas, USA

6.6.1 Division of the Work

My contribution, besides being the lead author, was to optimize the kinetics for the methane-air mixture and validate the mechanism, set up and perform the CFD simulations and the validation thereof. S. Sadasivuni provided the figures for the SGT-100 industrial gas turbine burner. S. Sadasivuni and D. Lörstad reviewed the article. L. E. Eriksson supervised the writing. The Turchemi test case was supplied by Siemens Industrial Turbomachinery Ltd, Lincoln, UK, and the experiment was previously carried out at the DLR Institute of Combustion Technology, Germany.

6.6.2 Results and Discussion

This paper deals with a new optimized and evaluated four-step reaction mechanism, called M4, for methane-air mixtures. The target for the optimization was to match the detailed mechanism based on the adiabatic flame temperature, the laminar flame speed and the species concentrations for fully burned conditions at different pressures. The validity of the M4 scheme is limited to operating pressure conditions from $1-6$ bar, inlet temperatures from $295K-650K$ and $\phi = 0.4-1.6$.

The M4 scheme was tested for a laboratory version of the Siemens SGT-100 DLE gas turbine combustor. Velocity profiles, flame temperatures and major species are compared with experiments (PLIF, chemiluminescence imaging, PIV and (1D) laser Raman scattering) for different global reaction mechanisms and turbulence models.

The SAS-SST simulations with the M4 global reaction mechanism predicted mixing and major species well. However, the SAS-SST simulations seem to overpredict the temperature at all locations. The RANS models predict the velocity profiles well using both global mechanisms (the WD2 and the M4 global mechanisms). Small differences are seen between the two reaction schemes with respect to the temperature profiles. The RANS simulations are found to predict well at upstream regions and no satisfactory results were obtained with the LES-WALE turbulence model mainly due to the lack of a suitable subgrid combustion model in the Ansys CFX flow solver.

6.7 Paper VII

B. Farcy, A. Abou-Taouk, L. Vervisch, P. Domingo and N. Perret, Two approaches of chemistry downsizing for simulating selective non catalytic reduction DeNOx Process, *Fuel*, 118 (2014) 291-299

6.7.1 Division of the Work

My contribution was to optimize the two-step mechanism for the kinetics based on the NO_x conversion. B. Farcy was the co-author and performed the parameterization of the detailed chemistry using a single progress variable. L. Vervisch and P. Domingo supervised the writing.

6.7.2 Results and Discussion

This paper discusses the influence of temperature and composition on the conversion of NO_x by ammonia under conditions representative of a SNCR (Selective Non Catalytic Reduction) DeNOx. It is experimentally observed that a narrow temperature window exists over which the efficiency of the process is maximum. Above this range, the transformation of ammonia into NO dominates, jeopardizing the NO_x conversion. It is concluded that temperature fluctuations of the order of $100K$ in a turbulent flow may be sufficient to strongly reduce the overall process efficiency.

An automated projection of detailed chemistry is discussed from a recently developed approach, Niu *et al.* (2013), and it is shown that the NO_x conversion may be tabulated from a progress variable defined from all chemical species involved in the detailed kinetics. A reduced two-step global mechanism is obtained from an automated optimization of the chemical rate parameters. It is shown that the optimized two-step reproduces most of the expected NO_x conversion behavior, specifically in the temperature range where the process would operate at its best.

For a given set of boundary conditions, a chemical look-up table obtained from a detailed chemical mechanism and parameterized with a single progress variable brings the possibility of introducing in the modeling loop refined chemistry information for the cost of solving a single variable, as would be the case with single-step chemistry. The reduction in computational cost is therefore significant, at least two orders of magnitude for the detailed scheme considered in this work. It will be about the same with the two-step scheme, except that more flexibility is allowed in terms of boundary conditions, since no look-up table is introduced.

6.8 Paper VIII

A. Abou-Taouk, B. Farcy, P. Domingo, L. Vervisch, S. Sadasivuni and L. -E. Eriksson, 2014, A new approach for Large Eddy Simulation of gas

turbine partially premixed combustion: Implicit modeling using optimized chemistry, *To be submitted to Combustion Theory and Modeling*

6.8.1 Division of the Work

The idea of and the contribution to the new sub-grid scale modeling for LES came about via a joint collaboration between A. Abou-Taouk, B. Farcy, P. Domingo, L. Vervisch and L. E. Eriksson. My contribution, besides being the lead author, was to perform the chemistry optimization and to set up and perform the 3D LES simulation of the SGT-100 industrial gas turbine burner. B. Farcy performed the filtering of the results for the detailed mechanism. S. Sadasivuni was included in the article due to the agreement to allow the project to use the Turchemi test case supplied by Siemens Industrial Turbomachinery Ltd, Lincoln, UK. L. Vervisch and L. E. Eriksson supervised the writing.

6.8.2 Results and Discussion

This paper discusses a novel approach to the sub-grid scale modeling of turbulent partially premixed combustion in gas turbines based on optimized chemistry. The kinetic optimization is based on simultaneously optimizing the Arrhenius coefficients and a correction to mixture-averaged molecular diffusion coefficients. The objective is to reproduce, with LES modeling of the burning rates and transport fluxes, spatially filtered detailed chemistry solutions for a given filter size. A four-step global chemical scheme and a corrective factor to the diffusive budget are automatically obtained from the optimization tool in order to match the flame speed response and major species profiles, as they appear in a Gaussian filtered flame that is sufficiently thick to be resolved over an LES grid. The method is applied to an industrial gas turbine, which has been studied experimentally by Stopper *et al.* (2010, 2013). Flame properties along with statistical data agree well with the measurements.

Chapter 7

Unpublished Results

THIS section presents some of the unpublished CFD results that were obtained for the SGT-100 and the downscaled SGT-750 test burners.

7.1 SGT-100 burner

The main results obtained for the SGT-100 burner in the Turchemi project, Stopper *et al.* (2010, 2013), are presented and discussed in papers VI and VIII. However, some of the prediction were not presented in the articles and are shown here. A comparison of the LES results with experimental data was carried out at four axial locations in the combustor (x/D = 1.21, 1.44, 1.66, 2.00 where D = 0.086 m is the burner exit diameter). Figures 7.1 - 7.3 provides comparison of PIV measured and simulated mean and RMS axial/radial velocities at the four mentioned locations for the non-reacting case (no combustion). The pressure in the burner was set to 5 bar according to the experimental set-up. The LES results agree well with the measured main flow field. Both (inner and outer) recirculation zones are well captured, and shear layer regions are correctly reproduced. Both the reacting and non-reacting flow simulations using LES show that the prediction of the velocities close to the center line is not fully correctly represented. The reason for this error does not seem to be connected to the combustion modeling since both cases show this behavior.

Figure 7.4 shows two different iso-surfaces: the second invariant of the velocity gradient tensor, λ_2 (in gray), and the CO mass fraction (in red). The figure also shows the instantaneous temperature (back plane) and the instantaneous heat release rate (bottom plane) for the reacting flow LES simulation. The flame in the core region of the burner seems to have thickened, wrinkled structures, and con-

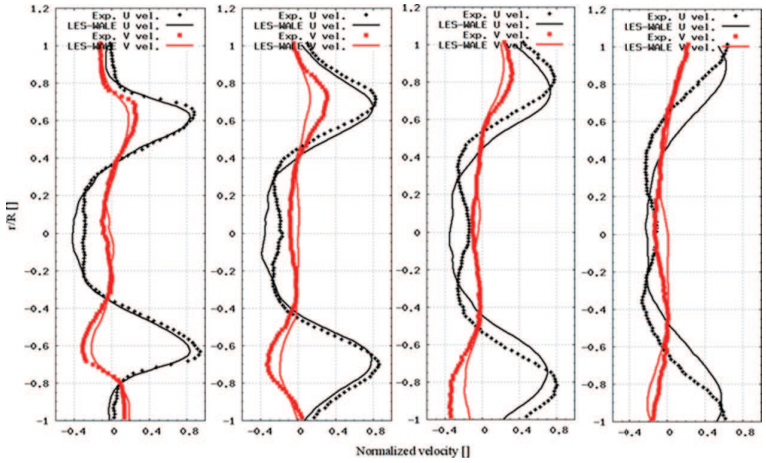

Figure 7.1: Comparison of U mean (black) and V mean (red) normalized velocity profiles for the four PIV axial plane locations

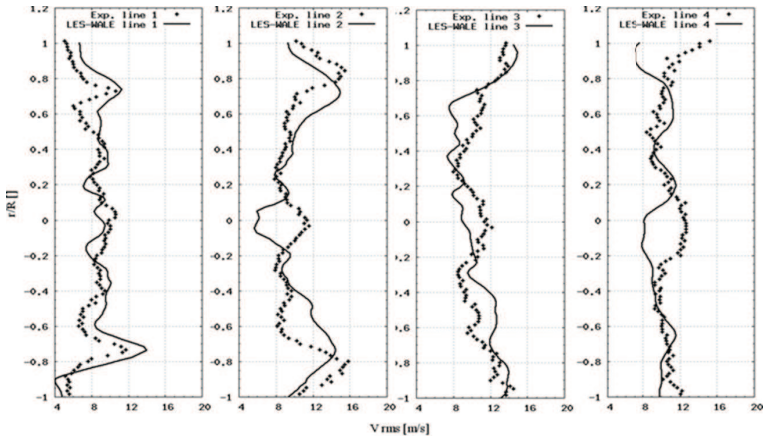

Figure 7.2: Comparison of V rms velocity (m/s) profiles for the four PIV axial plane locations

sequently appears to belong to the thin reaction zones regime in the diagram by Peters (2000). This regime is characterized by turbulent motions that are able to penetrate into the preheat zone and both affect and thicken it. However, the reaction zone is unaffected and remains thin. The flame in the shear layer is in the border of broken reaction zones regime (thickened flame regime). The small scales of turbulence can enter both the preheat and the reaction zones, and are strongly affected by turbulent motions. The strong mixing process due to the high swirl motion seems to dilute the mixture to equivalence ratios below the flammability limit and results in local extinction of the flame.

The burner is governed by a radial swirler, and the downstream part of the burner is therefore governed by a strong protruding vor-

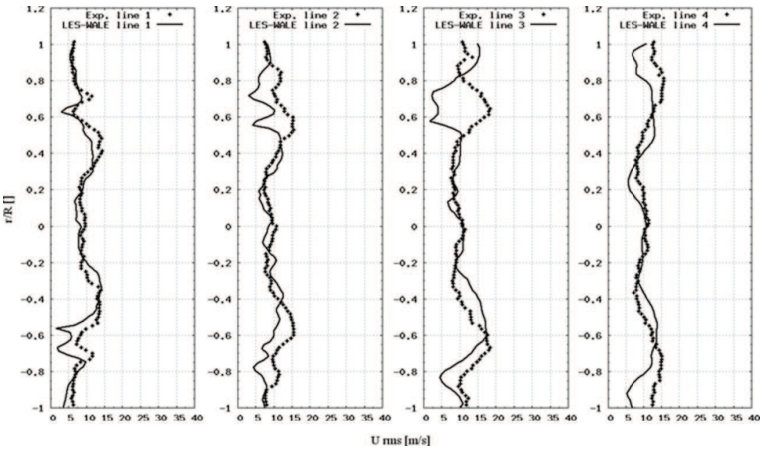

Figure 7.3: Comparison of U rms velocity (m/s) profiles for the four PIV axial plane locations

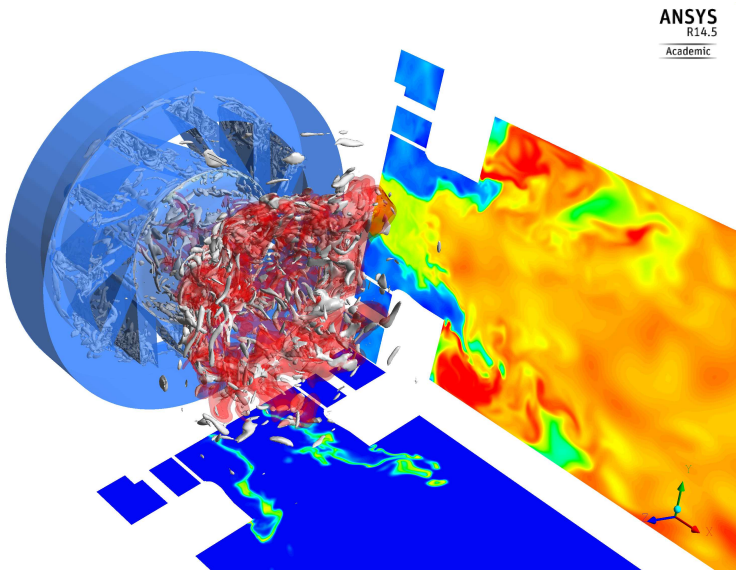

Figure 7.4: Iso-λ_2 (gray) and Iso-CO mass fraction (red). Bottom plane: instantaneous heat release rate. Back plane: instantaneous temperature

tex core extending from the outlet plane into the prechamber. The exhaust channel is longer in the experimental set-up, which may affect this vortex core upstream. This may be the reason why both the hybrid URANS/LES and LES simulations show a poor prediction of the velocities close to the center line in the combustor chamber. The swirling flame seems to be located in the upstream region of the combustor chamber and anchored close to the wall located at the beginning of the prechamber. Comparing the vortex core distributions in the up-

stream part of the combustor chamber, different vorticity distributions can be observed. The LES simulation predicts a comparatively small region of vortices that develops from vortex rings being continuously shed from the prechamber. The vortex interactions assisted by instabilities in the annular shear layer imply that the vortex rings break up rather quickly. Hence, a cloud of vortices is formed where the vortices continue to interact with each other.

Figure 7.5 shows an instantaneous contour plot of the equivalence ratio in the burner at an axial plane. The fuel (CH_4) stays relatively close to the cylindrical prechamber wall after it has been injected at the radial swirlers. The main reason for this is the high swirl number of the air-fuel mixture that passes through the prechamber. It is also obvious that the fuel is not perfectly mixed in the combustor chamber, but rather partially premixed. This also agrees well with the results of the experiments, Stopper *et al.* (2010).

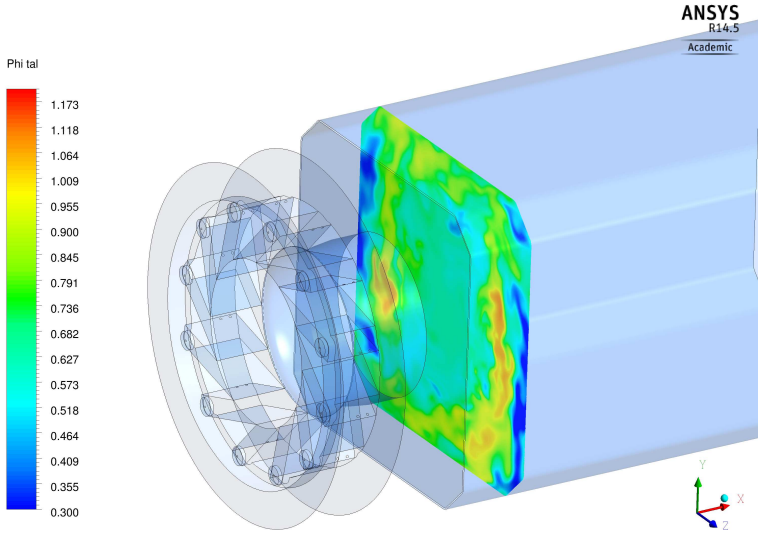

Figure 7.5: Instantaneous contour plot of the equivalence number in the burner at an axial plane

Figure 7.6 shows a scatter plot (14000 points) of the temperature in the inner shear layer taken from the work of Stopper *et al.* (2010). This plot provides insight into the degree of mixing of fuel and air entering the combustion chamber. The equivalence ratio ranges from lean mixtures with fuel concentrations below the ignition limit to slightly rich mixtures. A perfect mixing is almost impossible to achieve in industrial conditions since the higher pressure and the limited space imply a short residence time in the premix region.

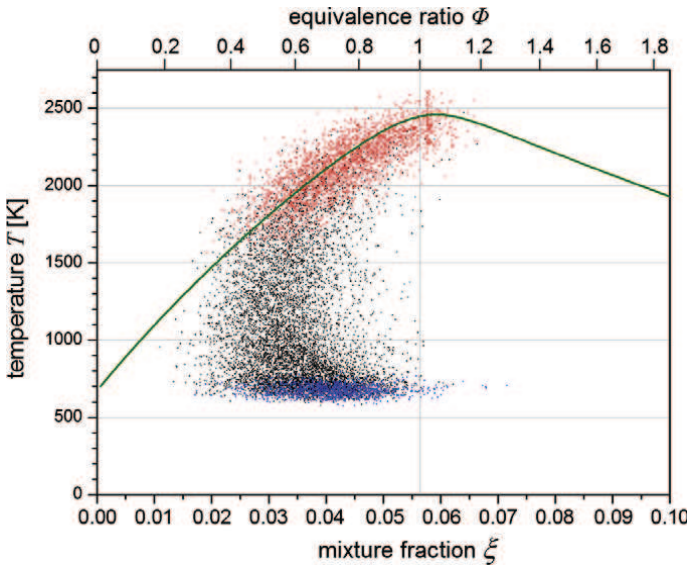

Figure 7.6: Scatter plot (14000 points) of the temperature measured in the inner shear layer. The curve represents the calculated adiabatic temperature of the reaction products; taken from the work by Stopper *et al.* (2010).

Figure 7.7 shows the instantaneous reaction rates for the four reactions using the new LES modeling approach (Abou-Taouk *et al.* (2014)). The kinetic rate data are shown in Table 7.1

Reaction	A_i	B_i	E_{a_i}	Reaction order
$CH_4 + \frac{1}{2}\,O_2 \rightarrow CO + 2H_2$	9.213E+14	0	31.5	$[CH_4]^{0.62}$, $[O_2]^{1.5}$
$H_2 + \frac{1}{2}\,O_2 \rightarrow H_2O$	1.606E+18	-1.2	40.67	$[H_2]^{0.425}$, $[O_2]^{1.694}$
$CO + \frac{1}{2}\,O_2 \rightarrow CO_2$	1.746E+15	0	40.6	$[CO]^{1.05}$, $[O_2]^{0.3}$, $[H_2O]^{0.5}$
$CO + H_2O \leftrightarrow CO_2 + H_2$	1.305E+15	0	20.5	[CO], $[H_2O]$

Table 7.1: Kinetic rate data (unit in cm, s, kcal and mol)

The reaction rates are expressed as:

$$\dot{\omega}_i = A_i f(\phi) \prod_{j \in \mathcal{A}_i} \left(\frac{\rho Y_j}{W_j} \right)^{\mu_{j,i}} T^{B_i} \exp\left(-E_{a_i}/(\mathcal{R}T)\right) \,, \tag{7.1}$$

where $\mathcal{A}_i$ is the ensemble of species involved in reaction i, ρ denotes the density and W_j is the molecular weight of species j. The highest reac-

tion rates are obtained in the reaction zone since the peak temperature is obtained in this region. However, the magnitudes differ between the four reactions. The fastest reactions seem to be reactions number one and three, which are the oxidation of the fuel and the oxidation of CO into CO_2. Perhaps unexpected, due to the high pre-exponential value, is the low reaction rate obtained for the second reaction (here hydrogen and oxygen are reacted into water). However, the strong negative temperature exponent, β, in equation 7.1, makes this reaction rate small at high temperatures.

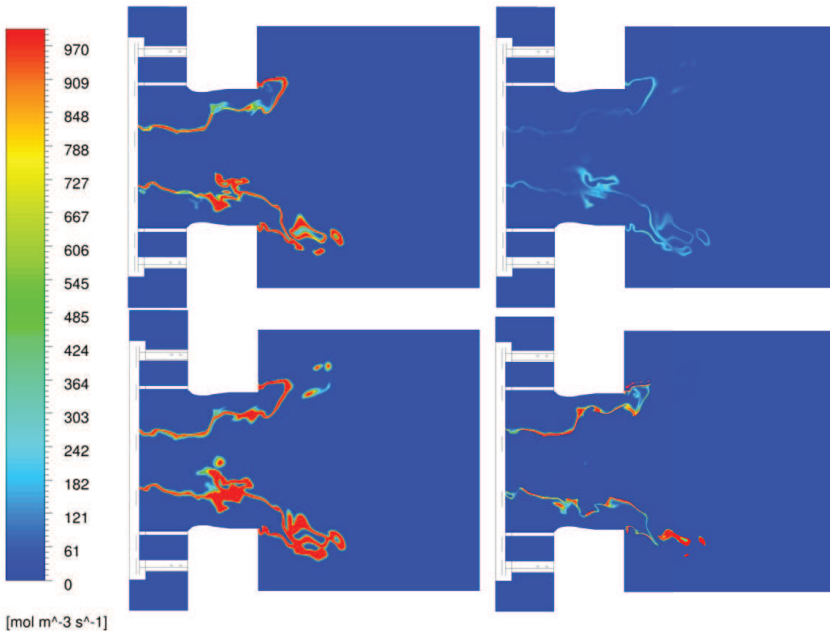

Figure 7.7: LES simulation of the SGT-100 burner (Abou-Taouk *et al.* (2014)). Instantaneous reaction rates: reaction 1 upper left, reaction 2 upper right, reaction 3 lower left and reaction 4 lower right

Abou-Taouk *et al.* (2013) presented CFD results for the Turchemi test case using the SAS-SST model. To determine which turbulence model was used by the solver in different regions, the different terms in the SAS-SST model must be visualized. The regions with LES-like solutions should have the following term dominating (Egorov & Menter (2007))

$$\rho\zeta_2\kappa S^2\left(\frac{L}{L_{\nu k}}\right)^2 \tag{7.2}$$

and the regions with RANS solutions should have the following term of the same magnitude as the term in equation 7.2:

$$\frac{2\rho k}{\sigma_\phi}\left(\frac{1}{\omega^2}\frac{\partial\omega}{\partial x_j}\frac{\partial\omega}{\partial x_j}\right) \tag{7.3}$$

The ratio between the terms in equations 7.2 and 7.3 is plotted in Figure 7.8, where the instantaneous ratio between the terms mentioned above is shown. LES-like solutions are provided for values larger than one. It is clearly seen that the major part of the burner is simulated by the SAS model since the flow is highly unsteady and three-dimensional.

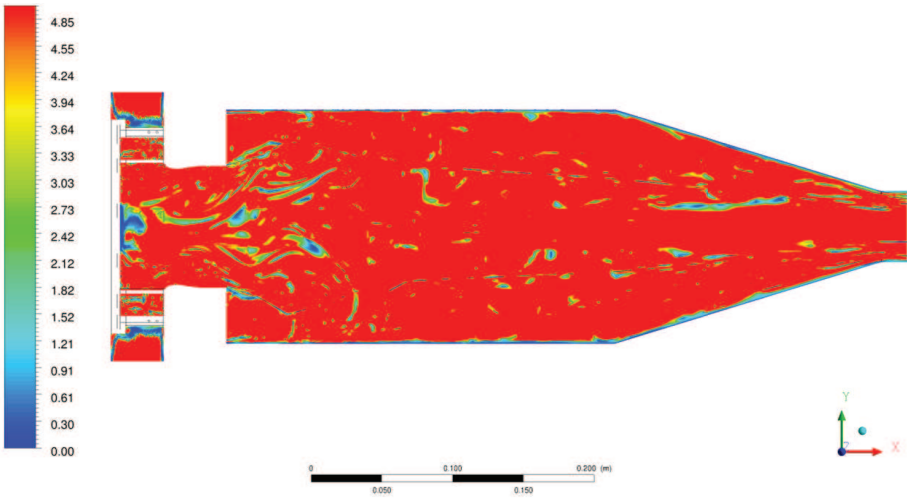

Figure 7.8: Instantaneous contour plot showing which turbulence model is activated. Red: the SAS model is used; Blue: the unsteady $k-\omega$ SST model is used.

7.2 Downscaled SGT-750 test burner

The main results obtained for the downscaled SGT-750 test burner are presented and discussed in papers I, II, IV and V. Figure 7.9 shows an iso-surface of the highest CO mass fraction (red), the instantaneous temperature (bottom plane) and the instantaneous heat release rate (back plane) using the SAS-SST model and a methane-air mixture. In this simulation, the prechamber is operating at a fuel-rich condition ($\phi = 1.6$) and the main flame at a fuel-lean condition ($\phi = 0.4$). The main swirling flame is located in the Quarl part and anchored close to the smallest section in the Quarl. It is clearly visible that the highest reaction rates are located close to the wall in the Quarl since the swirl is sufficiently high to push the fuel radially outwards. The flame in the

shear layer shows a broken reaction structure and thus seems to be associated with the thickened flame regime.

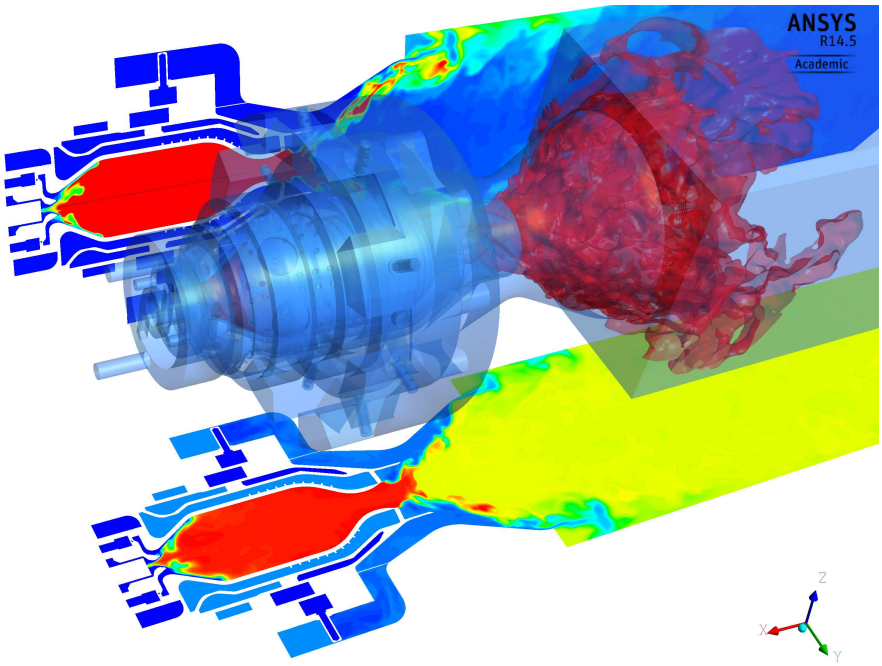

Figure 7.9: Iso-CO mass fraction (red). Bottom plane: instantaneous temperature. Back plane: instantaneous heat release rate

Figure 7.10 shows an instantaneous contour plot of the equivalence ratio, ϕ, in the burner at three different axial planes. Fuel, air and burned gases are relatively well mixed downstream in the burner due to the strong mixing (high swirl number). However, it is clear that the local equivalence ratio around the flame position, visible in Figure 7.9, varies from lean mixtures with fuel concentrations below the ignition limit to slightly below stoichiometric values. It is also this region that is measured, using PIV, in the experimental campaign, see Sigfrid (2013); Whiddon (2014); Abou-Taouk *et al.* (2012).

Figure 7.11 and Figure 7.12 show contour plots in order to determine which of the two models in the combined FRC/EDM is activated for reaction 1 (Figure 7.11) and reaction 2 (Figure 7.12) in the optimized two-step global scheme (Abou-Taouk & Eriksson (2011)). The expressions that calculate the reaction rates are based on either the EDM model or the FRC model and have been put into the Ansys CFX® software. The colors in the plot show the ratio between the reaction rates based on the FRC model (calculated according to equation 7.1) and the EDM model. Red means that the Arrhenius reaction rate is larger than the EDM reaction rate and consequently that the reaction

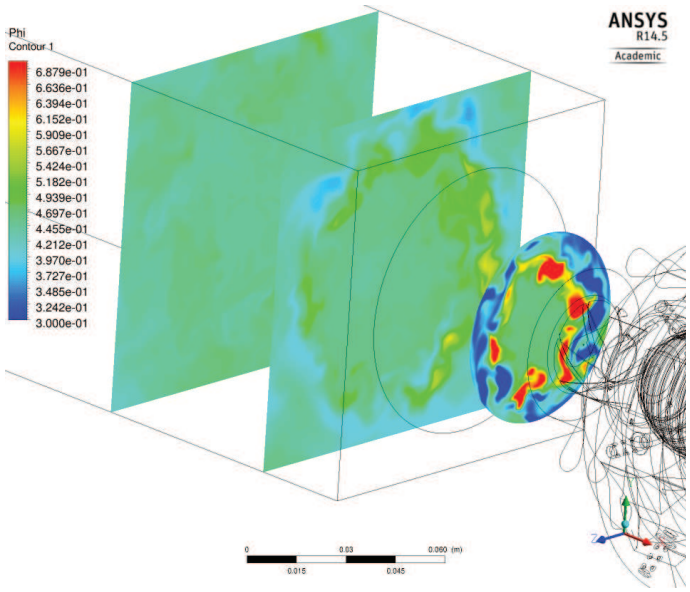

Figure 7.10: Instantaneous contour plot of the equivalence ratio in the downscaled SGT-750 test burner at three different planes

rate is limited by the turbulent mixing. Blue means the opposite, e.g. the FRC model is used by the solver. What is visible is that the reaction rates are based on the Arrhenius expression close to the interface between the hot and cold mixtures (see Figure 7.13), e.g. where the flame is located. The EDM model is activated where the temperature is high (since the Arrhenius rate comes to be large), consequently making the reaction rates limited by the mixing process.

The ratio between the terms in equations 7.2 and 7.3 is plotted in Figure 7.14 and shows which turbulence model is used by the solver. LES-like solutions are provided for values larger than one and the opposite gives $k - \omega$ SST solutions. The major part of the CFD domain is solved by the SAS model.

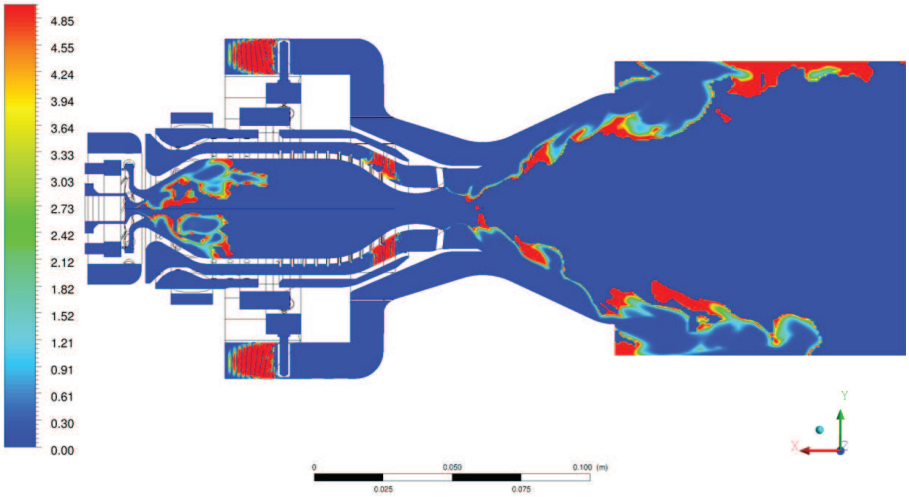

Figure 7.11: Instantaneous contour plot of the ratio between the reaction rate from the FRC and the EDM models, to determine which of the combustion models is activated in reaction 1 (optimized two-step global mechanism, Abou-Taouk & Eriksson (2011)). Values larger than one: the EDM model is used; values smaller than one: the FRC model is used.

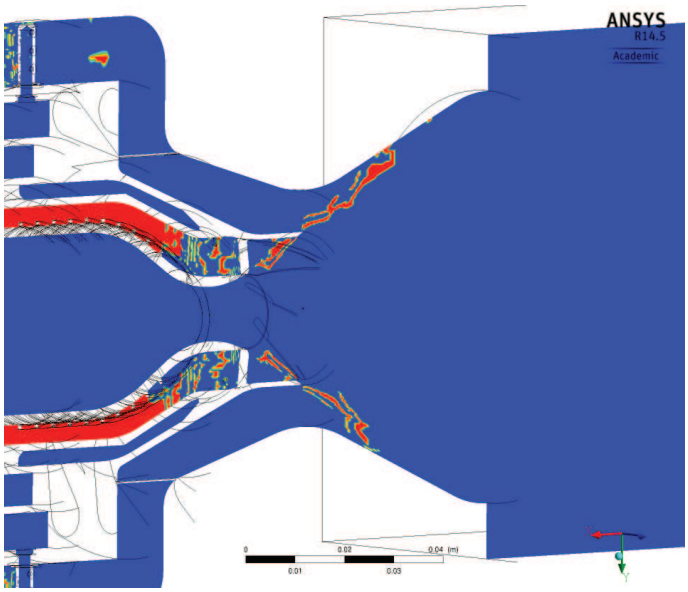

Figure 7.12: Instantaneous contour plot of the ratio between the reaction rate from the FRC and the EDM models, to determine which of the combustion models is activated in reaction 2 (optimized two-step global mechanism, Abou-Taouk & Eriksson (2011)). Values larger than one: the EDM model is used; values smaller than one: the FRC model is used, color scale same as previous figure

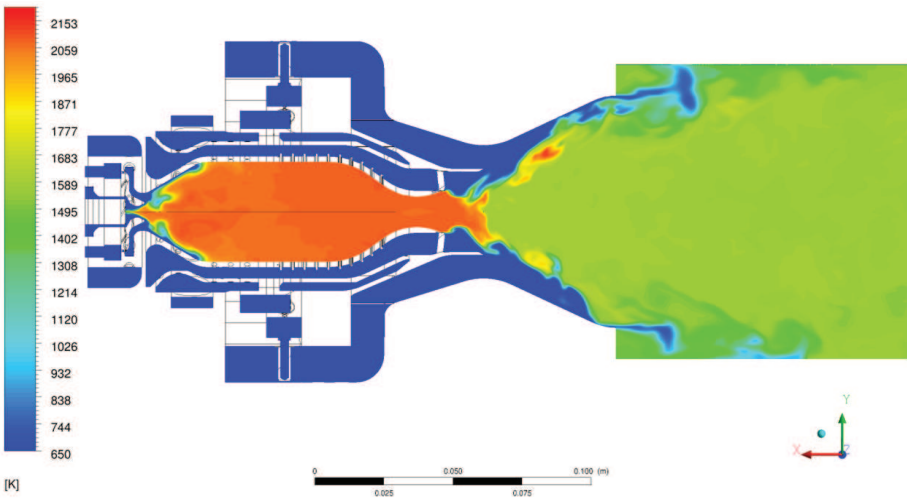

Figure 7.13: Instantaneous contour plot showing the temperature

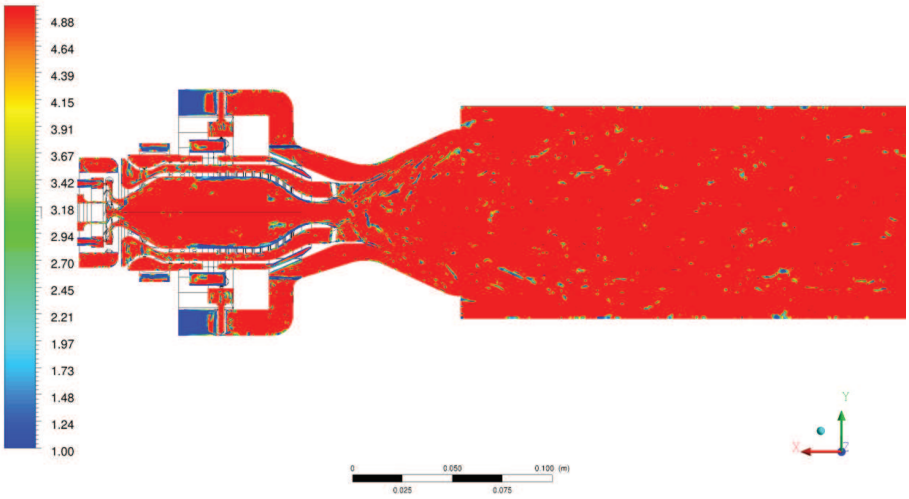

Figure 7.14: Instantaneous contour plot showing which turbulence model is activated. Red: the SAS model is used; Blue: the unsteady $k-\omega$ SST model is used.

Chapter 8

Concluding Remarks

MODELING turbulent combustion in industrial gas turbine applications is a challenging task. Combustion simulations based on RANS models are still very useful for industries. However, with increased computer capabilities, hybrid RANS/LES and LES are very promising models and are rapidly developing for turbulent combustion applications.

A detailed kinetic reaction scheme can contain hundreds of species and thousands of reactions, and the complexity of combustion chemistry needs to be reduced. The main part of this thesis involves the development of a methodology for optimizing global schemes in order to apply them for numerical studies. An optimization strategy has been developed using modeFRONTIER® as the optimization software coupled to the CHEMKIN® software. The optimization procedure, which dynamically adjusts the Arrhenius coefficients and the correction function for the transport properties to match a set of reference (even for Gaussian filtered) laminar flames computed with the fully detailed kinetics, has been shown to work well for the cases studied.

8.1 Optimization of Global Schemes

The main conclusions concerning optimization of reduced schemes are:

- The number of species and the reaction steps included in the global mechanism need to be chosen before any optimization can be performed. This is a tricky task, and there is no straightforward approach to how to accomplish this. The number of species to be involved in the global scheme can be determined by a preliminary equilibrium analysis. This study is based on varying the number of species in the global mechanism, and thus examine

whether the equilibrium conditions can be matched compared to a detailed mechanism, see Abou-Taouk *et al.* (2014).

- The GRI-Mech 3.0 detailed mechanism was used for gases that are based on methane and syngas mixtures. However, the San Diego mechanism was also tested for the syngas mixture, according to published literature, but without observing large differences compared to the GRI-Mech 3.0 mechanism.

- A number of settings and parameters need to be optimized in CHEMKIN in order to limit the simulation time. The most important parameters and settings are:

  ATOL and RTOL: These two tolerances (absolute and relative) are used by the solver to determine the convergence. Too small a value may increase the solver time from minutes to hours per iteration.

  GRAD and CURVE: These set the adaptive grid control based on the solution gradient and solution curvature, respectively. These parameters in the 1-D flame model control the maximum gradient and the maximum curvature allowed between grid points. A smaller value implies an increased number of grid points in the solver and consequently longer simulation time.

  Temperature profile: To decrease the simulation time, a user-specified temperature profile should be used as a start guess of the solution.

  Grid points: Both the number of adaptive grid points and the maximum number of adaptive grid points allowed should be chosen carefully to minimize the solution time and to obtain a mesh-independent solution.

  Continuation technique: This method allows the iterative iteration process to be divided into subparts. The continuation technique decreases the simulation time.

- Optimization based on the PSR model yields multiple reaction rate coefficient solutions that give accurate predictions of the species concentrations, but almost all of these solutions fail to predict the species concentration profiles and the laminar flame speed in a 1-D propagating flame. Both the lean and rich conditions cannot be simultaneously included in the optimization simulation due to different chemistry behavior.

- It is important to choose the maximum and minimum bounds for the Arrhenius parameters carefully during the optimization process to avoid convergence problems due to an improper modeling of chemistry. Choosing intervals outside the flammability limits will imply a long simulation time and may imply solutions that diverge.

Finally, a novel approach to the sub-grid scale modeling of turbulent, partially premixed combustion in gas turbines based on optimized chemistry is presented. A four-step global chemical scheme and a corrective factor to the transport properties are automatically obtained from the optimization set-up, in order to match the flame speed response and major species profiles, as they appear in a Gaussian filtered flame that is sufficiently thick to be resolved over a coarse LES grid.

8.2 CFD Simulations

High quality block-structured grids, based on hexahedral cells, were used throughout the work. The geometry features included are chosen carefully in order to decrease the dependency on the inlet boundary conditions. The main conclusions based on the preparation of the CFD domain are:

- **Grid size:** Keeping the mesh size as low as possible is preferred and is important since the simulation time is proportional to the mesh size. The quality of the hexahedral mesh type is high, and the resolution of this type of mesh is around five to eight times better than for the tetra cells for the same number of grid points. However, the creation of the block structure requires a great deal of experience and can be a time-consuming task depending on the complexity of the geometry.

- **CFD domain:** Locate the inlet boundary conditions as far as possible from the measuring planes. This is done by including the upstream cavities. However, including more cavities and geometry features implies larger grid sizes and consequently a longer simulation time.

Prototypes of the premixed/partially premixed burners of the SGT-100 and the downscaled SGT-750 test burners, and the Sandia Flame D, have been numerically investigated using RANS, hybrid URANS/LES and LES turbulence models. The kinetics has been modeled by the optimized global schemes and the combustion by the finite rate chemistry

model and the combined eddy dissipation model/finite rate chemistry model.

The main conclusions from the CFD results on the downscaled SGT-750 test burner are:

The predicted lean blowout limit using CFD is somewhat higher than the experimental data. The lean blowout equivalence ratio was significantly lower for the syngas mixtures compared to the methane based gases, which is in agreement with the observation made in the experimental testing, Sigfrid (2013). Furthermore, the comparisons of the POD modes from PIV measurements and CFD simulations were in good agreement. The RANS model captures well the mean values and predicts well the upstream regions, but had difficulties predicting the position and the maximum velocity of the recirculation zone. Finally, the recirculation zone and the magnitude of the maximum velocities are correctly predicted using the hybrid URANS/LES model. The simulation time is around six to seven times more expensive than the RANS simulation, but the increased flame structure resolution is valuable and compares well to the real flame structure. The hybrid URANS/LES model is a promising model for turbulent reacting flows, especially for industrial burner applications.

The main conclusions from the CFD results on the SGT-100 burner are:

The predicted burner pressure loss compares well with measured data from the experiment. The LES simulation with the new subgrid approach was tested for this burner, where the results showed that the flame dynamics along with statistical data agreed well with the measurements.

Finally, the CFD simulations show that the choice of both turbulence model and chemical kinetics mechanism has a large impact on the simulation results. The combustion modeling varies between RANS and LES models since the combustion is treated differently. Therefore, it is not straightforward how these models can be compared.

8.3 Future Work

It is important that high quality experimental data are available in order to validate existing and new kinetic models for turbulent reactive

flow. The limited published experimental data for low caloric fuel mixtures is a problem for being able to validate global mechanisms aimed for CFD with these types of mixtures.

What would be interesting to investigate in the future is the differences between the PSR and the 1D laminar flame model in the optimization methodology. A set-up using both these models in a combined optimization process will be an interesting research topic.

It is well known that confined turbulent flames may develop pressure oscillations. Further studies of how these global schemes predict pressure oscillations compared to measured data will therefore be of great interest in being able to correctly predict combustion instabilities.

Finally, further numerical studies using the downscaled SGT-750 test burner would be of interest. Unfortunately, the number of test cases available with published data is limited for turbulent swirling flow applications, and especially a burner that contains rich conditions. The downscaled SGT-750 test burner is thus of interest since the RPL part has the availability to operate from lean to rich conditions.

Bibliography

ABDEL-GAYED, R. G. & BRADLEY, D. 1989 Combustion regimes and the straining of turbulent premixed flames. *Combustion and Flame* **76**, 213–218.

ABDEL-GAYED, R. G., BRADLEY, D., HAMID, M. N. & LAWES, M. 1984 Lewis number effects on turbulent burning velocity. *Symposium (international) on combustion* pp. 505–512.

ABOU-TAOUK, A. & ERIKSSON, L. E. 2011 Optimized global mmechanisms for cfd analysis of swirl-stabilized syngas burner for gas turbines. *ASME Turbo Expo, Vancouver, Canada* pp. GT2011–45853.

ABOU-TAOUK, A., FARCY, B., DOMINGO, P., VERVISCH, L., SADASIVUNI, S. & ERIKSSON, L. E. 2014 A new approach for large eddy simulation of gas turbine partially premixed combustion: Implicit modeling using optimized chemistry. *Submitted to the Proceedings of the Combustion Institute* .

ABOU-TAOUK, A., SADASIVUNI, S., LORSTAD, D. & ERIKSSON, L. E. 2013 Evaluation of global mechanisms for les analysis of sgt-100 dle combustion system. *ASME Turbo Expo, San Antonio, Texas, USA* pp. GT2013–95454.

ABOU-TAOUK, A., SIGFRID, I., WHIDDON, R. & ERIKSSON, L. E. 2012 A four-step global reaction mechanism for cfd simulations of flexi-fuel burner for gas turbines. *Turbulence, Heat and Mass Transfer* **7**, 785–788.

ANDERSEN, J., RASMUSSEN, C. L., GISELSSON, T. & GLARBORG, P. 2009 Global combustion mechanisms for use in cfd modeling under oxy-fuel conditions. *Energy Fuels* **23(3)**, 1379–1389.

ANGELBERGER, C., VEYNANTE, D., EGOLFOPOULOS, F. & POINSOT, T. 1998 Large eddy simulations of combustion instabilities in premixed flames. *Proc. of the Summer Program, Center for Turbulence Research, Stanford,* pp. 61–82.

BOILEAU, M., STAFFELBACH, G., CUENOT, B., POINSOT, T. & BÉRAT, C. 2008 Les of an ignition sequence in a gas turbine engine. *Combustion and Flame* **154(1/2)**, 2–22.

BORGHI, R. 1988 Turbulent combustion modelling. *Progress in Energy and Combustion Science* **14**, 245.

BOUDIER, G., GICQUEL, L. Y. M., POINSOT, T., BISSIERES, D. & BERAT, C. 2008 Effect of mesh resolution on large eddy simulation of reacting flows in complex geometry combustors. *Combustion and Flame* **155:1-2**, 196–214.

BRAY, K. & LIBBY, P. 1976 Interaction effects in turbulent premixed flames. *Phys Fluids* **19**, 1687.

BRAY, K. & MOSS, J. 1977 A unified statistical model of the premixed turbulent flame. *Acta Astron* **4**, 291.

BULAT, G., JONES, W. P. & MARQUIS, A. J. 2013 Large eddy simulation of an industrial gas-turbine combustion chamber using sub-grid pdf method. *Proceedings of the Combustion Institute* **34(2)**, 3155–3164.

BUTLER, T. D. & O'ROURKE, P. J. 1977 A numerical method for two dimensional unsteady reacting flows. *Symposium (international) on combustion* **16:1**, 1503–1515.

BUZZI, G. F. & MANENTI, F. 2009 Kinetic models analysis. *Chemical Engineering Science* **64(5)**, 1061–1074.

BYKOV, V. & MAAS, U. 2007 The extension of the ildm concept to reaction-diffusion manifolds. *Combustion Theory Model* **11(6)**, 839–862.

CAVALLO-MARINCOLA, F., MA, T. & KEMPF, A. M. 2013 Large eddy simulations of the darmstadt turbulent stratified flame series. *Proceedings of the Combustion Institute* **34(1)**, 1307–1315.

CFX 2014 *http://www.ansys.com/default.asp* .

CHAKRAVARTHY, V. K. & MENON, S. 2000 Subgrid modeling of turbulent premixed flames in the flamelet regime. *Flow, Turbulence and Combustion* **65:2**, 133–161.

CHARLETTE, F., MENEVEAU, C. & VEYANTE, D. 2002 A power-law flame wrinkling model for les of premixed turbulent combustion. part i: Non-dynamic formulation and initial tests. *Combustion and Flame* **131**, 159–180.

CHEMKIN 2014 *http://www.reactiondesign.com* .

CHENG, R. K., LITTLEJOHN, D., STRAKEY, P. A. & SIDWELL, T. 2009 Laboratory investigations of a low-swirl injector with h2 and ch4 at gas turbine conditions. *Proceedings of the Combustion Institute* **32**, 3001–3009.

COLIN, O., DUCROS, F., VEYNANTE, D. & POINSOT, T. 2000 A thickened flame model for large eddy simulations of turbulent premixed combustion. *Physics of Fluids* **12:7**, 1843–1863.

CUOCI, A., FRASSOLDATI, A., FARAVELLI, T. & RANZI, E. 2009 Accuracy and flexibility of simplified kinetic models for cfd applications. *32nd Meeting on Combustion* .

CURTISS, C. F. & HIRSCHFELDER, J. O. 1949 *Journal of Chemical Physics* **17**, 550–555.

DUWIG, C., NOGENMYR, K. J., CHAN, C. & DUNN, M. J. 2011 Large eddy simulations of a piloted lean premix jet flame using finite-rate chemistry. *Combustion Theory and Modelling* **15**, 537–568.

EGOROV, Y. & MENTER, F. 2007 Development and application of sst-sas turbulence model in the desider project. *Second Symposium on Hybrid RANS-LES Methods, Corfu, Greece* .

ELLIOTT, L., INGHAM, D., KYNE, A., MERA, N., POURKASHANIAN, M. & WILSON, C. 2003 Multiobjective genetic algorithm optimization for calculating the reaction rate coefficients for hydrogen combustion. *Ind. Eng. Chem. Res.* **42**, 1215–1224.

ERLEBACHER, G., HUSSAINI, M. Y., SPEZIALE, C. G. & ZANG, T. A. 1992 Toward the large-eddy simulation of compressible turbulent flows. *Journal of Fluid Mechanics* **238**, 155–185.

FARCY, B., ABOU-TAOUK, A., VERVISCH, L., DOMINGO, P. & PERRET, N. 2014 Two approaches of chemistry downsizing for simulating selective non catalytic reduction denox process. *Fuel* **118**, 291–299.

FEDINA, E. & FUREBY, C. 2011 A comparative study of flamelet and finite rate chemistry les for an axisymmetric dump combustor. *Journal of Turbulence* **12(1)**.

FERNANDEZ-TARRAZO, E., SANCHEZ, A., LINAN, A. & WILLIAMS, F. 2006 *Combustion and Flame* **147:1-2**, 32–38.

FIORINA, B., VICQUELIN, R., AUZILLON, P., DARABIHA, N., GICQUEL, O. & VEYNANTE, D. 2010 A filtered tabulated chemistry model for les of premixed combustion. *Combustion and Flame* **157**, 465–475.

FRANZELLI, B., RIBER, E., SANJOSE, M. & POINSOT, T. 2010 A two-step chemical scheme for large eddy simulation of kerosene-air flames. *Combustion and Flame* **157(7)**, 1364–1373.

FUREBY, C. 2008 Towards the use of large eddy simulation in engineering. *Progress in Aerospace Sciences* **44**, 381–396.

FUREBY, C. 2010 Les of a multi-burner annular gas turbine combustor. *Flow, Turbulence and Combustion* **84**, 543–564.

GENRUP, M. & THERN, M. 2013 Ny gasturbinteknik, gas turbine developments 2012-2014. Technical report NO. 13:31. Elforsk.

GLASSMAN, I. 1996 *Combustion*, 3rd edn. Academic Press.

GOBBY, D. 2009 Piloted methane jet flame. Technical report. Ansys CFX.

DE GOEY, L. P. H., VAN OIJEN, J. A., BONGERS, H. & GROOT, G. R. A. 2003 New flamelet based reduction methods: the bridge between chemical reduction techniques and flamelet methods. *European Combustion Meeting* .

GOKULAKRISHNAN, P., KWON, S., HAMER, A., KLASSEN, M. & ROBY, R. 2006 Reduced kinetic mechanism for reactive flow simulation of syngas/methane combustion at gas turbine conditions. *ASME Turbo Power Expo, Power for land , Sea and Air, GT2006-90573* .

GOLOVITCHEV, V. I., NORDIN, N., JARNICKI, R. & CHOMIAK, J. 2000 3-d diesel spray simulations using a new detailed chemistry turbulent combustion model. *International Spring Fuels and Lubricants Meeting and Exposition Paris, France June 19-22* .

GRAN, I. & MAGNUSSEN, B. F. 1996 A numerical study of a bluff-body stabilized diffusion flame. part 2. influence of combustion modeling and finite-rate chemistry. *Combustion Science Technology* **119**, 191–217.

GRUNDY, P. 2008 Shell energy scenarios to 2050 .

GÜLDER, O. L. 1990 Turbulent premixed flame propagation models for different combustion regimes. *Proceedings of the Combustion Institute* **23**, 743–750.

GULLBRAND, J. 2003 Ctr stanford. *Annu. Res. Briefs* pp. 331–342.

GUSTAFSSON, B. 2010 Introduction to project area combustor technology. *Turbo Power Programme Conference* .

HAWKES, E. R. & CANT, R. S. 2001 Implications of a flame surface density approach to large eddy simulation of premixed turbulent combustion. *Combustion and Flame* **126:3**, 1617–1629.

IEA 2013 Key world energy statistics. *International Energy Agency* **www.iea.org**.

IRANNEZHAD, M. 2012 A numerical study of reacting flows using finite rate chemistry. *Ph.D. thesis, Chalmers University of Technology, Gothenburg, Sweden* .

JANICKA, J. & SADIKI, A. 2005 Large eddy simulation of turbulent combustion systems. *Proceedings of the Combustion Institute* **30(1)**, 537–547.

JAPIKSE, D. & BAINES, N. 1997 *Introduction to Turbomachinery*. White River Junction, Vt.:Concepts ETI, Oxford Uinversity Press.

JOHANSSON, E. 2010 Combustion modeling in jet engine combustors. *Master of science thesis, Chalmers University of Technology, Gothenburg, Sweden* .

JOHNSON, M. R., LITTLEJOHN, D., NAZEER, W. A., SMITH, K. O. & CHENG, R. K. 2005 A comparison of the flow fields and emissions of high-swirl injectors and low-swirl injectors for lean premixed gas turbines. *Proceedings of the Combustion Institute* **30**, 2867–2874.

JONES, W. P. & LINDSTEDT, R. P. 1988 Global reaction schemes for hydrocarbon combustion. *Combustion and Flame* **73**, 233–249.

KARMAN, T. V. & PENNER, S. S. 1954 Fundamental approach to laminar flame propagation in selected combustion problems. *(AGARD Combust. Colloq.)* pp. Butterworths, London.

KEMPF, A., SADIKI, A. & JANICKA, J. 2002 *Proceedings of the Combustion Institute* **29**, 1979–1985.

KUENNE, G., KETELHEUN, A. & JANICKA, J. 2011 Les modeling of premixed combustion using a thickened flame approach coupled with fgm tabulated chemistry. *Combustion and Flame* **158**, 1750–1767.

KUO, K. K. 2005 *Principles of Combustion*, 2nd edn. John Wiley Sons.

LAM, S. H. & GOUSSIS, D. A. 1994 The csp method for simplifying kinetics. *International Journal of Chemical Kinetics,* **26:4**, 461–486.

LEFEBVRE, A. H. 1999 *Gas Turbine Combustion*, 2nd edn. New York:Taylor & Francis.

LÉGIER, J. P., POINSOT, T. & VEYNANTE, D. 2000 Dynamically thickened flame les model for premixed and non-premixed turbulent combustion. *Proc. of the summer program* pp. 157–168.

LIPATNIKOV, A. N. & CHOMIAK, J. 2002 Turbulent flame speed and thickness: phenomenology, evaluation and application in multi-dimensional simulations. *Progress in Energy and Combustion Science* **28**, 1–74.

MAAS, U. & POPE, S. B. 1992*a* Implementation of simplified chemical kinetics based on intrinsic low-dimensional manifolds. *Symposium (international) on combustion* **24:1**, 103–112.

MAAS, U. & POPE, S. B. 1992*b* Simplifying chemical kinetics: Intrinsic low-dimensional manifolds in composition space. *Combustion and Flame* **88:3-4**, 239–264.

MAGNUSSEN, B. F. & HJERTAGER, B. H. 1976 On mathematical models of turbulent combustion with special emphasis on soot formation and combustion. *16th Symp. (Int'l.) on Combustion* .

MALLARD, E. & CHATELIER, H. L. 1883 *Ann. Mines* **4**, 379.

MARLOW, D. & NORTON, T. 1995 A reduced mechanism for low-heating-value gas combustion in a perfectly stirred reactor. *American Flame Research Committee International Symposium* .

MARZOUK, O. & HUCKABY, E. D. 2010 A comparative study of eight finite-rate chemistry kinetics for co/h_2 combustion. *Appl. Comp. Fluid Mech* **4**, 331–356.

MCBRIDE, B. J. & GORDON, S. 1996 Computer program for calculation of complex chemical equilibrium compositions and applications ii. user's manual and program description. Nasa rp-1311-p2. NASA.

MENTER, F. 1994 Two-equation eddy-viscosity turbulence models for engineering applications. *AIAA-Journal* **32**, 1598 – 1605.

MEREDITH, K. V. & BLACK, D. L. 2006 Automated global mechanism generation for use in cfd simulations. *44-th AIAA-Paper.–Reno, Nevada* pp. 1–13.

MODEFRONTIER 2014 *http://www.modefrontier.com* .

MOUSTAPHA, H. & ZELESKY, M. 2003 *Axial and Radial Turbines*. Concepts NREC.

NGUYEN, P. D., VERVISCH, L., SUBRAMANIAN, V. & DOMINGO, P. 2010 Multidimensional flamelet-generated manifolds for partially premixed combustion. *Combustion and Flame* **157(1)**, 43–61.

NICOUD, F. & DUCROS, F. 1999 Subgrid-scale stress modelling based on the square of the velocity gradient tensor. *Flow Turbulence and Combustion* **62**, 183–200.

NIU, Y.-S., VERVISCH, L. & TAO, P. D. 2013 An optimization-based approach to detailed chemistry tabulation: Automated progress variable definition. *Combustion and Flame* **160(4)**, 776–785.

NOGENMYR, K.-J. 2008 On the modeling of premixed combustion under varying equivalence ratios. PhD thesis, Division of Fluid Mechanics, Lund University , Lund.

NOGENMYR, K.-J., PETERSSON, P., BAI, X. S., NAUERT, A., OLOFSSON, J., BRACKMAN, C., SEYFRIED, H., ZETTERBERG, J., LI, Z. S., RICHTER, M., DREIZLER, A., LINNE, M. & ALDÉN, M. 2007 Large eddy simulation and experiments of stratified lean premixed methane/air turbulent flames. *Proceedings of the Combustion Institute* **31**, 1467–1475.

NOVOSSELOV, I. V. & MALTE, P. C. 2008 Development and application of an eight-step global mechanism for cfd and crn simulation of lean-premixed combustors. *Journal of Engineering for Gas Turbines and Power* **130**.

OIJEN, J. A. V. & GOEY, L. P. H. D. 2000 Modelling of premixed laminar flames using flamelet- generated manifolds. *Combustion Science and Technology* **161:1**, 113–137.

OIJEN, J. A. V., LAMMERS, F. A. & DEGOEY, L. P. H. 2001 Modeling of complex premixed burner systems by using flamelet-generated manifolds. *Combustion and Flame* **127(3)**, 2124–2134.

O'ROURKE, P. J. & BRACCO, F. V. 1979 Two scaling transformations for the numerical computation of multidimensional unsteady laminar flames. *Journal of Computational Physics* **33:2**, 185–203.

PERSSON, B. 2012 Modern gasturbines to meet the future market demands. *ICCI 18th International Energy and Environment Conference, Istanbul, Turkey* .

PETERS, N. 1984 Laminar flamelet concepts in turbulent combustion. *Prog. Energy Combust. Sci.* **10**, 319.

PETERS, N. 1985 Numerical and asymptotic analysis of systematically reduced reaction schemes for hydrocarbon flames. *Numerical simulation of combustion phenomena* **147:1-2**, 90–109.

PETERS, N. 1986 Laminar flamelet concepts in turbulent combustion. *Proc. Combust. Inst.* **21**, 1231–1250.

PETERS, N. 1999 The turbulent burning velocity for large scale and small scale. *Journal of Fluid Mechanics* **384**, 107–132.

PETERS, N. 2000 *Turbulent Combustion*, 1st edn. Cambridge University Press.

PETERS, N. & KANURY, A. M. 2001 Turbulent combustion. *Applied Mechanics Reviews* **54**, B73. 19.

PITSCH, H. 2006 Large-eddy simulation of turbulent combustion. *Annual Review of Fluid Mechanics* **38**, 453–482.

PITSCH, H. 2012 Combustion theory. *Princeton-CEFRC Summer School On Combustion* .

POINSOT, T. & VEYNANTE, D. 2001 *Theoretical and Numerical Combustion*. R. T. Edwards, Flourtown, PA.

POINSOT, T. & VEYNANTE, D. 2005 *Theoretical and Numerical Combustion*, 3rd edn. R. T. Edwards Inc.

POPE, S. B. 1985 Pdf methods for turbulent reactive flows. *Prog. Energy Combust. Sci.* **11**, 119–192.

POPE, S. B. 1990 Computations of turbulent combustion: Progress and challenges. *Proceedings of the Combustion Institute* **23**, 591–612.

REN, Z. & POPE, S. B. 2006 The use of slow manifolds in reactive flows. *Combustion and Flame* **147:4**, 243–261.

SADASIVUNI, S., BULAT, G., SANDERSON, V. & SWAMINATHAN, N. 2012 Numerical application of scalar dissipation rate combustion model to siemens dle combustors. *Proceedings of ASME Turbo Expo* pp. GT2012–68483.

SANDIA, F. 2014 Sandia national laboratories. *Turbulent Diffusion Flame Laboratory Web Site, http://www.ca.sandia.gov/tfd* .

SARAVANAMUTTOO, H., ROGERS, G. & COHEN, H. 2001 *Gas Turbine Theory*, 5th edn. Pearson Education Limited 1951, 2001.

SELLE, L., LARTIGUE, G., POINSOT, T., KOCH, R., SCHILDMACHER, K. U., KREBS, W., PRADE, B., KAUFMANN, P. & VEYNANTE, D. 2004 Compressible large eddy simulation of turbulent combustion in complex geometry on unstructed meshes. *Combustion and Flame* **137**, 489–505.

SEMENOV, N. 1942 Theory of normal flame propagation. *Translated in NACA Tech. Mem.* **1026**.

SIEMENS 2014 *http://www.sit-ab.se/* .

SIGFRID, I. 2013 Investigation of a prototype industrial gas turbine combustor using alternative gaseous fuels. *Ph.D. thesis, Lund University, Lund, Sweden* .

SIGFRID, I., WHIDDON, R., ABOU-TAOUK, A., COLLIN, R. & KLINGMANN, J. 2012 Experimental investigation of an industrial lean premixed gas turbine combustor with high swirl. *ASME Gas Turbine India Conference, GTIndia2012-9681* .

SIGFRID, I., WHIDDON, R., COLLIN, R. & KLINGMANN, J. 2010 Experimental investigation of laminar flame speed for medium calorific gas with various amounts of hydrogen and carbon monoxide content at gas turbine temperatures. *ASME Turbo Power Expo, Power for land , Sea and Air, GT2010-22275* .

SIGFRID, I., WHIDDON, R., COLLIN, R. & KLINGMANN, J. 2011*a* Experimental investigation of lean stability limit of an prototype syngas burner for low calorific value gases. *ASME Turbo Power Expo, Power for land , Sea and Air, GT2011-45694* .

SIGFRID, I., WHIDDON, R., COLLIN, R. & KLINGMANN, J. 2011*b* Parametric study of emissions from low calorific value syngas combustion, with variation of fuel distribution, in a prototype three sector burner. *ASME Turbo Power Expo, Power for land , Sea and Air, GT2011-45689* .

SIGFRID, I., WHIDDON, R., COLLIN, R. & KLINGMANN, J. 2013*a* Experimental and reactor network study of nitrogen dilution effects on nox formation for natural gas and syngas at elevated pressures. *ASME Turbo Power Expo, Power for land , Sea and Air, GT2013-94355* .

SIGFRID, I., WHIDDON, R., COLLIN, R. & KLINGMANN, J. 2014 Reactive species influence on the lean blow out limit for an industrial dle gas turbine burner. *Submitted to Combustion and Flame* .

SIGFRID, I., WHIDDON, R., COLLIN, R., KLINGMANN, J. & ALDEN, M. 2013*b* Investigation of a premixed gas turbine combustor central body burner using oh planar laser induced fluorescence at elevated pressures. *ASME Turbo Power Expo, Power for land , Sea and Air, GT2013-94443* .

SIT 2014 *www.energy.siemens.com/co/pool/hq/power-generation/gas-turbines/sgt-750/SGT-750Siemensgasturbine.pdf* .

SLAVINSKAYA, N. & UNKHOFF, M. B. 2008 Reduced reaction mechanisms for methane and syngas combustion in gas turbines. *Journal of Engineering for Gas Turbines and Power* **130(2)**, 021504.

SMITH, G. P., FRENKLACH, D. M. G. M., MORIARTY, N. W., EITENEER, B., GOLDENBERG, M., BOWMAN, C. T., HANSON, R. K., SONG, S., GARDINER, W. C., LISSIANSKI, V. V. & QIN, Z. 1999 Technical report. *http://www.me.berkeley.edu/gri-mech* .

SMOOKE, M. 1991 *Reduced kinetic mechanisms and asymptotic approximations of methane-air flames*. Springer-Verlag, Berlin.

SPALDING, D. B. 1971 Mixing and chemical reaction in steady confined turbulent flames. *Proc. Combust. Inst.* **13**, 649–657.

SPALDING, D. B. 1976 Development of the eddy-break-up model of turbulent combustion. *Proc. Combust. Inst.* **16**, 1657–1663.

STOPPER, U., AIGNER, M., AX, H., MEIER, W., SADANANDAN, R., STOHR, M. & BONALDO, A. 2010 Piv, 2d-lif and 1d-raman measurements of flow field, composition and temperature in premixed gas turbine flames. *Experimental Thermal and Fluid Science* **34(3)**, 396–403.

STOPPER, U., MEIER, W., SADANANDAN, R., STOHR, M., AIGNER, M. & BULAT, G. 2013 Experimental study of industrial gas turbine

flames including quantification of pressure influence on flow field, fuel/air premixing and flame shape. *Combustion and Flame* **160(10)**, 2103–2118.

STRAKEY, P. A. & EGGENSPIELER, G. 2010 Development and validation of a thickened flame modeling approach for large eddy simulation of premixed combustion. *Journal of Engineering for Gas Turbines and Power* **132**, 071501–1–071501–9.

SUBRAMANIAN, V., DOMINGO, P. & VERVISCH, L. 2010 Large eddy simulation of forced ignition of an annular bluff-body burner. *Combustion and Flame* **157(3)**, 579–601.

SYRED, N. & BEÉR, J. 1974 Combustion in swirling flows: A review. *Combustion and Flame* **23:2**, 143–201.

TANFORD, C. & PEASE, R. N. 1947 Theory of burning velocity. *J. Chem. Phys.* **15**, 861–865.

TENNEKES, H. & LUMLEY, J. 1972 *A first course in turbulence*. Cambridge: M.I.T. Press.

TIANFENG, L. & CHUNG, L. K. 2007 Diffusion coefficient reduction through species bundling. *Combustion and Flame* **148:3**, 117–126.

TIANFENG, L. & CHUNG, L. K. 2008 Strategies for mechanism reduction for large hydrocarbons: n-heptane. *Combustion and Flame* **154:1-2**, 153–163.

TURNS, S. R. 1996 *An Introduction to Combustion*. McGraw-Hill New York.

VANDERBEI, R. J. 2001 *Linear Programming: Foundations and Extensions*. Springer New York.

VEYNANTE, D. & VERVISCH, L. 2002 Turbulent combustion modeling. *Progress in Energy and Combustion Science* **28**, 193–266.

VEYNANTE, D. & VERVISCH, L. 2011 Turbulent combustion modeling. *VKI LS Course* .

WALSH, P. & FLETCHER, P. 2004 Gas turbine performance. *Blackwell, Oxford* pp. 193–195.

WANG, G., BOILEAU, M. & VEYANTE, D. 2011 Implementation of a dynamic thickened flame model for large eddy simulations of turbulent premixed combustion. *Combustion and Flame* **158**, 2199–2213.

WARNATZ, J., MAAS, U. & DIBBLE, R. W. 2006 *Combustion. Physical and chemical fundamentals, modeling and simulation, experiments, pollutant formation*, 4th edn. Springer.

WESTBROOK, C. K. & DRYER, F. L. 1984 Chemical kinetic modeling of hydrocarbon combustion. *Progress in Energy and Combustion Science* **10(1)**, 1–57.

WHIDDON, R. 2014 Application of laser-based diagnostics to a prototype gas turbine burner at selected pressures. *Ph.D. thesis, Lund University, Lund, Sweden* .

WILCOX, D. C. 2004 *Turbulence Modeling for CFD*, 2nd edn. DCW Industries, Inc.

WILLIAMS, F. 1985 *Turbulent Combustion.In: The mathematics of combustion*, jd ed edn. Buckmaster, SIAM, Philadelphia.

YAKHOT, V., ORSZAG, C., THANGAM, S., GATSKI, T. & SPEZIALE, C. 1992 Development of turbulence models for shear flows by a double expanision technique. *Physics of Fluids* **4:7**, 1510.

YAN, J., MOCKETT, C. & THIELE, F. 2005 Investigation of alternative length scale substitutions in detached-eddy simulation. *Flow, Turbulence and Combustion* **74**, 85–102.

ZELDOVICH, Y. H., BARENBLATT, G. I., LIBROVICH, V. B. & MAKVILADZE, G. M. 1985 The mathematical theory of combustion and explosions. *Eng. tran., Plenum, New York* .

ZIMONT, V. L. 2000 Gas premixed combustion at high turbulence. turbulent flame closure combustion model. *Experimental Thermal and Fluid Science* **21**, 179–186.

ZIMONT, V. L. & LIPATNIKOV, A. 1995 A numerical model of premixed turbulent combustion of gases. *Chemical Physics Reports* **14**, 993–1025.

Appendix A

Equations

THIS section describes both the RANS models $k-\omega$ SST and RNG $k-\epsilon$. The hybrid SAS-SST turbulence model is also described, and the equations follow here:

A.1 $k-\omega$ SST

The $k-\omega$ SST model is an industry standard for complex flows with separation and has become very popular. The $k-\omega$ SST model combines two different approaches. The model can be used all the way down to the wall without any extra damping functions. In the outer region (free-stream), the SST formulation switches to a $k-\epsilon$ behavior. The k equation reads:

$$\frac{\partial \rho k}{\partial t} + \frac{\partial}{\partial x_j}\left(\rho \bar{U}_j k\right) = \frac{\partial}{\partial x_j}\left[\left(\mu + \frac{\mu_t}{\sigma_k}\right)\frac{\partial k}{\partial x_j}\right] + P_k - \rho\beta^* k\omega \tag{A.1}$$

and the ω equation reads:

$$\frac{\partial \rho \omega}{\partial t} + \frac{\partial}{\partial x_j}\left(\rho \bar{U}_j \omega\right) = \frac{\partial}{\partial x_j}\left[\left(\mu + \frac{\mu_t}{\sigma_\omega}\right)\frac{\partial \omega}{\partial x_j}\right] + \alpha\frac{\omega}{k}P_k - \rho\beta\omega^2 + (1-F_1)\frac{2\rho}{\sigma_{\omega 2}}\frac{1}{\omega}\frac{\partial k}{\partial x_i}\frac{\partial \omega}{\partial x_i} \tag{A.2}$$

A.2 RNG $k-\epsilon$

The RNG model was developed by Yakhot *et al.* (1992) to renormalize the Navier-Stokes equations. The RNG approach is based on the equation attempting to account for the different scales of motion in the

flow through modifications of the production term, P_k. The k equation reads:

$$\frac{\partial \rho k}{\partial t} + \frac{\partial}{\partial x_j}\left(\rho \bar{U}_j k\right) = \frac{\partial}{\partial x_j}\left[\left(\mu + \frac{\mu_t}{\sigma_k}\right)\frac{\partial k}{\partial x_j}\right] + P_k - \rho\epsilon \tag{A.3}$$

and the ϵ equation reads:

$$\frac{\partial \rho \epsilon}{\partial t} + \frac{\partial}{\partial x_j}\left(\rho \bar{U}_j \epsilon\right) = \frac{\partial}{\partial x_j}\left[\left(\mu + \frac{\mu_t}{\sigma_\epsilon}\right)\frac{\partial \epsilon}{\partial x_j}\right] + C_{1\epsilon}\frac{\epsilon}{k}P_k - \rho C^{\star}_{2\epsilon}\frac{\epsilon^2}{k} \tag{A.4}$$

A.3 SAS-SST

The SAS approach represents a new class of the URANS models. The von Karman length scale explicitly enters the transport equations to the SAS model. The model gives suitable RANS solutions for stable flows. For flows with transient behavior, the model reduces its eddy viscosity according to the locally resolved vortex size represented by the von Karman length scale. The SAS model can under those conditions allow the break-up of large unsteady structures into a turbulent spectrum and avoid RANS-typical single-mode vortex structures. SAS modeling is based on the use of a second mechanical scale in the source/sink terms of the underlying turbulence model. The modified ω equation reads:

$$\frac{\partial \rho \omega}{\partial t} + \frac{\partial}{\partial x_j}\left(\rho \bar{U}_j \omega\right) = \frac{\partial}{\partial x_j}\left[\left(\mu + \frac{\mu_t}{\sigma_\omega}\right)\frac{\partial \omega}{\partial x_j}\right] + \alpha\frac{\omega}{k}P_k - \rho\beta\omega^2 + (1 - F_1)\frac{2\rho}{\sigma_{\omega 2}}\frac{1}{\omega}\frac{\partial k}{\partial x_i}\frac{\partial \omega}{\partial x_i} + S_{SAS} \tag{A.5}$$

The term S_{SAS} stands for the SAS source term and comes from a term in Rotta's transport equation for the correlation-based length scale, see Menter (1994); Egorov & Menter (2007). The source term reads:

$$S_{SAS} = max\left[\rho\zeta_2\kappa S^2\left(\frac{L}{L_{\nu k}}\right)^2 - C\frac{2\rho k}{\sigma_\phi}max\left(\frac{1}{\omega^2}\frac{\partial \omega}{\partial x_j}\frac{\partial \omega}{\partial x_j}, \frac{1}{k^2}\frac{\partial k}{\partial x_j}\frac{\partial k}{\partial x_j}\right), 0\right] \tag{A.6}$$

and the $L_{\nu k}$, L and constants read:

$$L_{\nu k} = \frac{\kappa\frac{\partial \bar{U}}{\partial y}}{\frac{\partial^2 \bar{U}}{\partial y^2}}, L = \frac{k^{1/2}}{\omega C_\mu^{1/4}}, C = 2, \zeta = 3.51 \tag{A.7}$$

Paper I

Paper II

Paper III

Paper IV

Paper V

Paper VI

Paper VII

Paper VIII